MULTI-SITE STATISTICAL DOWNSCALING OF DAILY TEMPERATURE EXTREMES FOR CLIMATE-RELATED IMPACT ASSESSMENT STUDIES

BY

Ju Eun Kim

Department of Civil Engineering and Applied Mechanics

McGill University

Montreal, Quebec, Canada

A thesis submitted to McGill University in partial fulfillment of the requirement of the degree of Master of Engineering

December 2012

TABLE OF CONTENTS

ABSTRACT

Global climate change has been considered in many engineering studies due to its drastic impacts on the design and planning of various infrastructures. In order to reduce the risks of those impacts, the present study focuses on accurate prediction of daily temperature extremes for future periods under different climate change scenarios. The main objectives of this study are therefore: (a) to detect the evidences of climate change from the statistical analysis of existing observed daily extreme temperature data; (b) to assess the performance of single-site and multi-site statistical downscaling (SD) approaches in order to identify the best SD model that could describe accurately the linkage between global scale climate variables and the observed statistical properties of daily temperature extremes at a given local site; and (c) to provide a prediction of daily temperature extremes for future periods based on the best SD model identified under different climate change scenarios.

Firstly, a detailed statistical analysis of daily extreme temperature data available during the 1973-2009 period from a network of 25 weather stations located in South Korea was carried out to identify the possible trends in 18 different temperature characteristics. Results of this data analysis have indicated significant changes in the characteristics of daily maximum temperature (Tmax) and daily minimum temperature (Tmin) during this period. In particular, the positive trends in annual means of Tmax and Tmin were found statistically significant. In addition, the number of cold events tends to decrease while the number of warm events tends to increase at most of the stations considered.

Secondly, statistical downscaling methods were used to describe the linkage between the coarse resolution of General Circulation Model (GCM) climate variables and the daily extreme temperature characteristics at a local site for impact assessments. Most previous studies have been dealing with downscaling of daily temperature extremes at a single site. However, more recent studies have been conducted to develop improved downscaling methods for many sites concurrently. This study was carried out to assess

the performance of the multi-site SD method based on the Singular Value Decomposition (SVD) method as compared with the performance of the popular SDSM for single-site downscaling. The application of the multi-site and single-site SD methods was performed using the observed daily Tmax and Tmin data from the 25 stations in South Korea and the corresponding NCEP re-analysis data for the 1973-2001 period. It was found that the multi-site SD method and the single-site SDSM could accurately reproduce basic properties of Tmax and Tmin at each local site. However, the multi-site SD method could describe more accurately the temporal and spatial correlations of daily temperature extremes than the SDSM. Overall, the multi-site SD method was found to be more accurate than the SDSM.

Finally, future prediction of daily extreme temperatures was accomplished based on the multi-site SD method under the A1B and A2 climate scenarios provided by the third version of the Canadian Global Climate Model (CGCM3). The increasing trends were found in the monthly means of Tmax and Tmin, the monthly90^{th} percentiles of Tmax, and the monthly10^{th} percentiles of Tmin for the future 2010-2100 period over South Korea.

Résumé

Le changement climatique global a été introduit dans les études d'ingénierie en raison de ses impacts importants sur la conception et la planification des infrastructures. Afin de réduire ces impacts, la présente étude se concentre sur la possibilité d'obtenir des prévisions précises des températures extrêmes pour les périodes futures sous divers scénarios de changement climatique. Les objectifs principaux de cette étude sont alors (a) de détecter les éléments reliés au changement climatique à partir de l'analyse statistique des données disponible de températures extrêmes journalières; (b) d'évaluer la performance des techniques de mise en échelle statistique (SD : Statistical Downscaling) en un site et en plusieurs sites pour identifier le meilleur modèle SD qui est capable décrire correctement le lien entre les variables climatiques globales et les propriétés statistiques observées des températures extrêmes journalières en un site choisi; et (c) de fournir une prévision des températures extrêmes pour le futur en se basant sur le meilleur modèle SD identifié pour divers scénarios de changement climatique.

Premièrement, une analyse statistique détaillée des données de températures extrêmes journalières disponibles pour la période de 1973-2009 d'un réseau de 25 stations météorologiques situé en la Corée du Sud a été effectuée pour identifier les tendances possibles dans les 18 propriétés de température. Les résultats de cette analyse des données ont indiqué des changements significatifs sur les caractéristiques de température maximale journalière (Tmax) et de température minimale journalière (Tmin) pendant cette période. En particulier, des tendances positives statistiquement significatives dans les moyennes annuelles de Tmax et Tmin ont été identifiées. De plus, le nombre d'événements froids a eu une tendance de diminution tandis que le nombre d'événements chauds a eu une tendance d'augmentation pour la plupart de stations considérées.

Deuxièmement, les méthodes SD ont été utilisées pour établir le lien entre la résolution grossière des variables climatiques du modèle de circulation générale (MCG) et les propriétés de températures extrêmes journalières en un site pour les évaluations d'impact. La plupart des études antérieures ont été effectuées sur la mise en échelle des températures extrêmes journalières en un seul site. Cependant, des études plus récentes

ont été réalisées pour élaborer des méthodes de mise en échelle en plusieurs sites simultanément. Cette étude a été effectuée pour évaluer la performance de la méthode SD en multi-sites basée sur la technique de décomposition en valeurs singulières (SVD) en comparant avec celle de la méthode de mise en échelle statistique populaire SDSM en un site. L'application de ces deux méthodes a été réalisée en utilisant les données observées de températures extrêmes journalières Tmax et Tmin de 25 stations météorologiques en Corée du Sud et les données de NCEP correspondantes pour la période de 1973 à 2001. On a trouvé que les méthodes de mise en échelle multi-sites et en un site SDSM sont capables de reproduire correctement les caractéristiques statistiques de base de Tmax et Tmin en chaque site. Toutefois, l'approche multi-site peut reproduire d'une façon plus précise les corrélations temporelle et spatiale que la méthode SDSM.

En général, l'approche multi-site peut fournir des estimations plus précises des caractéristiques Tmax et Tmin que celles données par la méthode SDSM. Enfin, la prévision des températures extrêmes quotidiennes est faite en appliquant l'approche multi-sites SD pour les scénarios de changement climatique A1B et A2 fournis par le modèle climatique global canadien (MCCG3). Les résultats de cette prévision ont indiqué une tendance croissante dans les valeurs moyennes mensuelles de Tmax et Tmin, la 90e percentile de Tmax et la 10e percentile de Tmin pour la période de 2010 à 2100 à travers de la Corée du Sud.

ACKNOWLEDGEMENTS

First of all, I wish to express my most sincere gratitude to my supervisor, Prof. V-T-V Nguyen, Department of Civil Engineering and Applied Mechanics, McGill University, Quebec, Canada for his expert guidance, encouragement, and comprehension in this research.

I would like to my appreciation to Dr. Malika Khalili, Myeong-Ho Yeo and Ju-Eun Kim (Mechanical Engineering) for their assistance and advice during my research work.

The most grateful thanks are due to my husband, Luzhuo Liu, my parents, my parents-in-law and my brother, Tae-Eun Kim for their love and financial support. Special thanks go to my friends, Min-Young Lee and Joo-Wan Kim for their encouragement and support.

LIST OF FIGURES

LIST OF TABLES

1 INTRODUCTION

1.1 Statement of Problems

Increase in surface temperature has been observed all over the globe during the last century. Warming of the Earth is widely accepted as a result of change in atmospheric composition by greenhouse gases – majorly carbon dioxide (CO_2) and methane (CH4) emission from human activities. Actually, the recent increasing trends of greenhouse gases level in atmosphere and historical temperature record were closely matched. The instrumental records show that 0.6 ± 0.2 degree of the global average annual temperature and around 30% of atmospheric concentration of CO_2 has simultaneously increased since 19^{th} century (IPCC, 2007). The changes in air temperature may affect the climate system. Increase of sea surface temperature, derived from increment of air temperature plays an important role of accelerating evaporation mechanism and adding more energy to the water cycle. These hydrological changes are possibly related to more severe climatic events in recent years. Held and Soden (2000) reported that wet regions get wetter and dry regions get drier according to changes in hydrological cycle in response to global warming.

The unexpected extreme weather events could significantly affect civil engineering practices such as water resource management, coastal development and flood control. Failure risk in hydraulic structures and their maintenance costs could be increased by those extreme events. In order to avoid economical and technical uncertainties caused by these extreme weather events, it is urgently critical for civil engineers, hydrologists and environmental policy makers to better understand the current weather patterns and to accurately estimate the possible future change of climate and hydrologic processes such as the temperature extremes. Therefore, the main objective of the present study is to provide a reliable prediction of the possible change in the future temperature extremes based on a robust and accurate modeling method under different climate change scenarios.

General Circulation Models (GCMs) have been widely used to project future climate conditions. In general, GCMs perform reasonably well to simulate climate parameters at a global scale (usually larger than 200 km), but they could not provide accurate estimates of climate variables at smaller scales (e.g., less than 30 km) for impact assessment studies due to their coarse temporal and spatial resolution. A common method to overcome this scale mismatch is so-called 'downscaling'. Downscaling techniques are broadly divided into two groups (Nguyen, 2002; Wilby, 2002): dynamical downscaling (DD) methods and statistical downscaling (SD) procedures. The DD methods provide regional climate simulations at the spatial resolution of 20 to 50km based on physical formulas and boundary conditions derived from GCMs outputs, while the SD techniques are based on the empirical relationship between the global atmospheric variables given by GCMs and the surface weather variables at a local site. Compared to DD methods, SD techniques are more widely adopted in hydrological studies due to their simpler computational requirement and their more accurate adaptation to the climate conditions at a given local site.

For instance, the Statistical DownScaling Model (SDSM) developed by Wilby et al. (2002) is one of the popular SD methods. The SDSM is based on a combination of a statistical regression model and a stochastic component for downscaling of of daily extreme temperature and daily precipitation processes at a single site. However, these single-site SD methods such as the SDSM are limited to reproduce realistic characteristics of climate processes at a given location, but they could not describe accurately the spatial dependency of climate series at different locations concurrently. Ignorance of the spatial dependency in weather data can affect the reliability of impact assessments (Srikanthan and McMahon, 2001 and Maraun et al., 2010). For example, the spatial distribution of rainfall over the watershed is an important factor to determine the magnitude and the duration of floods. Khalili et al. (2006) showed that using simulated precipitation without considering the spatial dependency in a hydrologic model may lead to underestimating or overestimating the extreme stream flows for summer and autumn seasons over Quebec region.

Recent studies have proposed multi-site downscaling approaches in order to reproduce more realistically the spatial dependency of observed climate series. In particular, Malika and Nguyen (2012) have proposed a multi-site SD method based the Singular Value Decomposition (SVD) technique for downscaling of daily temperature extremes at many sites concurrently. In addition, the SVD-based stochastic simulation models have been successfully used for simulation of streamflow series (Cavadias, 1986; Chaleeraktrakoon, 1995) and weather data (Nguyen, 2001) at many sites. Those previous studies however did not provide a detailed comparison of the performance of a multi-site SD method as compared to the performance of a single-site SD method such as the SDSM. Therefore, in the present study, the multi-site SD method based on the SVD technique is examined as compared with the SDSM to identify the best method that could provide accurate and reliable extreme temperature simulations for the current period and for temperature predictions in the future.

1.2 Objectives of Study

As mentioned above, the main aim of this research is to identify the best SD method that could provide accurate and reliable simulation and prediction of daily extreme temperature series under changing climate conditions. To achieve this aim, the present study focuses on the following four specific objectives using daily extreme temperature data available in South Korea:

1. To detect the evidence of climate change over South Korea based on a detailed statistical analysis of the variability of daily extreme temperature characteristics;
2. To assess the feasibility of the SVD-based multi-site SD method and the single-site SDSM in the downscaling of daily maximum and minimum temperature processes in South Korea;
3. To compare the performance of the SVD-based multi-site SD and the SDSM in terms of their abilities to reproduce accurately the temporal and spatial statistical properties of the observed daily extreme temperature series at different locations; and

4. To provide the predictions of the changes in daily temperature extremes for future periods under different climate change scenarios using the best SD method identified.

1.3 Organization of Thesis

The remaining chapters of this thesis are organized as follows: Chapter 2 summarizes a review of the literature regarding climate change and global warming, statistical characterization of temperature extremes, and downscaling techniques. Chapter 3 provides a description of the data used in this study, the detailed methodology of the downscaling methods considered, and the comparison criteria for assessing the performance of these SD methods. Chapter 4 provides the detailed statistical analyses of the observed daily extreme temperature data over South Korea. Chapter 5 presents the comparison of the performance of the multi-site SD method and the SDSM for downscaling daily temperature extremes. Chapter 6 presents the prediction of changes in future temperature extremes. Finally, Chapter 7 gives the conclusions of this study and the recommendations for further studies.

2 LITERATURE REVIEW

This chapter presents a brief review of previous works concerning the current assessment of the global climate change with a special emphasis on temperature changes using different temperature variability indices, and the existing downscaling techniques for climate impact assessment studies.

2.1 Climate Change and Global Warming

IPCC (2001) defined that climate change as any change in the mean of weather condition or in statistical distribution of weather pattern for over decades. Climate change in long-term periods is caused by natural factors such as variations in solar radiation, deviation in the Earth's orbit, volcano activity and continental drift, or anthropogenic factors. Although global climate is naturally fluctuated, many climatologists (IPCC, 2001 and 2007) believe that recent dramatic climate change is particularly associated with human-induced causes. Rapid population growth and industrialization results an unusual rise in concentration of greenhouse gases (GHGs). GHGs such as water vapor, carbon dioxide (CO_2), methane (CH_4), nitrous oxide (N_2O) and ozone (O_3) in an atmosphere play a critical role for green house effect. Those gases warm the Earth by absorbing and emitting radiation within the thermal infrared range.

For last two decades, global climate has apparently been warming. Besides, increases in GHGs emission and in global temperature occurred at the similar time. A close correlation between temperature and atmospheric concentration of GHGs is proved by an analysis of isotopic contents in ice cores (Petit et al., 1999). This analysis allows investigating palaeoclimate series in the past million years: local temperature and precipitation, moisture source conditions, wind strength and aerosol fluxes of marine, volcanic eruptions, and solar variability. Palaeoclimate information from the analysis supports that current inclement in global surface mean temperature is highly correlated to the increased emission of GHGs by human activities. Also, IPCC (2001) has concluded that recent dramatic increase of GHGs emission by human activities has played the most significant role in global warming.

In 2010, the average annual concentration of CO_2 in the atmosphere measured by Mauna Loa Observatory is 389.78 parts per million (ppm) which is the highest level in at least the past 650,000 years (IPCC, 2007). The concentrations of CO_2 and CH_4 have increased by 36% and 148% respectively since 1750 (EPA, 2007). In addition, the global average annual temperature has increased 0.6 ± 0.2 degree for the past century (IPCC, 2001). Figure 2.1 shows that surface mean temperature over the Northern Hemisphere from AD 1000 to 1999. The graph is shaped like a hockey stick since increase in surface temperature for the Northern Hemisphere over the 20th century is remarkably greater than any other century in the last thousand years.

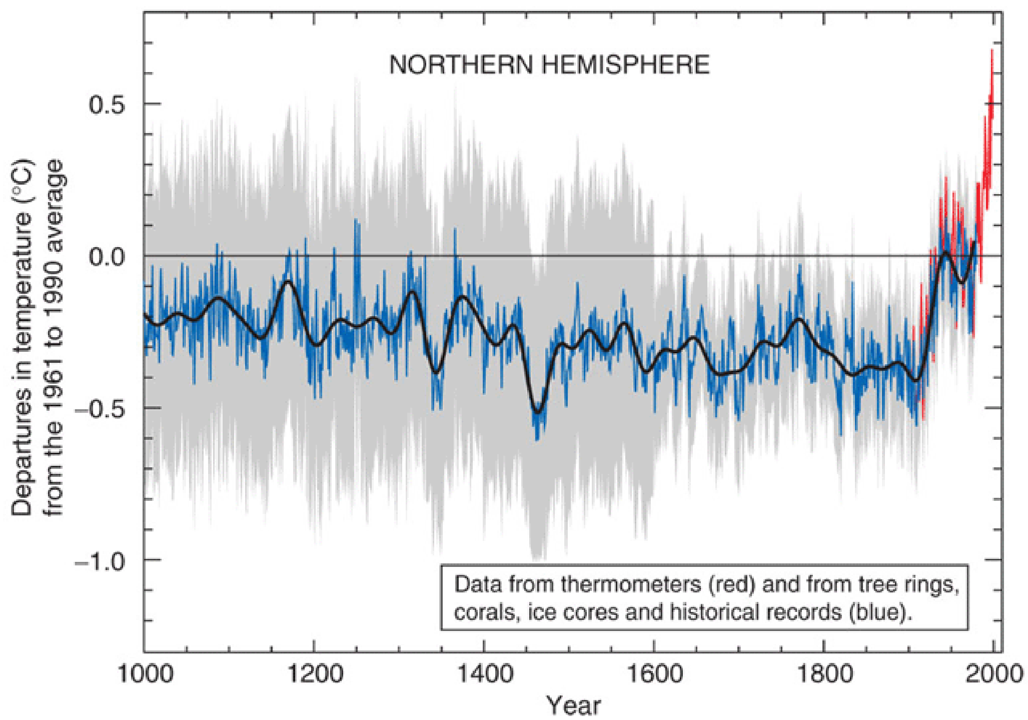

Figure 2.1 Variations of Northern Hemisphere surface mean temperature from AD 1000 to 1999. Annual mean temperature reconstructed by tree rings, corals, ice cores and historical records (blue line) and instrumental data (red line). Gray shaded region represents a 95% confidence range of the annual temperature estimates (Mann et al, 1999).

Global warming can cause variety of impacts on environment and human society. Global mean temperature increase directly affects to global mean sea-level. A rate of a sea level rise over the 20th century observed by Church and White (2006) is 1.7 ±0.3 mm per year. Based on future global temperature scenarios of IPCC's fourth assessment report, Vermeer (2010) projected a future sea-level rise ranging from 75 to 190 cm for the period 1990-2100. A sea level rise possibly results in submerging of low-lying coastal areas. Other indirect impacts of global warming are increase in extreme weather events (Katz et al., 1992; Easterling, 2000), loss of biodiversity (Walther, 2002) and risk to human health (Patz et al., 2000). Held and Soden (2000) refer that wet regions get wetter and dry regions get drier according to changes in hydrological cycle in response to global warming. Changes in global hydrological cycle and energy circulation are highly possible to increase frequency and magnitude of extreme weather events. Consequently, flood protection structures such as damns, spill ways and levees need to be altered their capacity and management system. Furthermore, global warming can modify plant communities and ocean acidification that result in extinction of species. Also human health can be threatened by weather-related stress and disease, and acceleration of the spread of infectious disease.

2.2 General Circulation Models

Due to increase of interests in global climate change, many climate centres have designed mathematical models with physical, fluid dynamical and chemical equations to describe the general circulation of the atmosphere and ocean of the Earth. These models are known as general circulation models (GCMs). Different GCMs use different model resolution, assumption and boundary conditions. Commonly used GCMs are the third version of the Canadian Global Climate Model (CGCM3), the third version of the Hadley centre coupled model (HadCM3) and the fifth generation European centre Hamburg general circulation model (ECHAM5).

GCMs typically structure in three-dimensional grid and the resolutions of the models that are between 1 and 5 degrees in latitude and longitude. HadCM3 has a horizontal resolution of 3.75 °in longitude and 2.5 °in latitude, and uses 19 levels in the vertical. CGCM3 is modeled over a grid of 3.75 °in longitude and 2.5 °in latitude, and has 31 levels in the vertical.

Scenario	**Storyline**	**Global Warming until 2100**	**CO_2 Emission**
A1	➢ Rapid economic growth ➢ The quick spread of technologies ➢ A global population reaches 9 billion in 2050 and generally declines ➢ A convergent world Subsets of A1 based on technological emphasis A1F1 - Fossil fuel intensive A1B - All energy source A1T – Non-fossil fuel energy sources	1.4 - 6.4 ℃	High (A1F1: Highest)
A2	➢ Economic growth and technological improvements per capita income are slower and more fragmented. ➢ Continuously increasing global population ➢ A heterogeneous world, with regional diversity ➢ Self-reliance nations, preservation of local identities	2.0 - 5.4 ℃	High-medium
B1	➢ Rapid economic growth as in A1 ➢ Reduction in material intensity and introduction of clean and resource efficient technologies ➢ Population peaks in 2050 and declines as A1 ➢ Emphasis on global solutions to economic, social and environmental sustainability	1.1 - 2.9 ℃	Low
B2	➢ Intermediate levels of economic development ➢ Less rapid and more diverse technological change than in the B2 ➢ Continuously increasing global population at a lower rate than A2 ➢ Emphasis on local solutions to economic, social and environmental sustainability	1.4 - 3.8 ℃	Low-medium

Table 2.1 Special Report on Emission Scenarios (SRES) storylines and outcome (IPCC, 2001)

For projections of future climate change, GCMs requires of application of various possible scenarios to estimate the level of GHGs emission. In recent, special report on emissions scenarios (SRES) which released in 2001 by IPCC is most commonly used due to its reasonable consideration of driving forces of emissions such as demographic development, socio-economic development and the rate and direction of technological change. Table 1.1 summarized the detailed characteristics of storylines and range of possible outcomes of SRES.

2.3 Statistical Characterization of Temperature Variability

2.3.1 Temperature Variability Indices

Indices of climate data are commonly used as statistical measures to describe changes in mean and variability of climate. Many climate studies have used several climate extreme indices such as means, variations and extremes of weather indicators. There was a remarkable consistency in the results of different regional temperature studies using indices of daily temperature. In North America, the number of cold events has decreased significantly but the number of warm events has increased significantly (Easterling et al., 2000; Kunkel et al., 2004). In Europe, the warming trends in temperature extremes are also indicated, and at the same time fewer cold nights and more warm days are detected (Klein Tank et al., 2003). In Africa (Mokssit A., 2003), Australia (Plummer et al., 1999), South America (Vincent et al., 2005) and Asia (Zhai et al., 2003), results are similar to that obtained from North America and Europe studies.

Global studies on extreme weather were done by Frich et al. (2002) and Alexander et al. (2006). The global studies using indices of daily temperature agreed with the annual averages of daily maximum temperature (Tmax) and daily minimum temperature (Tmin) have increased significantly for the last half-century. The number of cold events tends to decrease but the number of warm events tends to increase in many locations of the world. Moreover, the decreasing trend in diurnal temperature range (DTR) has been observed in several regions due to stronger decrease of minimum temperature and relatively weaker increase of maximum temperature (Qian and Lin, 2004).

2.3.2 Trends on Temperature Extreme in South Korea

South Korea has a temperate climate with four distinct seasons. Although Korea mainly has cold and dry winters and hot and humid summers, the regional weather characteristics is not identical because of complex topography. High mountain range crisscrosses the peninsula and only 30% of the area of South Korea consists of lowland that lies mainly along coasts. Complicated mountainous terrain in South Korea causes the high spatial variation in characteristics of regional climate. Besides, the global trend in climate change or the results from climate analysis of adjacent regions cannot always represent changes in local-scale climate. Therefore, local-scale climate studies are urgently required to achieve reliable climate information over South Korea.

Unfortunately, not many studies have analyzed local climate in South Korea using various indices. Jung et al. (2002) examined daily temperature records of 16 stations over South Korea. They investigated the increasing trends in means of daily Tmax and Tmin, which were the same as the global trends. Kwon (2005) and Choi (2004) also observed increases in annual means of daily Tmin, Tmax and daily mean temperature (Tmean). The study of extreme climatic indices done by Choi (2004) found significant decrease in the number of frost days and increase in growing season length (GSL) at most stations. In addition, the trends in variability of extreme temperature were negative for more than half of region over the country. Im et al. (2011) analyzed the trends in five different indices of temperature extremes - frost days (FD), hot days (HD), averaged daily Tmax above 95th percentile (TX95), averaged daily Tmin below 5th percentile (TN5) and the maximum duration of consecutive hot days (HW) using the Mann-Kendall test. The trends in TX95, HD and HW remain constant or slightly increase. Yet, the negative trends in FD and TN5 were statistically significant at the 90% confidence level in more than half of the country in recent 30 years (1971-2000).

2.4 Downscaling Methods

Downscaling is a common technique in order to bridge the gap between the coarse resolution of GCMs and the required resolution for impact assessments such as agriculture, energy, health and civil construction at a regional or local scale. Typically, the resolutions of GCMs are larger than 250km but the favorable resolution for impact applications is less than 30km. The strategy of downscaling is to connect global-scale climate variability and local-scale observation for generating more regionally specific forecasts. Downscaling techniques could be divided into two broad categories; dynamic downscaling (DD) and statistical downscaling (SD).

2.4.1 Dynamic Downscaling

Dynamic downscaling (DD) methods involve nesting a higher resolution regional climate model (RCM) within a coarse GCM resolution (Wilby et al., 2002). RCMs dynamically simulate climate features using the formulas and boundary conditions from GCMs. In general, there are three different types of DD methods (Yarnal et al.,2001):

1) Running a regional-scale limited-area model with the coarse GCM data as geographical or spectral boundary conditions (as known as 'one-way nesting').
2) Performing global-scale experiments with high-resolution Atmosphere GCMs (AGCMs) with coarse GCM data as initial boundary condition.
3) Using a variable-resolution global model with the highest resolution over the area of interest.

The main advantage of RCMs is that they are able to resolve regional climate dynamic processes such as convective or orographic precipitation at the much finer spatial resolution of 20-50km. However, these models still cannot meet the finer spatial resolution needs of explicit models of ecosystem or hydrological system. Also, the scope of modeling and simulations using DD approaches is limited because their computational demanding is as expensive to run as GCMs (Wilby et al., 2002).

2.4.2 Statistical Downscaling

Statistical downscaling (SD) techniques rely on the empirical relationship between global-scale atmospheric variables and local-scale observed surface environmental parameters such as temperature and precipitation (Nguyen, 2002). The main advantage of SD methods over DD methods is the low computational requirements (Wilby et al., 2002; Nguyen, 2002). SD methods are attractive for hydrologic analysis due to their easy application and modification achieved by the requirements of relatively less number of parameters compared to DD methods (Wilby et al., 2004). However, SD techniques have several limitations related to accessibility of the local meteorological data and the unverifiable background assumptions of SD approaches. Firstly, the reliable time series data archived for a long term periods are required but it is not easy to obtain for the target region. Secondly, this technique is affected by bias in GCMs variables used as predictor in SD models (Goodess et al., 2001). More recently, many developers of SD methods achieved improvement in previously mentioned limitations. SD techniques are classified into three strategies according to studies of Wilby and Wigley (1997): weather typing approaches, stochastic weather generators and regression-based downscaling methods.

2.4.2.1 Weather typing

Weather typing approaches involve grouping local meteorological variables related to atmospheric circulation patterns into limited number of types (Bardossy and Plate, 2002; Yarnal et al., 2001). Weather schemes are identified by applying objective statistical methods such as principal component analysis (PCA), neural networks or cluster analysis, or using subjective weather classification schemes (Yurnal et al.,2001). The main assumption of these approaches is the relationship between local climate variables and weather types is valid in future. Future regional climate pattern is derived from the comparison of produced weather types using GCM and observed weather data at a local scale (Wilby et al., 2002).

Weather typing downscaling methods can yield physically sensible linkage of global scale climate and local scale surface weather (Wilby et al., 2002). However, weather typing downscaling may not capture variations in surface climate since the schemes are often parochial (Wilby et al., 2002).

2.4.2.2. Stochastic Weather Generators

Stochastic weather generators produce synthetic time series of weather data based on the statistical characteristics of local weather. Most well-known stochastic weather generators are Richardson's weather generator (WGEN) (Richardson, 1981) and Long Ashton Research Station Weather Generation (LARG-WG) (Semenov et al., 1997). Weather generation initiates with calculating site specific weather parameters based on the statistical attributes of observed local weather variables. Daily climate scenarios are generated stochastically by using these computed parameters with outputs from a host GCM.

Weather generating approaches are particularly useful for risk analysis due to its efficient production of large ensembles (Kilsby et al., 2007). However, adjusting parameters in the process to generate future climate scenarios should be realistic and consistent since unanticipated effect can be caused when the parameters are varied (Wilby and Wigley, 1997).

2.4.2.3 Regression-based Methods

Regression models build depend on the linear or nonlinear empirical relationships between local scale predictand variables and global scale atmospheric predictor variables (Wilby et al., 2002). Similar to weather typing methods, the basic assumption of the regression-based downscaling methods is that parameters derived in the present climate will valid in future climate conditions (Wilby et al. 2004). Commonly applied regression methods are based on multivariate regression, canonical correlation analysis (CCA) (Busuioc et al., 2008) and artificial neural networks (ANNs) (Crane and Hewitson, 1998). The most popularly used tools are the Statistical Downscaling Model (SDSM) (Wilby et al., 2002) and the Automated Statistical Downscaling (ASD) (Hessami et al., 2008).

The main strength of regression-based downscaling methods is their relatively easy application and low computational demands with their use of the observable trans-scale relationships (Wilby et al., 2002). However, an application of regression-based procedures is relatively sensitive to the selection of predictor variables, mathematical transfer function or statistical fitting procedure (Wilby et al., 2002).

2.4.3 Multi-site Downscaling

Recent studies have interested in development of multi-site downscaling approaches. Multi-site downscaling methods allow downscaling weather data at multiple sites concurrently. The generated results from the popularly used single site downscaling models such as the SDSM and the ASD are unable to account the spatial dependency between stations. Ignorance of the spatial dependency in weather data is possible to affect reliability of hydrological impact studies (Wilks, 1998; Qian et al., 2002; Srikanthan and McMahon, 2001). For example, the realistic spatial distribution of precipitation in watershed is important for the accurate estimation of stream flow. Khalili et al. (2006) showed that using simulated precipitation without considering the spatial dependency in a hydrologic model may lead underestimating or overestimating the extreme streamflows for summer and autum seasons over Quebec region.

Although the needs of developing multi-site downscaling methods are often emphasized in many studies, relatively little work has been done on multi-site generation of climate data. Wilks (1998) extended a single-site WGEN stochastic weather generator model for downscaling precipitation at multiple sites simultaneously. For this extension, serially independent but spatially correlated random numbers are used to produce the spatial correlation in the synthetic time series (Wilks, 1998). Qian et al. (2002) extended the stochastic weather generator model using parameters conditioned on daily circulation patterns. Palutikof et al. (2002) also used a stochastic weather generator to simulate daily multi-site weather scenarios of future climates. The multi-site rainfall scenarios were achieved by uniform random sampling. The temperature scenarios were simulated using linear transfer functions initiated by free atmospheric variables. Charles et al. (2004) applied a stochastic weather typing approach conjunction with a Nonhomogeneous Hidden Markov Model (NHMM) for multi-site downscaling.

Regression-based multi-site SD methods have been realized by extending single-site downscaling models such as multivariate regression, artificial neural networks (ANNs) and Generalized Linear Models (GLMs). Wilby et al. (2003) extended the SDSM using conditional resampling method of Palutikof et al. (2002). Cannon (2008) used the ANN approach with the expanded Bernoulli-gamma Density Network (EBDN) for probabilistic multi-site precipitation downscaling. Generalized Linear Model (GLM)-based flamework interpreting the spatial-temporal structure to simulate multi-site rainfall sequences were used by Chandler and Wheater (2002) and Yang et al. (2005).

Harpham and Wilby (2005) compared three different regression-based multi-site downscaling models for simulating heavy daily precipitation occurrence and amounts; a Radial Basis Function (RBF) ANN, a Multi-Layer Perceptron (MLP) ANN and a Conditional Resampling Method using the SDSM. Both of the multi-site ANN procedures performed relatively poor in term of inter-site correlation compared to the SDSM resampling procedure due to the fully deterministic nature of ANN models. Buerger and Chen (2005) questioned about three regression-based methods of randomization (RND), inflation (IFN) and expanded downscaling (EDS) suggested by IPCC report. However, they found all of the models did not accurately estimate the spatial correlations between precipitation data at multiple sites.

In this study, singular value decomposition (SVD) is used to achieve multi-site downscaling. The SVD technique is computationally efficient for transforming a large matrix of correlated data into its matrix of independent components (Chaleeraktrakoon, 1995). The main advantage of the SVD technique is preserving the meaningful statistical properties (e.g., means, standard deviations, whitin-the year correlations, and inter-site cross correlations) in the generated data sequences (Cavadias, 1985 and Chaleeraktrakoon, 1995). Canvadias (1985) first used in hydrological study for multivariate stochastic simulation of river flow. Chaleeraktrakoon (1995) used the SVD technique combined with a first order autoregressive (AR) model to generate synthetic streamflows in multiple seasons and at multiple sites simultaneously. Some of these stochastic models applying SVD techniques were employed for simulating time series of weather data. Nguyen (2001) employed combination model of the first-order autoregressive model and the SVD technique to simulate rainfall at multiple sites concurrently. Besides, Khalili and Nguyen (2012) employed the SVD technique combined with the multiple regression model for multi-site downscaling of daily temperature extremes. It seems that the proposed combination methods successfully reproduce the basic statistic properties of the observed weather time series.

3 METHODOLOGY

In the first part of this chapter, the description of the observed daily extreme temperature data from a network of 25 stations in South Korea as well as the atmospheric predictors given by NCEP re-analysis data and the CGCM3 is provided. The remaining part of this chapter introduces the multi-site statistical downscaling (SD) method and the SDSM that commonly used for single-site statistical downscaling.

3.1 Data Description

The local-scale observed data over South Korea are used as predictands in the regression models of downscaling techniques. Global-scale atmospheric variables provided by the National Centers for Environmental Prediction (NCEP) are used as predictors in the regressions model.

3.1.1 Local-scale Observed Variables

The observed weather datasets archived for the long term are required to achieve reliable results from our analysis. It is however difficult to obtain consistent long-term temperature datasets over South Korea due to Japanese colonial period (1910-1945) and Korean War period (1951-1953). The longest consistent temperature data have been recorded since 1961 at only 15 stations over South Korea. The weather data from these 15 stations cannot represent the overall climate condition of South Korea since the majority of the stations are located near west and south coast; consequently, ten more stations were added. The selection is based on homogeneity of data, the archived period and station density. Therefore, our study uses daily maximum temperature (Tmax) and daily minimum temperature (Tmin) at 25 stations over South Korea. Figure 3.1 shows the specific locations of these selected 25 weather stations. More detailed information of the selected weather stations is described in Appendix A.

Generally, the long-term climate datasets are often inhomogeneous due to site relocations, replacement of measurements, urbanization, alteration in observing procedures and missing data (Vincent, 1997). Choi et al. (2003) tested homogeneity of Korean temperature time series data at 16 stations for the period from 1968 to 1999 using the median rank-score method. Their results show that no datasets retain distinct inhomogeneity problem. In this study, break points of temperature time series are observed for the period of 1973-2009. The evidences of inhomogeneity are not found in any temperature data series at all 25 stations.

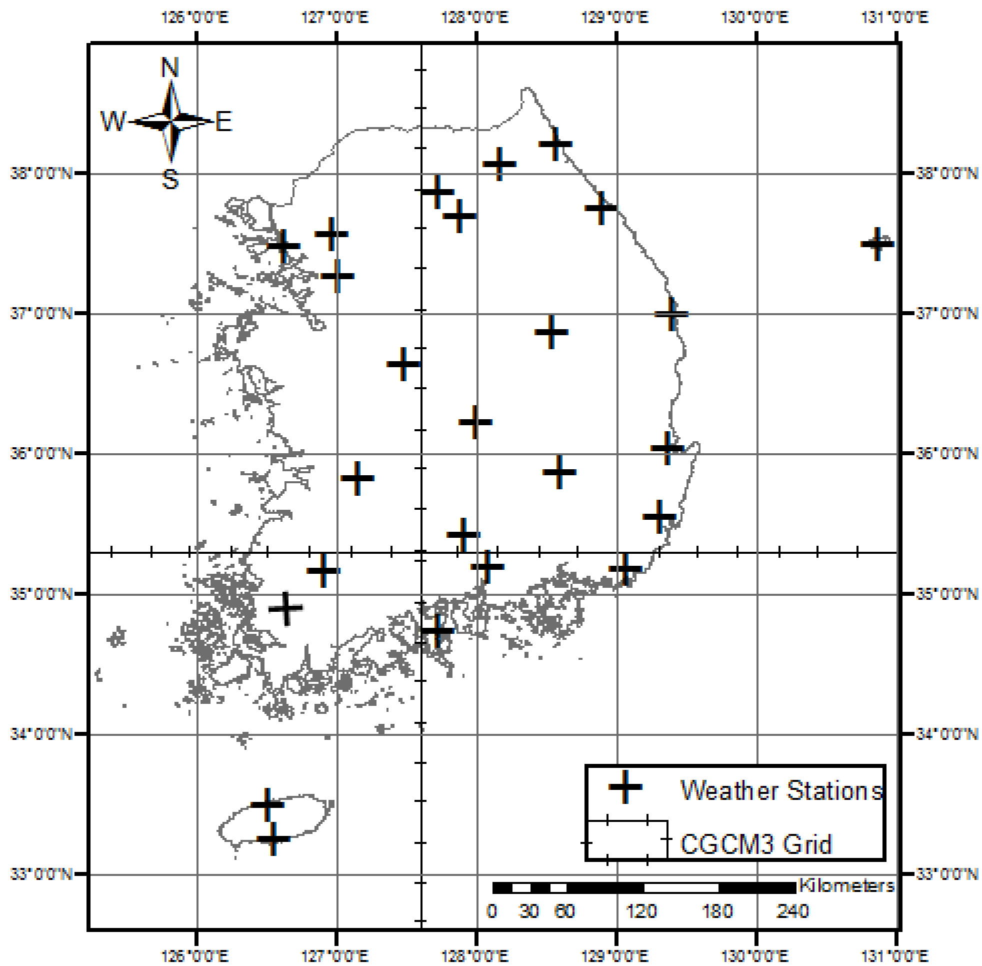

Figure 3.1 Location of 25 weather stations in study area and CGCM3 grid (3.75 º longitude × 3.75 ºlatitude)

The temperature datasets are provided by Korea Meteorological Administration (KMA). Most of stations have no missing data while Seoguipo has 12 missing data for both of Tmax and Tmin, and Hongcheon has one missing data for Tmax.

3.1.2 Global-scale Climatic Variables

Global-scale atmospheric variables are describing atmospheric circulation, thickness, stability and moisture over the area. The variables are produced from the National Centers for Environmental Prediction (NCEP), the National Centers for Atmospheric Research (NCAR) or the European Center for Medium-range Weather Forecasts (ECMWF) re-analysis (Kalnay et al., 1996). Some of them are secondary variables derived from re-analysis data (e.g. daily vorticity is derived from mean sea level pressure) (Wilby et al., 2002). Table 3.1 defines daily NCEP atmospheric variables.

Variable	Description	Variable	Description
mslp	Mean sea leve pressure	p__f	Surface geostrophic airflow velocity
p5_f	Geostrophic airflow velocity at 500 hPa	p__u	Surface horizontal wind
p5_u	Horizontal wind at 500 hPa	p__v	Surface zonal wind
p5_v	Zonal wind at 500 hPa	p__z	Surface vorticity
p5_z	Vorticity at 500 hPa	p_zh	Surface divergence
p5zh	Divergence at 500 hPa	p_th	Surface wind direction
p5th	Wind direction at 500 hPa	p500	Geopotential height at 500 hPa
p8_f	Geostrophic airflow velocity at 850 hPa	p850	Geopotential height at 850 hPa
p8_u	Horizontal wind at 850 hPa	s500	Specific humidity at 500 hPa
p8_v	Zonal wind at 850 hPa	s850	Specific humidity at 850 hPa
p8_z	Vorticity at 850 hPa	shum	Near surface specific humiditiy
p8zh	Divergence at 850 hPa	temp	2m air temperature
p8th	Wind direction at 850 hPa		

Table 3.1 Atmospheric NCEP predictor variables for downscaling procedure

Variables of the NCEP re-analysis and the GCM outputs require re-gridding and standardization. Re-gridding is needed because the grid spacing of observed or re-analysis climate datasets do not always correspond onto the grids of GCMs (Wilby et al., 2004). In this study, NCEP/NCAR variables have been interpolated onto the Guassian grids (3.75 º longitude × 3.75 ºlatitude) of the third version of the Canadian Global Climate Model

(CGCM3). Guassian grids of CGCM3 over South Korea region are described on Figure 3.1. Both NCEP re-analysed and GCM-derived predictor variables have been standardized using means and standard deviations for the baseline period 1961-1990 to avoid systematic biases contained within variables.

3.2 Downscaling Techniques

In this study, the SDSM is selected as representative of single-site statistical downscaling approach. The SDSM has been identified as one of leading single-site statistical downscaling tools. The examined Multi-site SD method is the combination of the multiple regression model and the SVD technique. Figures 3.2 and 3.3 schematically illustrate the downscaling procedure of the SDSM and the multi-site SD method respectively with description of required data.

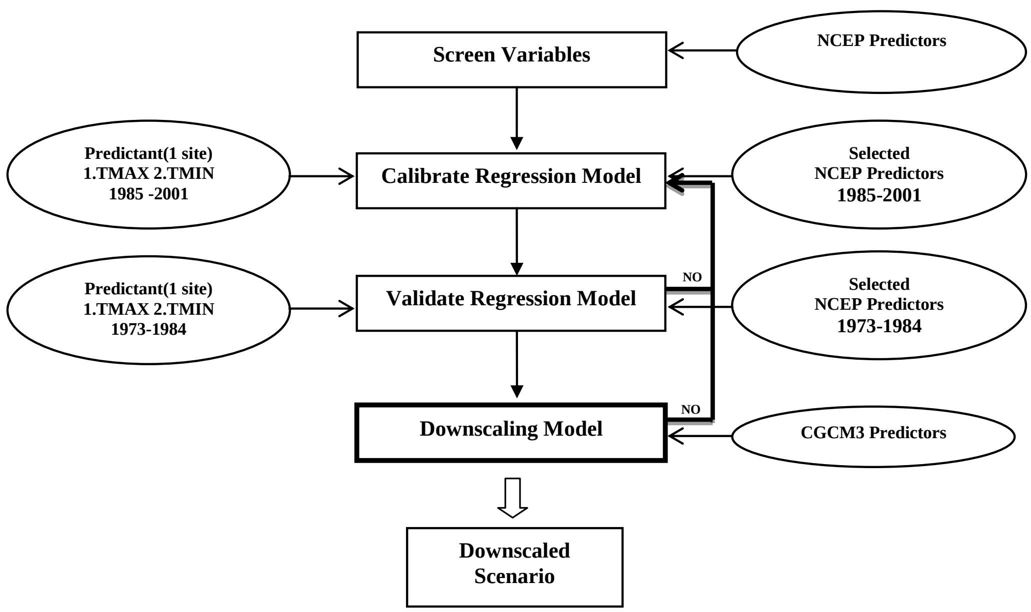

Figure 3.2 Schematic diagram of the SDSM

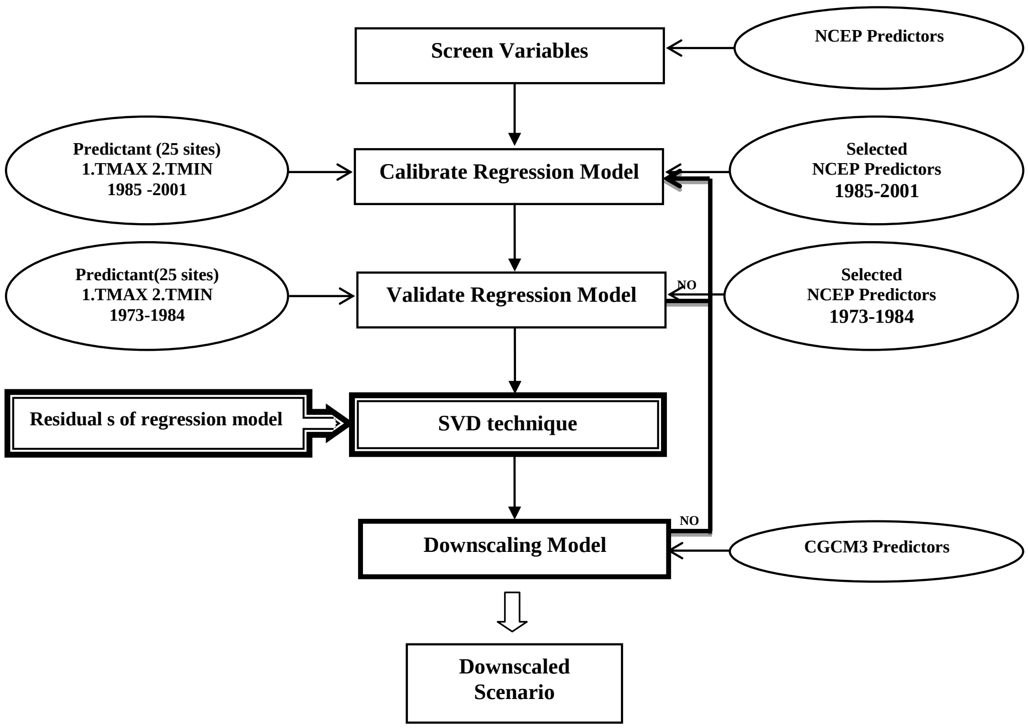

Figure 3.3 Schematic diagram of the multi-site SD method

.

Downscaling procedures of the SDSM and the multi-site SD method are similarly divided into the following steps; screen variables, develop the regression models and generate the downscaled future scenarios.

The regression model is consisted of the deterministic and stochastic components. The deterministic components of the regression models of the SDSM and the multi-site SD method are exactly same. Yet, the procedures of two methods to simulate stochastic components are different. The SDSM directly generates the stochastic components while the multi-site SD method uses the SVD technique to simulate them at multiple sites simultaneously. More detailed mechanism of the SDSM and the multi-site SD method is explained in the following sub-sections.

3.2.1 Screen Variables

This stage is the most challenging for users to develop a downscaling model since the selected variables determine the characteristic of downscaled climate scenario (Wilby et al., 2002). Thus, a user needs to select appropriate global-scale atmospheric predictors being significantly related to a local-scale observation.

The SDSM has its own screen variable system based on the partial explained variance and the correlation analysis. The screening procedure of the SDSM is tricky for a user because it requires statistically judicious concern. This difficulty can be avoided through using methods that select significant variables automatically. Wilby et al. (2002) suggested using offline partial correlation or step-wise regression analyses in their study.

Therefore, this study applied two different methods to determine the most appropriate set of predictors automatically: (a) stepwise regression with backward selection; (b) Variable Importance in the Projection (VIP) scores obtained from Partial Least Square (PLS) regression (called the PLS-VIP method).

Backward stepwise regression initiates with all independent variables and removes the least significant variable sequentially from a full model. Most commonly used criterion to eliminate an insignificant variable from the regression model is based on partial F-test. Partial F-statistics with degrees of freedom 1 and $n-p-1$ is determined as follows:

$$F = \frac{\left({R_P}^2 - {R_{P-1}}^2\right)(n-p-1\ \ )}{(1-{R_P}^2)} \tag{3.1}$$

where ${R_P}^2$ and ${R_{P-1}}^2$ are the coefficients of determination of more complex model with p explanatory variables and less complex model with $p-1$ variables respectively, n is the number of observations, and p is the number of predictors.

PLS regression is frequently used to analyze data with strongly collinear, noisy and numerous predictor variables. VIP scores obtained by PLS regression are used to select the most influential variables. In common, a predictor variable that has VIP score above 1 is considered as an important variable (Wold et al., 2001). The VIP score for the j-th X predictor variable can be calculated as follows:

$$\mathrm{VIP}_j = \sqrt{\frac{p}{R_d(y; t_1, \ldots, t_h)} \sum_{c=1}^{h} R_d(y; t_c) {w_{cj}}^2} \tag{3.2}$$

where R_d is defined as the mean of squares of the correlation coefficients (R), p is the number of predictors and y is a response variable, t_c, w_c ($c = 1, 2, 3 \ldots h$) respectively stand for the c-th column vector of a score matrix, T and a weight matrix, W of the predictor variable matrix, X. These matrices are obtained from PLS regression where h is the number of latent variables. More detailed methodology of PLS regression and VIP score can be referred in Chong et al. (2005).

Among two methods, the method performs better to select significant predictors will be employed for the variable selection. Performances of the methods are evaluated by the predictive accuracy of regression models using the predictors selected by the stepwise method and the PLS-VIP method respectively.

3.2.2 Develop Regression Models

Synthetic temperature extremes are computed by adding the simulated stochastic components to the deterministic components. As indicated above, the deterministic components of the SDSM and the multi-site SD method are exactly same. Both of the methods use the same predictors to calibrate the regression models. For stochastic components, the SDSM directly simulates the residual matrix with single column or row while the multi-site SD method requires using the SVD technique for multi-site simulating of the squared residual matrix with multiple columns and rows.

3.2.2.1 SDSM

The following expression is the regression model of the SDSM for calibrating Tmax, and the similar equation is applied for Tmin as well:

$$Tmax_{i,m} = \sum_{k=1}^{p} \alpha_{k,m} A_{ki,m} + \cdots + E_{Tmax_{i,m}} \tag{3.3}$$

where $Tmax_{i,m}$is the Tmax on day i, $\alpha_{k,m}$ is the k-th regression parameter for month m estimated from linear least squares regression, $A_{ki,m}$ (k = 1, 2, 3, ... , p) is the k-th significant predictor on day i in month m where p is the number of predictors, and E_{Tmax_i} is the model residual value on day i in month m.

The weather generation of the SDSM is based on the Monte Carlos simulation. The residuals are stochastically generated using pseudo random numbers following a normal distribution with standard deviation equal to the standard error of the regression model. The daily weather is computed by adding the simulated stochastic component (residual) to the deterministic component on each day at each station.

The generation procedure is repeated several times to simulate ensembles of synthetic weather series. Each synthesized ensemble is considered as an equally plausible local downscaled climate scenarios. The calibrated regression models are verified through synthesizing daily time series of weather data for the validation period that are not used for the calibration.

3.2.2.2 Multi-site SD method

The Multi-site SD method proposed in this study is the combination of a regression model and the SVD technique.

3.2.2.2.1 Multi-site Multivariate Regression Model

The multi-site multivariate regression model for the multi-site SD method is similarly calibrated as the regression model of the SDSM. The model for Tmax is expressed as follows:

$$\begin{pmatrix} Tmax_{i,m,1} \\ Tmax_{i,m,2} \\ . \\ . \\ Tmax_{i,m,n} \end{pmatrix} = \begin{pmatrix} \alpha_{Tmax_{0,m,1}} \\ \alpha_{Tmax_{0,m,2}} \\ . \\ . \\ \alpha_{Tmax_{0,m,n}} \end{pmatrix} + \begin{pmatrix} \sum_{k=1}^{p} \alpha_{Tmax_{k,m,1}} A_{Tmax_{ki,m,1}} \\ \sum_{k=1}^{p} \alpha_{Tmax_{k,m,2}} A_{Tmax_{ki,m,2}} \\ . \\ . \\ \sum_{k=1}^{p} \alpha_{Tmax_{k,m,n}} A_{Tmax_{ki,m,n}} \end{pmatrix} + \begin{pmatrix} E_{Tmax_{i,m,1}} \\ E_{Tmax_{i,m,2}} \\ . \\ . \\ E_{Tmax_{i,m,n}} \end{pmatrix} \qquad (3.4)$$

where $Tmax_{i,m,s}$ (s = 1, 2, 3, ... , n) is the Tmax on day i in month m at station s and n is the number of stations, $A_{Tmax_{ki,m,s}}$ (k = 1, 2, 3, ... , p) is the k -th significant predictor where p is the number of predictors, $\alpha_{Tmax_{k,m,n}}$ is the k-th regression parameter for month m at station s, and $E_{Tmax_{i,m,s}}$is the residual value on day i in month m at station s.

The obtained matrix of residual values E_{Tmax} from the multiple regression model will be used in following steps to simulate the synthetic residual matrix $\hat{E}$. The regression model for Tmax above is similarly applied for Tmin.

3.3.2.2.2 Singular Value Decomposition (SVD) Technique

Singular value decomposition (SVD) is a useful statistical technique to decompose a large and complex matrix into simpler matrices with preserving meaningful statistical properties of original matrix. Due to its advantages, the SVD technique has been popularly used for many study areas dealing multivariate data such as signal procession, image compression and weather prediction. Moreover, SVD is intimately related to the basis of the widespread statistical decomposition methods such as eigenvector decomposition, principal components analysis (PCA) and non-negative matrix factorization (NNMF).

Theologically, the idea of SVD is from an extension of the eigenvalue-eigenvector decomposition which is limited to decomposing symmetric squared matrices into two simpler matrices. Unlike eigen-decomposition, the SVD technique (Golun and Reinsch, 1970) provides a decomposition of any rectangular $m \times n$ matrices into three matrices: two orthogonal matrices and one diagonal matrix. Suppose A is an $m \times n$ rectangular matrix and it is expressed as:

$$A = SDV^T \tag{3.5}$$

$D = diag(\sigma_1, \sigma_2, \sigma_3, \dots, \sigma_r)$ satisfies $\sigma_1 \geq \sigma_2 \geq \sigma_3 \geq \cdots \geq \sigma_r$

where S is an $m \times m$ orthogonal matrix whose columns called the left singular vectors are the eigenvectors of AA^T, V is an $n \times n$ orthogonal matrix whose columns called the right singular vectors are the eigenvectors of A^TA, and D is an $m \times n$ diagonal matrix of non-zero ordered singular values of A. The non-zero singular values of A are the square roots of the non-zero eigenvalues of AA^T or A^TA. In present study, the SVD technique is used to simulate stochastic components of the multiple regression model. The following SVD procedure is applied on the residual matrix E.

First of all, an $m \times n$ data matrix, X is standardized by subtracting means of columns and dividing by their standard deviations to overcome different scales of residuals at different stations. The $m \times n$ standardized data matrix X_s is computed as:

$$X_{sij} = \frac{X_{ij} - \bar{X}_j}{S_j} \tag{3.6}$$

where X_{ij} is the value of X at i^{th} row and j^{th} column. $\bar{X}_{ij}$ and S_j are the mean and the standard deviation of the j^{th} column respectively.

Secondly, the SVD technique is applied to decompose the correlation matrix of X_s. Depends on the sizes of column and row of X_s, two different correlation matrices of the

$n \times n$ matrix, P and the $m \times m$ matrix, R can be computed. The correlation matrices P and R are expressed as follows:

$$P = \frac{1}{m-1} \times {X_s}^T \times X_s \tag{3.7}$$

$$R = \frac{1}{m-1} \times X_s \times {X_s}^T \tag{3.8}$$

Whichever the correlation matrix whose size is smaller is used for the next step. The SVD technique is applied to decompose the smaller correlation matrix.

If the correlation matrix P is smaller, the decomposition can be obtained as follows:

$$P = V_P \times D_P \times {V_P}^T \tag{3.9}$$

where $V_P$is the $n \times n$ matrix of the eigenvectors of P, and D_P is the $n \times n$ matrix of the singular values of P. The important notice is that only the r non-zero singular values of P in descending order are diagonal elements of D_P. r is rank of X_s and it is at least one and at most min(*m*,*n*). Thus, D_P is the $r \times r$ diagonal matrix of r ordered non-zero singular values of , and V_P is the $n \times r$ matrix of the corresponding *r* eigenvectors of P.

The principal components of X_s is computed as follows:

$$Z = X_s \times V_P \times D_P^{-\frac{1}{2}} \tag{3.10}$$

where Z is the $m \times r$ matrix of the r standardized principal components of X_s. The large number of possibly correlated observed variables (columns of X_s) transforms in to the small number of uncorrelated variables(columns of Z). The principal components (Columns of Z) are very closed to normal distribution because they are linear combinations of original variables (Columns of X_s).

The matrix Z is consisting of the orthogonal columns, which means that:

$$\frac{1}{m-1} Z^T Z = I_r \tag{3.11}$$

in which $I_r$is the identity matrix of order *r*.

Therefore, this property allows that the columns (principal components) of the $m \times r$ synthetic matrix $\hat{Z}$ can be generated independently following a standard normal distribution with zero mean and unit variance.

If the correlation matrix P is selected, V_P and D_P are simply obtained from the equation (3.9); however, for the correlation matrix R, an intermediate equation to calculate V_P is required such as:

$$V_P = \frac{1}{\sqrt{m-1}} \times {X_s}^T \times V_R \times {D_R}^{-\frac{1}{2}} \tag{3.12}$$

where D_R is the $r \times r$ diagonal matrix of R, and V_R is the $m \times r$ matrix of the eigenvectors of R. They are obtained by applying the equation (3.9) to R instead of P.

The correlation matrices P and R have the very similar diagonal matrices D_R and D_P respectively. Therefore, there is no need of intermediate equation to compute D_P .

If R is selected as the correlation matrix, the $m \times r$ matrix Z of the standardized principal components of X_s is computed as:

$$Z = \sqrt{m-1} \times V_R \tag{3.13}$$

Thirdly, the simulation of the synthetic standardized matrix $\hat{X}_s$ using the simulated matrix of principal components $\hat{Z}$ is based on the SVD theorem such as:

$$\hat{X}_s = \hat{Z} \times {V_P}^T \times {D_P}^{\frac{1}{2}} \tag{3.14}$$

The simulated $\hat{Z}$ is not perfectly orthogonal due to sampling variation. However, perfectly orthogonal $m \times r$ matrix $\hat{Z}_o$ is required for the equation (3.14). To obtain $\hat{Z}_o$, the SVD procedure above is applied to $\hat{Z}$: firstly, the $m \times r$ standardized matrix $\hat{Z}_s$ of $\hat{Z}$ is computed using equation (3.6); secondly, the $r \times r$ correlation matrix Q of $\hat{Z}_s$ is obtained from equation (3.7); thirdly, Q is decomposed into the $r \times r$ matrix V_Q of the eigenvectors of Q and the $r \times r$ diagonal matrix D_Q of the singular values of Q using equation (3.9), and finally, the $m \times r$ perfectly orthogonal matrix $\hat{Z}_o$ of standardized principal components of $\hat{Z}$ is computed from equation (3.10).

Finally, the non-standardized simulated matrix $\hat{X}$ is obtained as follows:

$$\hat{X}_{ij} = \hat{X}_{sij} \times S_j + \bar{X}_j \tag{3.15}$$

As mentioned above, the SVD technique has an advantage to preserve the statistical properties of the original data in the simulated sequences. The following demonstration shows that the correlation matrix $\hat{P}$ of the simulated standardized matrix $\hat{X}_s$ is similar to the correlation matrix P of the standardized data matrix X_s .

$$\begin{aligned}
\hat{P} &= \frac{1}{m-1} \times {X_s}^T \times X_s \\
&= \frac{1}{m-1} \times V_P \times D_P^{\frac{1}{2}} \times {\hat{Z}_o}^T \times \hat{Z}_o \times D_P^{\frac{1}{2}} \times {V_P}^T \\
&= \frac{1}{m-1} \times V_P \times D_P^{\frac{1}{2}} \times (m-1) \times I_r \times D_P^{\frac{1}{2}} \times {V_P}^T \\
&= V_P \times D_P \times {V_P}^T \\
&= P
\end{aligned} \tag{3.16}$$

Additionally, instead of using the $m \times r$ matrix of $\hat{Z}$ following a standard normal distribution to generate, first-order autoregressive model is fitted to columns of the matrix Z. The first-order autoregressive model (AR(1)) for $\hat{Z}$ is defined as (Haan, 1977):

$$\hat{Z}_{i,j} = \phi_1 Z_{i-1,j} + E_{Zij} \tag{3.17}$$

in which $\hat{Z}_{i,j}$is the value of $\hat{Z}$ at i^{th} row and j^{th} column, E_{Zij} is the value at i^{th} row and j^{th} column of the residual matrix of the AR(1) model, E_Z having zero mean and variance σ^2, and $\phi_1$is the parameter of the AR(1) model. $\phi_1$and σ^2can be estimated as:

$$\phi_1 = \rho_1 \tag{3.18}$$

$$\sigma^2 = 1 - {\phi_1}^2 \tag{3.19}$$

where $\rho_1$is the lag-one autocorrelation coefficient of the j^{th} column of the matrix Z.

In this study, AR(1) model was not applied for generating stochastic components.

The synthetic weather series are obtained by adding simulated residual matrix $\hat{E}$ to the deterministic part obtained from the regression model on each day at multiple stations. Similar to the SDSM, the ensembles of synthetic weather series are generated by repeating the generation procedure. The calibrated regression model is verified by using temperature extreme data for the validation period.

3.2.3 Generate Future Scenarios

For generating the daily time-series of future weather, atmospheric predictor variables of the reanalysis are replaced into predictor variables of the GCMs.

One thing to check for the future generation is that the length of year and month of GCM data are different. For instance, the HadCM3 developed by the Hadley centre has year length of 360 days and 30days per a month whereas the CGCM3 developed by Canadian centre for climate modelling and analysis (CCCma) has 365 days in each year with ignorance of leap days.

As mentioned in literature review, there are mainly 4 different types of the future emission scenarios (A1, A2, B1 and B2). In our study, prediction of the future temperature extremes is based on the scenarios of A1B and A2 provided from the CGCM3.

3.3 Statistical Measures for Numerical Evaluation

The graphical and numerical measures were used to evaluate the predictive ability of the models statistically. Graphical measures are beneficial to display easily the entire relationships between the model and the data at once whereas numerical measures are suitable to focus on a particular aspect of the data.

For numerical evaluation of the goodness of model, the following statistical measures such as the coefficient of determination (R^2) and the Root Mean Square Error (RMSE) were employed:

$$R^2 = 1 - \frac{\sum_{i=1}^{t} (\hat{y}_i - y_i)^2}{\sum_{i=1}^{t} (y_i - \bar{y})^2} \tag{3.20}$$

$$RMSE = \sqrt{\frac{1}{t}\sum_{i=1}^{t}(\hat{y}_i - y_i)^2} \tag{3.21}$$

where t is the length of the time series, $\hat{y}_i$ is the daily simulated temperature, y_i is the daily observed temperature, and $\bar{y}$ is the mean of the daily observed temperature on day i. R^2 is ranged between 0 to 1, and a value closer to 1 representing the better performance of the model. RMSE is also ranged between 0 and 1, and a value closer to 0 indicating the better performance of the model.

4 ANALYSES OF TEMPERATURE EXTREMES

This chapter provides a detailed statistical analysis of the temperature variability over South Korea by computing 18 different temperature indices using data at 25 stations during the period 1973-2009.

4.1 Indices and Computational Methodology

In the present study, a total of 18 different temperature indices are used to investigate change in the statistical characteristics of temperature extremes over South Korea. The indices are selected from the indicators recommended by the Canadian Climate Change Scenarios Network (CCCSN) and the Expert Team on Climate Change Detection and Indices (ETCCDI). More detailed information of extreme indices is available on CCCSN (http://cccsn.ca/) and ETCCDI (http://cccma.seos.uvic.ca/ETCCDI/) websites. The selected indices are described in Table 4.1.

The analysis uses daily temperature extremes at 25 stations over South Korea. Twenty five stations are selected according to homogeneity of data, the archived period and station density. The complete records of temperature data at 25 stations are available from 1961 to 2009.

A linear trend analysis is performed for all 18 indices. The slope is computed using the least squares fitting. The statistical significances of the trends in these indices are evaluated by the non-parametric Mann-Kendall trend test (Mann, 1945; Kendall, 1975). This test is widely used to detect the significance of the trends in time series data since it is simple and robust, and easily dealing with missing values (Im et al. 2011). Moreover, the non-parametric statistical tests are more feasible for non-normally distributed data series compared to parametric statistical tests.

Code	Unit	Description
TmaxMean	℃	Annual Mean of daily Tmax
TminMean	℃	Annual Mean of daily Tmin
TmoyMean	℃	Annual Mean of daily Tmean
TmaxSD	℃	Annual Standard deviation of daily Tmax
TminSD	℃	Annual Standard deviation of daily Tmin
TmoySD	℃	Annual Standard deviation of daily Tmean
Tmax90p	℃	Annual 90th percentile of daily Tmax
Tmin10p	℃	Annual 10th percentile of daily Tmin
FD	days	Frost Days: Annual count when Tmin < 0 ℃
SU25	days	Summer Days: Annual count when Tmax > 25 ℃
ID	days	Ice Days: Annual count when Tmax < 0 ℃
TR20	days	Tropical Nights: Annual count when Tmin > 20 ℃
FSL	days	Frost season length: Tmean < 0 ℃ more than 5 days and Tmean > 0 ℃ more than 5days
GSL	days	Growing season length: Tmean > 5 ℃ more than 5 days and Tmean < 5 ℃ more than 5days
FrTh	days	Days with freeze and thaw cycle(Tmax > 0 ℃ and Tmin < 0 ℃)
DTR	℃	Mean of diurnal temperature range
WSDI	days	Warm spell duration indicator: Annual count of days with at least 6 consecutive days when Tmax > 90th percentile
CSDI	days	Cold spell duration indicator: Annual count of days with at least 6 consecutive days when Tmin < 10th percentile

Table 4.1 Temperature indices and description

The Mann-Kendall trend test depends on the ranks of a time series and their time order, rather than their actual values. The null hypothesis H_0 is that there is no trend in the time series. For a time series$X = \{X_1, X_2 \dots X_n\}$, the Kendall score S is computed using following the equations.

$$S = \sum_{i=1}^{n-1} \sum_{j=i+1}^{n} sgn(X_j - X_i) \tag{4.1}$$

$$sgn(X_j - X_i) = \begin{cases} +1 & \quad X_j - X_i > 0 \\ 0 & if \quad X_j - X_i = 0 \\ -1 & \quad X_j - X_i < 0 \end{cases} \tag{4.2}$$

where X_i and X_j are the sequential data values on day i and j respectively ($j > i$), and n is the dataset record length.

If n ≥8, Mann (1945) and Kendall (1975) documented that S is approximately normally distributed under H_0 with zero mean and variance as follows:

$$Var(S) = \frac{1}{18}\, n(n-1)(2n+5) - \frac{1}{18}\sum_{i=1}^{m} t_i\,(t_i - 1)(2t_i + 5) \tag{4.3}$$

where m is the number of tied groups and t_i is the number of data values in the i^{th} group. If there are no ties in ranking, the last term of the equation (4.3) is 0. The Mann-Kendall trend test statistics Z is estimated as:

$$Z = \begin{cases} \dfrac{S-1}{\sqrt{Var(s)}} & \quad S > 0 \\ 0 & if \quad S = 0 \\ \dfrac{S+1}{\sqrt{Var(s)}} & \quad S < 0 \end{cases} \tag{4.4}$$

The statistically significant trend is evaluated using the Z value. H_0 is rejected if $|Z| > Z_{1-\alpha/2}$ where $Z_{1-\alpha/2}$ is the $1 - \alpha/2$ quantile of the standard normal distribution and α is the significance level.

4.2 Computation of Temperature Indices for Seoul Station

The temporal variation of temperature extremes indices for Seoul station is shown in Figure 4.1 to 4.4. The Seoul station is located in the Northwest of South Korea at latitude 37°34′N and longitude 126°58′E.

Figure 4.1 shows the temporal variation of annual means of daily Tmax (TmaxMean), daily Tmin (TminMean), daily Tmean (TmoyMean) and annual standard deviations (SDs) of daily Tmax (TmaxSD) at Seoul station during the period 1973-2009. The solid red lines indicate the trend lines, and the equations of the trend lines are given in the top of each diagram. The negative trends in TmaxMean (0.02 ℃ per year), TminMean (0.05 ℃ per year) and TmoyMean (0.04 ℃ per year) are detected. As mentioned above, the Mann-Kendall test is applied to assess the statistical significance of those trends. The negative trends in TmaxMean, TminMean and TmoyMean are significant at the 95% confidence level corresponds to α=0.05 since the all p values for TmaxMean (1.79E-02), TminMean (9.30E-06) and TmoyMean (2.63E-04) are less than α.

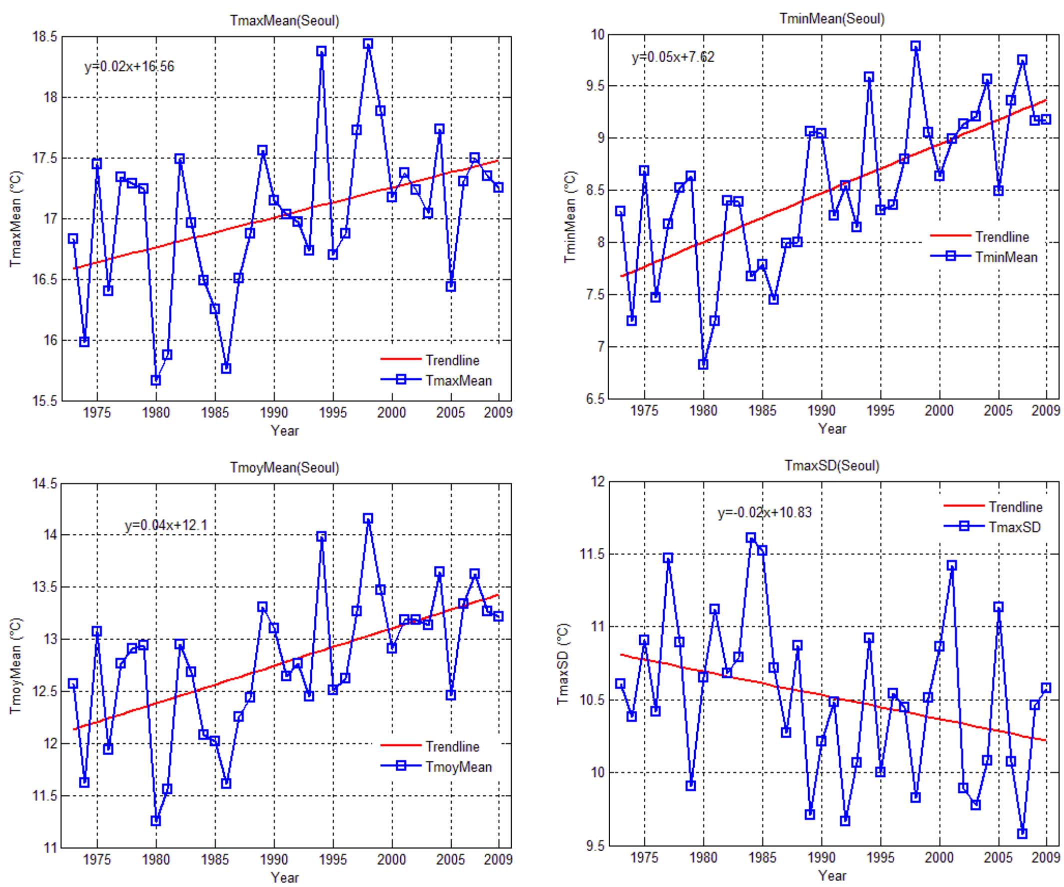

Figure 4.1 Trends in TmaxMean (upper left), TminMean (upper right), TmoyMean (lower left), and TmaxSD (lower right) for Seoul station during the period 1973-2009

The temporal variations of annual SDs of daily Tmin (TminSD) and daily Tmean (TmoySD), and annual 90th percentiles of daily Tmax (Tmax90p) and annual 10th percentiles of daily Tmin (Tmin10p) at Seoul station for the period 1973-2009 are displayed in Figure 4.2. The trends for TmaxSD (-0.02 ℃ per year), TminSD (-0.02 ℃ per year) and TmoySD (-0.02 ℃ per year) are negative. Although the slope coefficients are similar, only the decreasing trend in TminSD is significant at the 95% confidence level according to the Mann-Kendall test. The trend line of annual Tmax90p (0.01 ℃ per year) increases slightly while the trend line of annual Tmin10p (0.07 ℃ per year) increase noticeably during the period 1973 to 2009. On the basis of the Mann-Kendall test, only the increasing trend in annual Tmin10p is significant at the 95% confidence level.

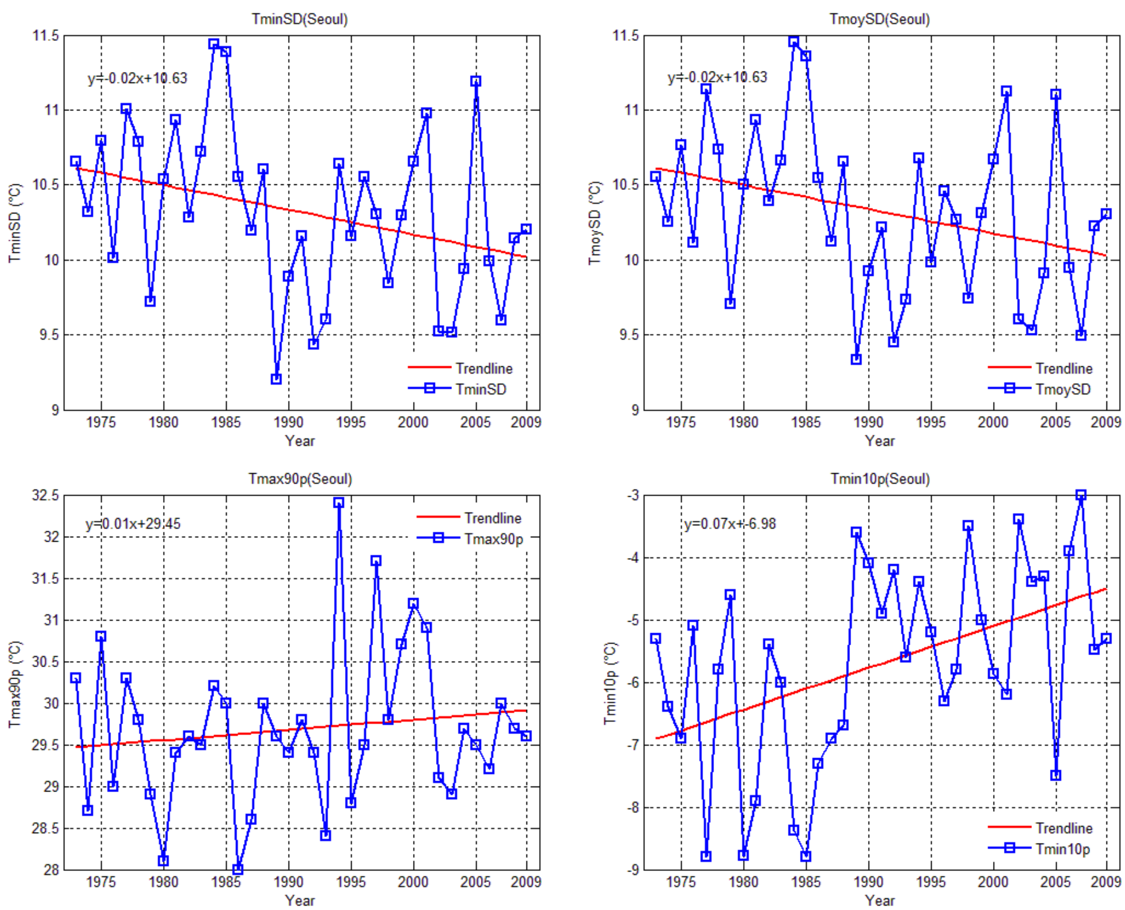

Figure 4.2 Trends in TminSD (upper left), TmoySD (upper right), and annual Tmax90p (lower left) and annual Tmin10p (lower right) for Seoul station during the period1973-2009

The temporal variations of frost days (FD), summer days (SD25), ice days (IC), tropical nights (TR20), frost season length (FSL) and growing season length (GSL) at Seoul station during the period 1973-2009 are shown in Figure 4.3.

In this study, FD is defined as annual counting of days with daily Tmin below 0 ℃. The significant decreasing trend in FD (-0.55 days per year) is observed at the 95% confidence level according to the Mann-Kendall test. SU25 is delineated as annual counting of days with daily Tmax above 25 ℃. The trend in SU25 (0.17 days per year) is positive during 1973 to 2009; however this trend is not significant at the 95 % confidence level. ID is determined as annual counting of days with daily Tmax below 0 ℃. The decreasing trend in ID (-0.3 days per year) is significant at the 95% confidence level. TR20 is defined as annual counting of days with daily Tmin above 25 ℃. The significant positive trend in TR20 (0.41 days per year) is noticed at the 95% confidence level.

Furthermore, FSL and GSL can be outlined as follows: Frost season begins when there are more than five consecutive days with daily Tmean below 0 ℃ and ends when there are more than five consecutive days with daily Tmean above 0 ℃; Growing season begins when there are more than five consecutive days with daily Tmean above 5 ℃ and ends when there are more than five consecutive days with daily Tmean below 5 ℃. The trend in FSL is negative and the trend in GSL is positive. Based on the Mann-Kendall test, both of the trends in FSL (-0.45 days per year) and GSL (0.56 days per year) are not significant at the 95% confidence level.

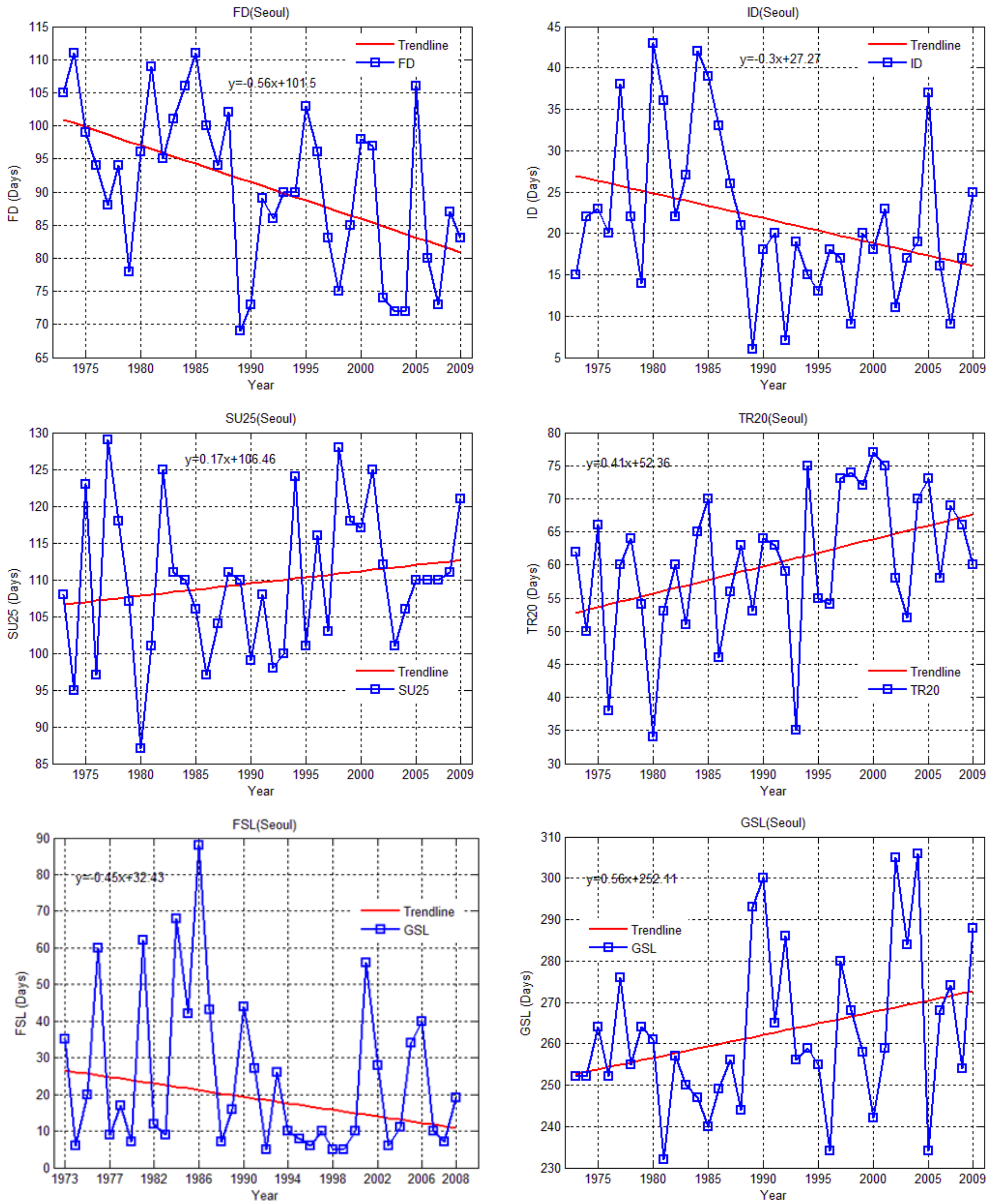

Figure 4.3 Trends in FD (top left), SU25 (top right), ID (middle left), TR20 (middle right), FSL (bottom left) and GSL (bottom right) for Seoul station during the period 1973-2009

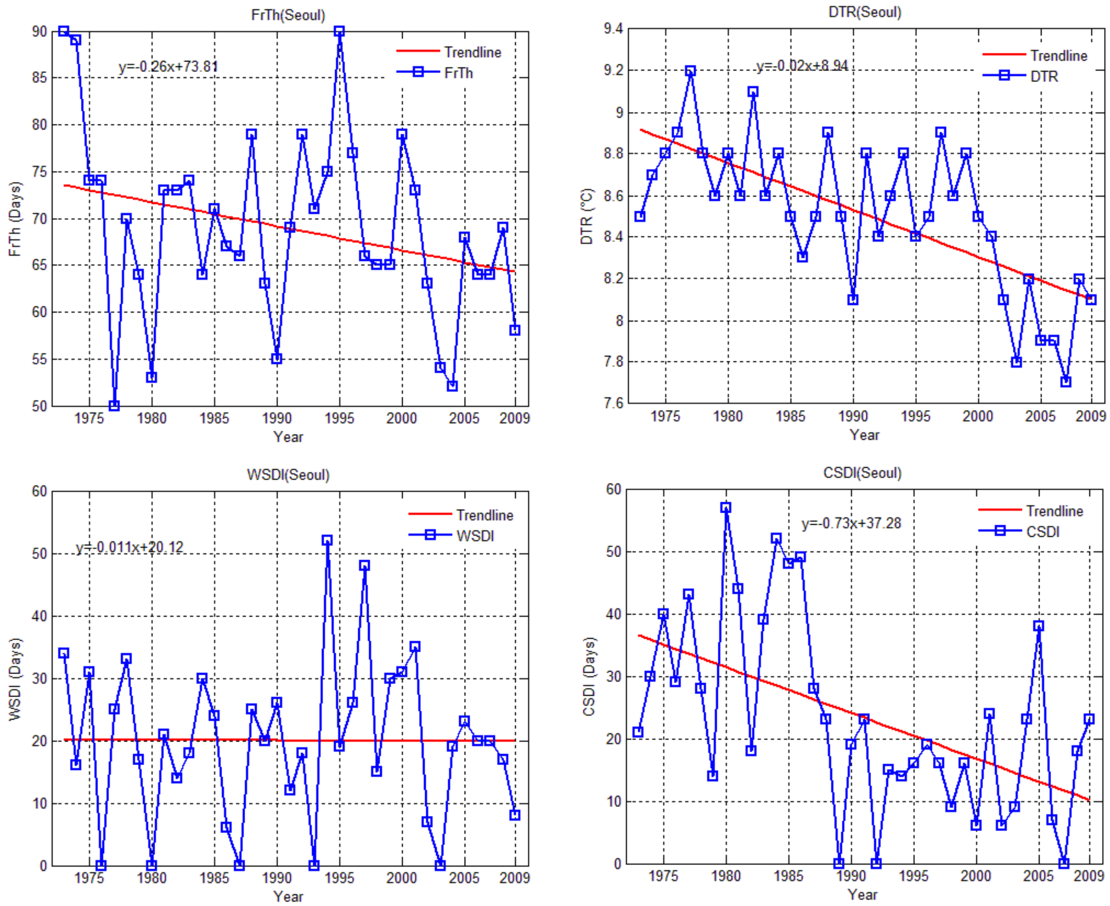

Figure 4.4 Trends in FrTh (upper left), annual means of DTR (upper right), WSDI (lower left) and CSDI (lower right) for Seoul station during the period 1973-2009

Figure 4.4 shows the temporal variations of freeze and thaw cycle (FrTh), annual means of diurnal temperature range (DTR), warm spell duration indicator (WSDI) and cold spell duration indicator (CSDI) during the period 1973-2009. The definition of FrTh is annual counting of days with freeze and thaw cycle (Tmax>0 ℃ and Tmin<0 ℃). DTR is computed by subtracting Tmin from Tmax. Both of FrTh (-0.26 days per year) and DTR (-0.02 ℃ per year) have the decreasing trends. Only the trend for DTR is significant at the 95% confidence level based on the Mann-Kendall test. WSDI is decided by annual counting of days with at least 6 consecutive days when Tmax exceeds 90^{th} percentile of the climatology (1973-2009). Similarly, CSDI is obtained by annual counting of days with a least 6 consecutive days when Tmin below 10^{th} percentile of the climatology. The negative trends are observed for WSDI (-0.01 days per year) and CSDI (-0.75 days per year). Only the trend for CSDI is statistically significant.

4.3 Computation of Temperature Indices for 25 Stations South Korea

In order to analyze temperature indices over South Korea, time series of temperature extreme at 25 stations are used. The results of the trend analysis are illustrated in the following maps.

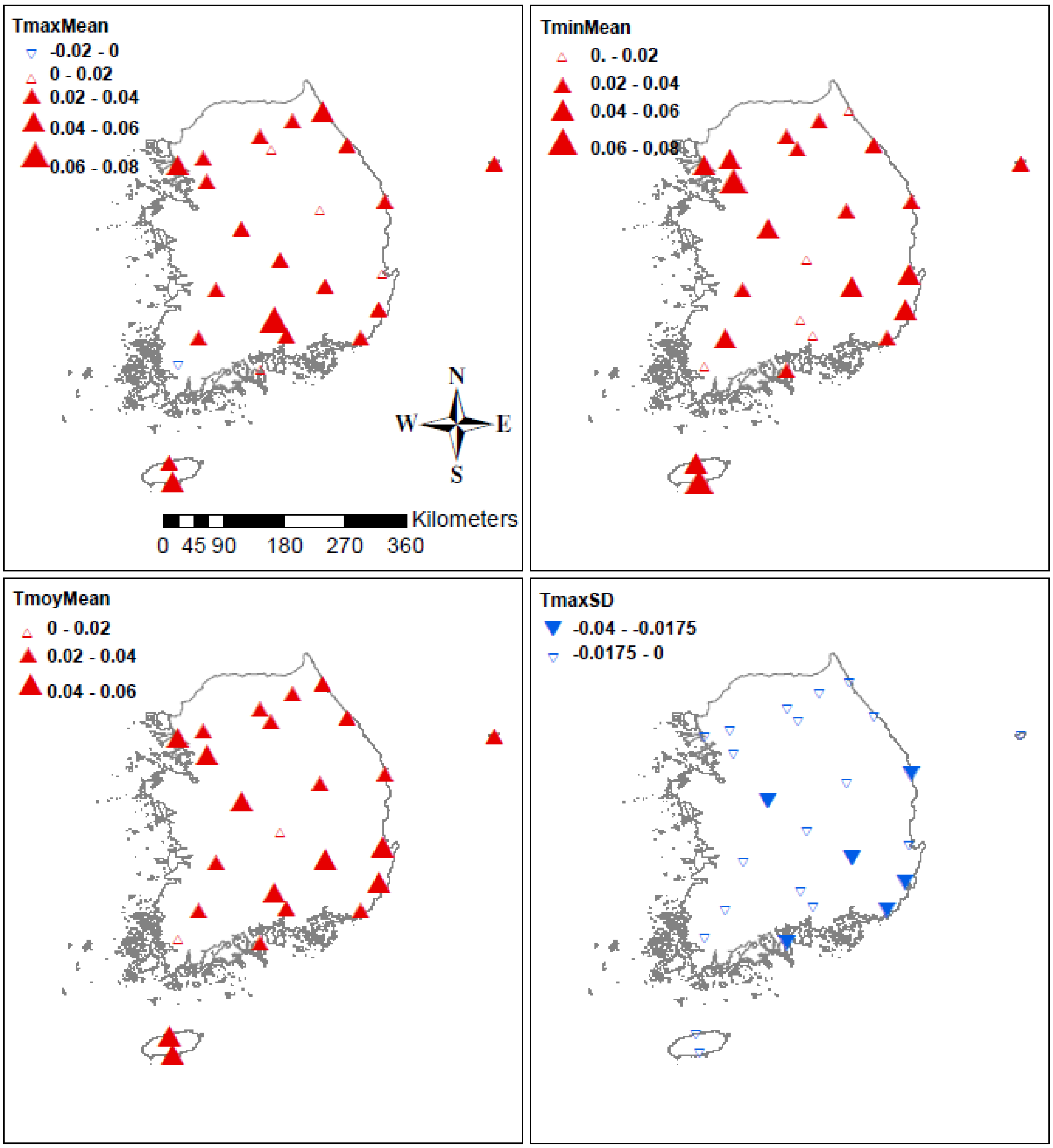

Figure 4.5 Trends in TmaxMean (upper left), TminMean (upper right), TmoyMean (lower left) and TmaxSD (lower right) for the 25 stations over South Korea during the period 1973-2009

The spatial distributions of the trends in TmaxMean, TminMean, TmoyMean and TmaxSD for 25 stations over South Korea during the period 1973-2009 are shown in Figure 4.5. The positive and negative trends are indicated by upward and downward triangles respectively. Solid triangles represent the significant trends at the 95% confidence level according to the Mann-Kendall test. In addition, sizes of triangles represent magnitudes of the annual trends. The remarkably steep positive trends in TmaxMean, TminMean and TmoyMean are statistically significant for the majority of the country except in few stations at the 95% confidence level. The steepest trend for TmaxMean is found in Hapcheon with a slope coefficient of 0.063 ℃. Besides, the largest slope coefficients of 0.079 ℃ and 0.058 ℃ per year respectively for TminMean and TmoyMean are observed in Suwon. The positive trends in all of three indices are not significant in Mokpo located edge of western south coast and are quite week in Chupungnyeong located in the mountainous region in the middle of the country. In the case of TmaxSD, the negative trends are observed in all of stations but the trends were only significant at 6 stations. The largest slope coefficient for TmaxSD is found in Cheongju with -0.369 ℃ per year.

Figure 4.6 shows the spatial distribution of the trends in TminSD, TmoySD, annual Tmax90p and annual Tmin10p for 25 stations over South Korea during the period 1973-2009. Similar to TmaxSD, the trends in both TminSD and TmoySD are negative for the most of stations in the country. The negative trends in TminSD and TmoySD are significant for 15 station and 11 stations respectively at the 95% confidence level based on the Mann-Kendall test. The steepest slope coefficients for both TminSD and TmoySD are detected in Yeongju with -0.029 ℃ and -0.022 ℃ per year respectively. The significant trends for annual Tmax90p are not found at the most of stations except in Hapcheon and Seogwipo. Different to annual Tmax90p, the positive trends for annual Tmin10p are generally strong over South Korea. The positive trends for more than half of all stations are statistically significant at the 95% confidence level. The largest trend for annual Tmin10p is detected in Suwon with slope coefficients of 0.103 ℃ per year.

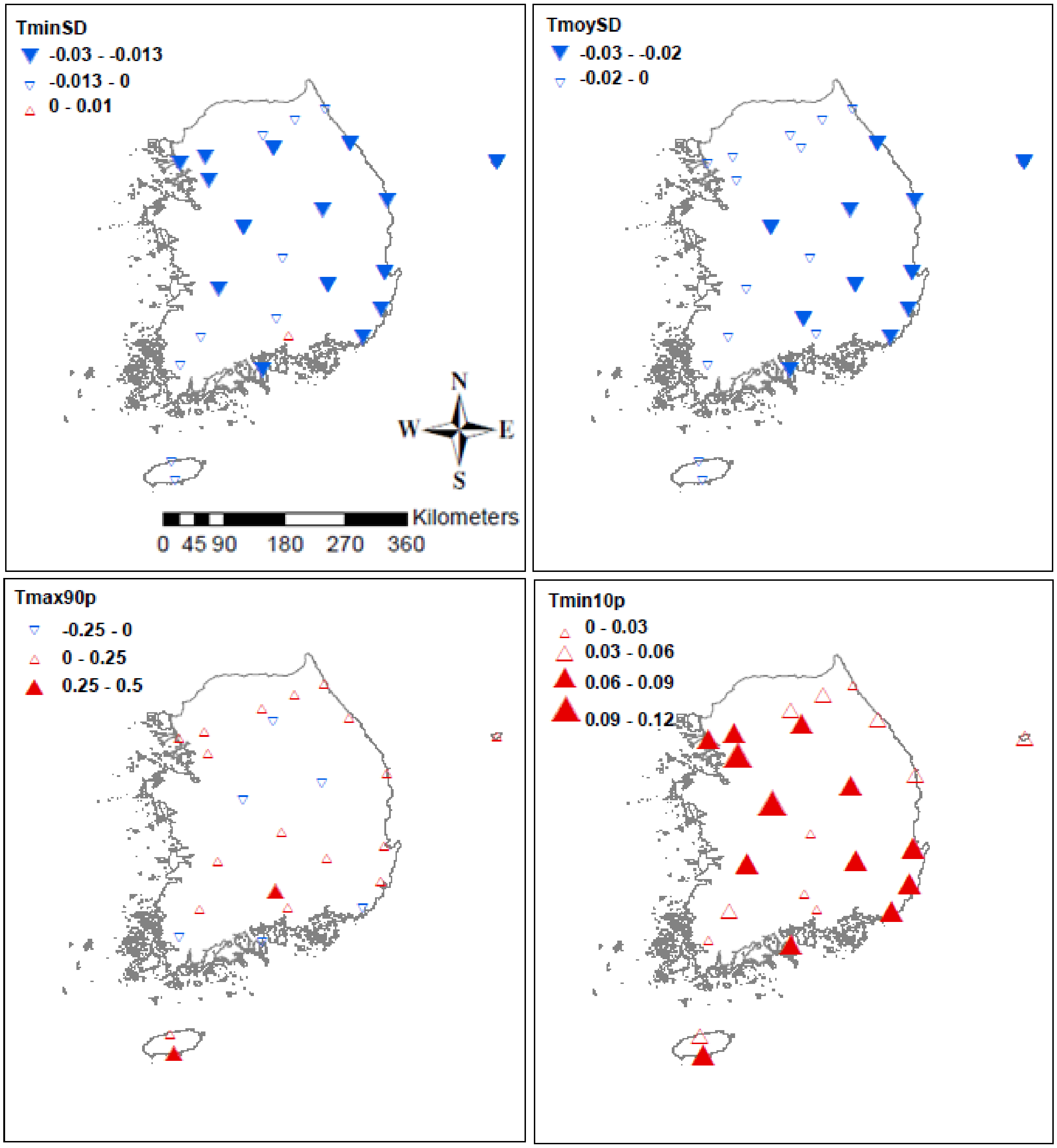

Figure 4.6 Trends in TminSD (upper left), TmoySD (upper right), and annual Tmax90p (lower left) and annual Tmin10p (lower right) for the 25 stations over South Korea during the period 1973-2009

The spatial distributions of the trends in FD, SU25, ID and TR20 for 25 stations over South Korea during the period 1973-2009 are shown in Figure 4.7. In the more than two-thirds of the country, statistically the negative trends for FD are observed at the 95% confidence level on the basis of the Mann-Kendall test. The steepest slope coefficient of -0.935 days per year are observed in Daegu located in the middle of the country. All 25 stations demonstrate the negative trends for ID. However, the negative trends in southern regions such as Yeosu, Jeju and Seogwipo are not meaningful because there are less than 3 ice days in most of years. The negative trends for ID are statistically significant in the most of the country except for 6 stations at the 95% confidence level. The largest slope coefficient of -0.47 days per year are obtained in Incheon located northern west coast. For the most of stations, the trends in SU25 and TR20 are positive. The positive trends in SU25 and TR20 are statistically significant for 8 stations and 13 stations respectively at the 95% confidence level. The largest trends for SU25 and TR20 are found in Seogwipo with slope coefficients of 0.8 and 0.79 days per year respectively.

Figure 4.8 shows the spatial distributions of the trends in FSL, GSL, FrTh and DTR for 25 stations over South Korea during the 1973-2009 periods. Apart from Jeju and Seogwipo in Jeju island located the southern ocean where there are no frost season, the negative trends in FSL are shown in all station over the country. For 6 stations, the negative trends in FSL are significant at the 95% confidence level using the Mann-Kendall trend test. The steepest trend of FSL is observed in Yeongju with a slope coefficient of -0.874 days per year. The positive trends in GSL are significant for the most of stations at the 95% confidence level. The largest trend of 1.2 days per year in GSL is detected in Ulsan located southern east coast. More than half of the country shows the negative trends in FrTh and DTR. The trends in FrTh and DTR are statistically significant for 13 and 15 stations respectively. The steepest slope coefficient of -0.826 days per year for FrTh is found in Pohang. Moreover, the strongest trend for DTR is observed in Hapcheon with slope coefficients of 0.052 ℃ per year.

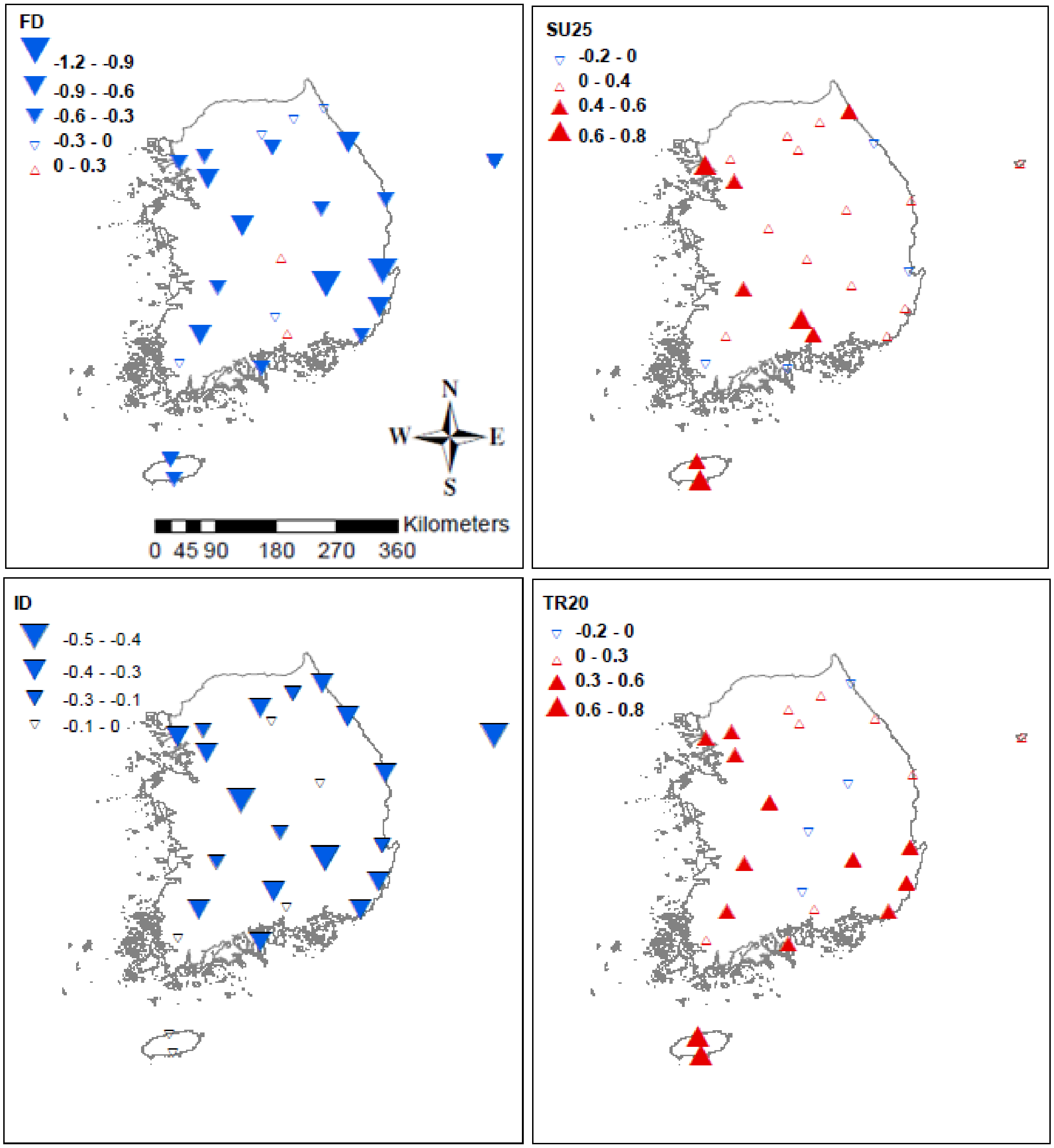

Figure 4.7 Trends in FD (upper left), SU25 (upper right), ID (lower left) and TR20 (lower right) for the 25 stations over South Korea during the period 1973-2009

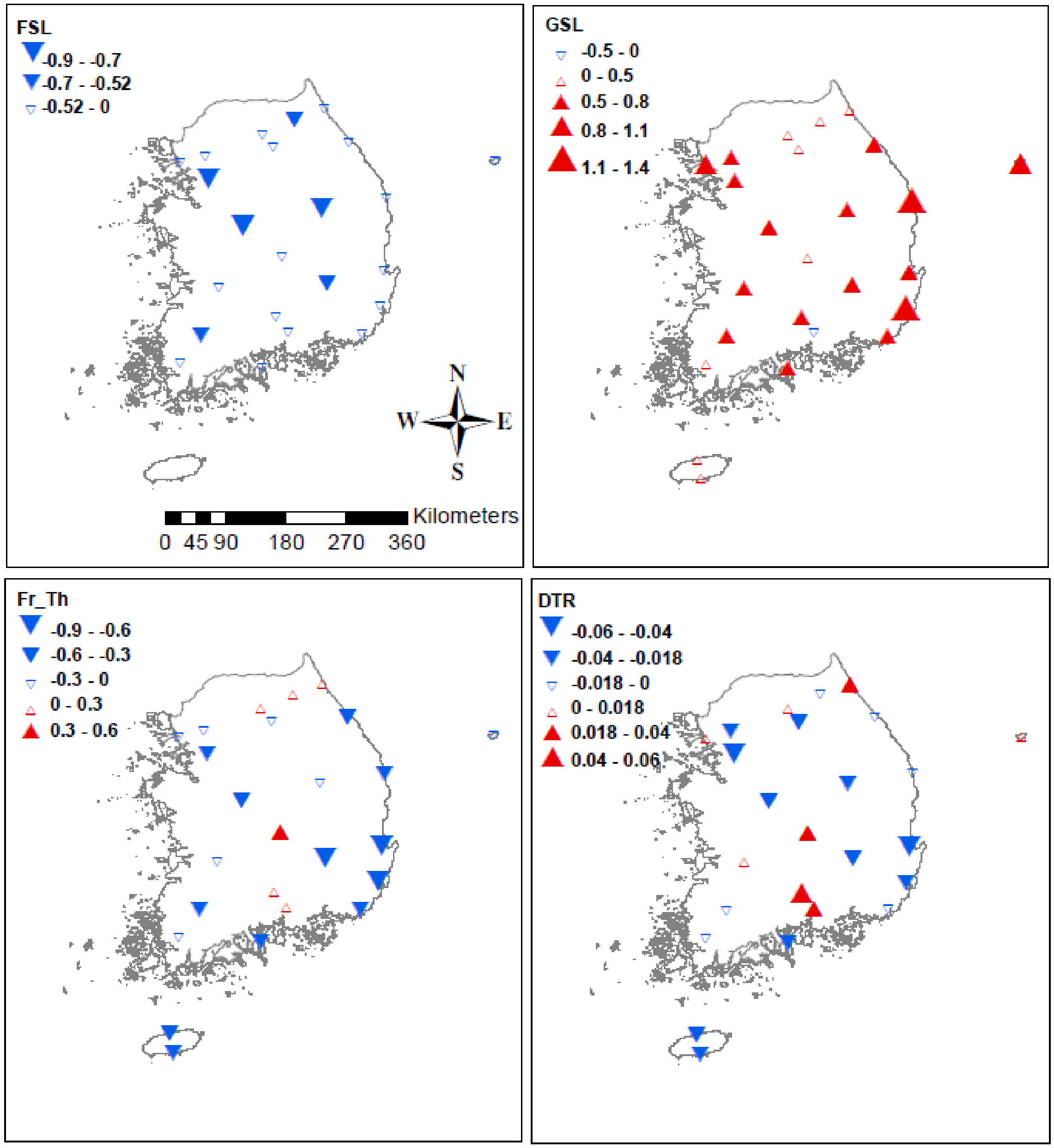

Figure 4.8 Trends in FSL (upper left), GSL (upper right), FrTh (lower left) and DTR (lower right) for the 25 stations over South Korea during the period 1973-2009

The spatial distributions of the trends in CSDI and WSDI for 25 stations over South Korea during the period 1973-2009 are shown in Figure 4.9. As seen from the figure below, the trends in WSDI for the most of stations show statistically non-significant. Only in Yeosu located southern coastal region, the negative trend is significant with a slope coefficient of -0.404 days per year. Contrasts of WSDI, the negative trends in CSDI are detected in all stations. Also, the trends in most of stations are significant at the 95% confidence level according to the Mann-Kendall test. The strongest trend in CSDI is obtained in Ulsan with the slope coefficient of -0.978 days per year.

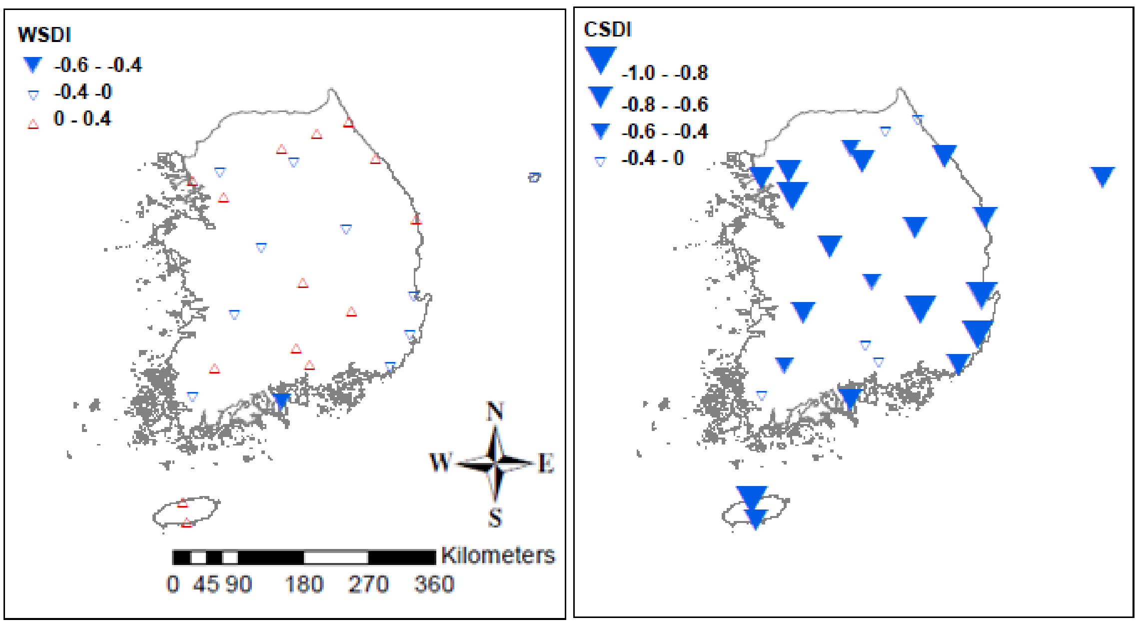

Figure 4.9 Trends in CSDI (left) and WSDI (right) for the 25 stations over South Korea during the period 1973-2009

5. DOWNSCALING MODELS FOR TEMPERATURE EXTREMES

Applying a downscaling technique that can reproduce the present weather properly is important to develop reliable local-scale climate scenario. Single-site downscaling methods have been widely applied for weather prediction in previous researches. However, recent several studies of downscaling methods have proposed multi-site SD methods. This chapter presents the comparison of the performance of the popular SDSM and the performance of the SVD-based multi-site SD procedure. This comparison allows the identification of the best SD method for accurate temperature simulations and projections.

A regression model consists of a deterministic component and a stochastic component. The deterministic components of the SDSM and the multi-site SD method are similar. However, their stochastic components are simulated by different procedures. The multi-site SD method uses the SVD technique to simulate the stochastic components at multiple stations concurrently while the SDSM simulates the values at single station directly. Synthetic temperature extremes are computed by adding the simulated stochastic components to the deterministic components. Hence, this chapter is divided by three parts: The first part presents the computation of the deterministic components; the second part provides the simulation of the stochastic components; the last part compares performances of the SDSM and the multi-site SD to reproduce characteristics of the observation in the synthetic results.

5.1 Deterministic Components of Regression Models

As mentioned above, the deterministic components of the regression models of the SDSM and the multi-site SD method are similar. Hence, both models used the same predictands and predictors for the calibration.

The regression models are developed using the observed local-scale predictands and the selected global-scale atmospheric predictors from variable screening process. Daily maximum temperature (Tmax) and daily minimum temperature (Tmin) at 25 stations over South Korea are used as predictands. Twenty five stations are selected according to homogeneity of data and station density. For candidate predictors, there are twenty five NCEP (Natural Centre for Environmental Prediction) climate variables covering the period from 1961 to 2001. In this study, two atmospheric variables, air temperature at 2m and surface specific humidity are eliminated before applying the variable selection operation since those two variables may have assimilated to the observed temperature extremes. The similarity between the information in a predictor and a predictand may lead to biased inference of the regression coefficients (Achen et al., 2000).

As described in methodology chapter, two different methods are used for screening variables: (a) stepwise regression with backward selection; (b) Variable Importance in the Projection (VIP) scores obtained from the Partial Least Square (PLS) regression (called the PLS-VIP method). The method that can screen significant variables more properly is employed for the variable selection operation. The effectiveness of methods is assessed by comparing performances of the regression models. Performances of the regression models are expressed in coefficient of determination (R^2) and Root Mean Square Error (RMSE). Furthermore, only five significant predictors are used in each regression model to avoid multicolinearity and to achieve the model efficiency (Gachon et al. 2005; Hessami et al. 2008).

5.1.1 Deterministic Component for Tmax

The predictand and predictor datasets cover the period from 1973 to 2001 at all 25 stations. The first 12 years (1973-1984) of datasets are used for the validation and the last 21 year (1985-2001) of datasets are utilized for the calibration. Each regression model is calibrated for each month and station. Table 5.1 shows model performances for Tmax using predictors selected by the stepwise method and the PLS-VIP method. R^2 and RMSE values are averages of 25 stations for each month. The results of both methods show closely similar R^2 and RMSE values in the calibration and validation periods.

Tmax	Calibration Period				Validation Period			
	PLS_VIP		Stepwise		PLS_VIP		Stepwise	
Month	R^2	RMSE	R^2	RMSE	R^2	RMSE	R^2	RMSE
January	0.42	2.75	0.45	2.67	0.47	3.28	0.51	3.18
February	0.51	2.62	0.53	2.56	0.50	3.12	0.51	3.05
March	0.39	3.12	0.38	3.12	0.38	3.71	0.39	3.72
April	0.41	3.20	0.41	3.22	0.25	3.81	0.26	3.83
May	0.26	3.24	0.23	3.32	0.29	3.86	0.30	3.95
June	0.25	2.81	0.20	2.90	0.18	3.34	0.12	3.46
July	0.38	2.78	0.37	2.81	0.34	3.30	0.31	3.34
August	0.30	2.53	0.28	2.56	0.32	3.01	0.31	3.04
September	0.32	2.50	0.31	2.51	0.17	2.98	0.20	2.99
October	0.43	2.49	0.45	2.44	0.41	2.97	0.43	2.90
November	0.52	2.89	0.55	2.81	0.48	3.44	0.55	3.35
December	0.46	2.97	0.52	2.80	0.52	3.54	0.57	3.34
Mean	**0.39**	**2.83**	**0.39**	**2.81**	**0.36**	**3.36**	**0.37**	**3.35**

Table 5.1 Model calibration and validation results for Tmax using predictors selected by the stepwise method and the PLS-VIP method

5.1.2 Deterministic Component for Tmin

Table 5.2 shows model performances for Tmin using predictors selected by the stepwise method and the PLS-VIP method. R^2 and RMSE values are averages of 25 stations for each month. The stepwise method provides more accurate estimation of Tmin than the PLS_VIP method does. It is indicated by higher R^2 values and the lower RMSE values in both calibration and validation periods.

Tmin	Calibration Period				Validation Period			
	PLS_VIP		Stepwise		PLS_VIP		Stepwise	
Month	R^2	RMSE	R^2	RMSE	R^2	RMSE	R^2	RMSE
January	0.33	3.26	0.42	3.06	0.29	3.88	0.36	3.64
February	0.40	2.87	0.47	2.72	0.41	3.41	0.44	3.24
March	0.37	2.49	0.42	2.42	0.30	2.97	0.35	2.88
April	0.48	2.50	0.51	2.49	0.34	2.97	0.36	2.96
May	0.31	2.30	0.34	2.28	0.30	2.73	0.36	2.71
June	0.38	1.82	0.43	1.80	0.36	2.16	0.43	2.14
July	0.50	1.72	0.52	1.74	0.45	2.05	0.47	2.07
August	0.39	1.64	0.41	1.65	0.32	1.95	0.37	1.96
September	0.54	2.11	0.59	2.04	0.47	2.51	0.53	2.43
October	0.46	2.55	0.55	2.37	0.40	3.03	0.47	2.82
November	0.44	2.93	0.53	2.71	0.40	3.49	0.51	3.23
December	0.32	3.05	0.42	2.83	0.39	3.63	0.46	3.37
Mean	**0.41**	**2.44**	**0.47**	**2.34**	**0.37**	**2.90**	**0.43**	**2.79**

Table 5.2 Model calibration and validation results for Tmin using predictors selected by the stepwise method and the PLS-VIP method

Although the stepwise method and the PLS-VIP method perform similar to determine predictors for Tmax, the stepwise method preforms slightly better to select suitable predictors for Tmin as compared with the PLS-VIP method does. Therefore, this study employs the stepwise method for the variable selection process.

5.2 Stochastic Components of Regression Models

Synthetic temperature extremes are computed by adding the simulated stochastic component (residual matrix) to the deterministic component of regression models. The SDSM directly simulates the residual matrix with single column or row while the multi-site SD method requires using the SVD technique for multi-site simulating of the squared residual matrix with multiple columns and rows.

The detailed computational procedures of the SDSM and the multi-site SD method are described in the following subsections.

5.2.1 Procedure of SDSM

The SDSM generates the stochastic component at each station individually. The computational procedure of the SDSM for simulating synthetic Tmax and Tmin time series is summarized as follows:

Step 1: Obtain the 1×6205 residual matrix E from the calibrated regression models for the 17 years calibration period (1985-2001), and for each station.

Step 2: Compute the 1×6205 synthetic residual matrix $\hat{E}$ using random numbers following the standard normal distribution N (0, 1)

Step 3: Compute the simulated values, $\hat{Y} = \alpha A + \hat{E}$

Step 4: Repeat 25 times from step1 to step 3 to simulate weather sequences at 25 stations.

5.2.2 Procedure of Multi-site SD Method

The SVD technique is used to simulate stochastic components of regression model at multiple sites concurrently. The detailed computational procedure of the multi-site SD method using the SVD technique to generate synthetic Tmax and Tmin time series is summarized as follows:

Step 1: Obtain the 25 ×6205 residual matrix E from calibrated regression models for the 17 years calibration period (1985-2001), and for 25 stations.

Step 2: Compute the standardize matrix E_S of E.

Step 3: Select the correlation matrix R instead of P because the dimension of the 25×25 matrix R is smaller than the dimension of the 6205×6205 matrix P.

Step 4: Apply the SVD technique to decompose the matrix R for obtaining the 24×24 diagonal matrix D_R of the ordered 24 non-zero singular values of R, and the 25×24 matrix V_R of the corresponding 14 eigenvectors of R. (r=24)

Step 5: Compute the matrix $V_P$of eigenvectors of P using the matrix V_R.

Step 6: Compute the 25×24 matrix Z of the 24 standardized principal components of E_S.

Step 7: Generate the 25×24 matrix $\hat{Z}$ whose columns independently follow a standard normal distribution N(0,1).

Step 8: Using the SVD technique to the matrix $\hat{Z}$, obtain the 25×24 perfect orthonormal matrix $\hat{Z}_o$.

Step 9: Compute the synthetic standardized matrix $\hat{E}_S = \hat{Z} \times {V_P}^T \times {D_P}^{\frac{1}{2}}$

Step 11: Compute the non-standardized synthetic matrix $\hat{E}$.

Step 12: Compute the simulated values, $\hat{Y}$ using the calibrated parameters and the synthetic residual matrix $\hat{E}$.

5.3 Results and Evaluation of SDSM and Multi-site SD Method

Performances of the SDSM and the multi-site SD method are compared by the three criteria: the effectiveness of the methods to reproduce (a) the basic statistical properties (means, standard deviations and extremes); (b) the emporal dependency at each station, and (c) the spatial dependency among stations.

5.3.1 Goodness of fit

The following results are based on 100 simulations of daily Tmax and Tmin time series. Performances of the SDSM and the multi-site SD method are evaluated by how accurately they reproduce basic statistical properties of observed data in the simulated results. The basic statistical properties of temperature extremes are indicated by four indices; monthly means and standard deviations (STDs) of Tmax and Tmin, monthly 90th percentiles of Tmax (Tmax90ps), and monthly10th percentiles of Tmin (Tmin10ps).

Tables 5.3 and 5.4 report monthly means and STDs of Tmax and monthly Tmax90ps computed from the observations and the simulated results at Seoul station. The multi-site SD method predicts basic statistical properties of Tmax accurately compared to observed data in both calibration and validation periods. Also the results obtained from the multi-site SD method are comparable to the results from the SDSM.

Tmax	Calibration period (1985-2001)								
	Mean			STD			Tmax90p		
Month	OBS	SDSM	Multi-SD	OBS	SDSM	Multi-SD	OBS	SDSM	Multi-SD
January	1.59	1.59	1.59	4.11	4.24	4.05	6.48	6.95	6.76
February	4.55	4.54	4.55	4.20	4.19	4.21	9.80	9.91	9.97
March	10.43	10.44	10.43	4.12	4.26	4.28	15.80	15.85	15.93
April	17.97	17.98	17.97	4.53	4.52	4.53	23.80	23.75	23.67
May	22.95	22.95	22.95	3.70	3.77	3.80	27.60	27.77	27.79
June	26.98	26.98	26.98	3.22	3.19	3.22	31.00	31.05	31.05
July	28.84	28.83	28.84	3.04	3.05	3.09	32.66	32.72	32.81
August	29.82	29.81	29.82	2.99	2.97	3.02	33.40	33.60	33.56
September	25.79	25.79	25.79	3.13	3.11	3.11	29.70	29.74	29.74
October	19.79	19.80	19.79	3.70	3.91	3.88	24.28	24.68	24.64
November	11.65	11.67	11.66	4.76	5.02	4.74	17.60	17.96	17.62
December	4.61	4.61	4.61	4.42	4.35	4.41	10.30	10.18	10.29

Table 5.3 Monthly means and STDs of Tmax, and monthly Tmax90ps computed from the observations and the simulated results by the SDSM and the multi-site SD method at Seoul station during the calibration period (1985-2001)

Tmax	Validation period (1973-1984)								
	Mean			STD			Tmax90p		
Month	OBS	SDSM	Multi-SD	OBS	SDSM	Multi-SD	OBS	SDSM	Multi-SD
January	1.08	1.35	1.36	4.55	4.44	4.26	6.90	7.19	6.92
February	3.44	3.92	3.93	4.97	4.70	4.72	9.59	9.85	9.88
March	10.17	9.93	9.97	4.42	4.28	4.37	15.80	15.38	15.66
April	17.46	18.09	18.10	4.27	4.34	4.35	23.10	23.63	23.66
May	22.82	22.84	22.86	3.88	3.94	3.99	27.60	27.83	27.96
June	26.77	26.89	26.84	2.91	3.19	3.22	30.25	30.95	30.93
July	28.83	28.76	28.75	3.11	3.07	3.12	32.60	32.72	32.76
August	29.37	29.88	29.86	2.98	2.98	3.04	32.80	33.72	33.74
September	25.66	25.57	25.59	2.58	2.97	2.94	28.60	29.38	29.35
October	19.76	19.49	19.49	4.27	3.93	3.91	24.80	24.39	24.38
November	11.20	10.96	10.99	5.34	4.99	4.73	17.70	17.26	16.92
December	3.69	3.92	3.86	4.90	4.45	4.65	9.80	9.65	9.81

Table 5.4 Monthly means and STDs of Tmax, and monthly Tmax90ps computed from the observations and the simulated results by the SDSM and the multi-site SD method at Seoul station during the validation period (1973-1984)

In order to assess performances of methods over South Korea, monthly means and STDs of Tmax and monthly Tmax90ps are computed for 25 stations. Figures 5.1 to 5.6 display boxplots of Tmax indices computed from the observations and the simulated results by the SDSM and the multi-site SD method. Each boxplot represents monthly Tmax indices aggregated at all 25 stations during the calibration period (Figure 5.1, 5.2 and 5.3) and the validation period (Figure 5.4, 5.5 and 5.6). For both of the SDSM and the multi-site SD method, it is found that a very close agreement between boxplots of the observations and the simulated results in both calibration and validation periods. In addition, the accuracy of models is numerically measured by RMSE. Table 5.5 reports RMSE values for monthly Tmax indices at all stations. For example, the SDSM results in RMSE values that are ranged from 0.56 ℃ to 1.37 ℃ for monthly means of Tmax, from 0.50 ℃ to 0.70 ℃ for monthly STDs of Tmax, and from 1.13 ℃ to 1.89 ℃ for monthly Tmax90ps in the validation period. The multi-site SD method results in RMSE values that are ranged from 0.84 ℃ to 1.84 ℃ for monthly means of Tmax, from 0.51 ℃ to 0.98 ℃ for monthly STDs of Tmax, and from 1.28 ℃ to 2.36 ℃ for monthly Tmax90ps in the validation period. For the all three Tmax indices, the SDSM provides slightly lower RMSE values than the multi-site SD method does in both calibration and validation periods.

Overall, the multi-site SD method performs well to estimate basic statistical properties of Tmax compared to the observations in all stations over South Korea. Besides, the multi-site SD method achieves similar accuracy in predicting statistical properties of Tmax as compared to the SDSM.

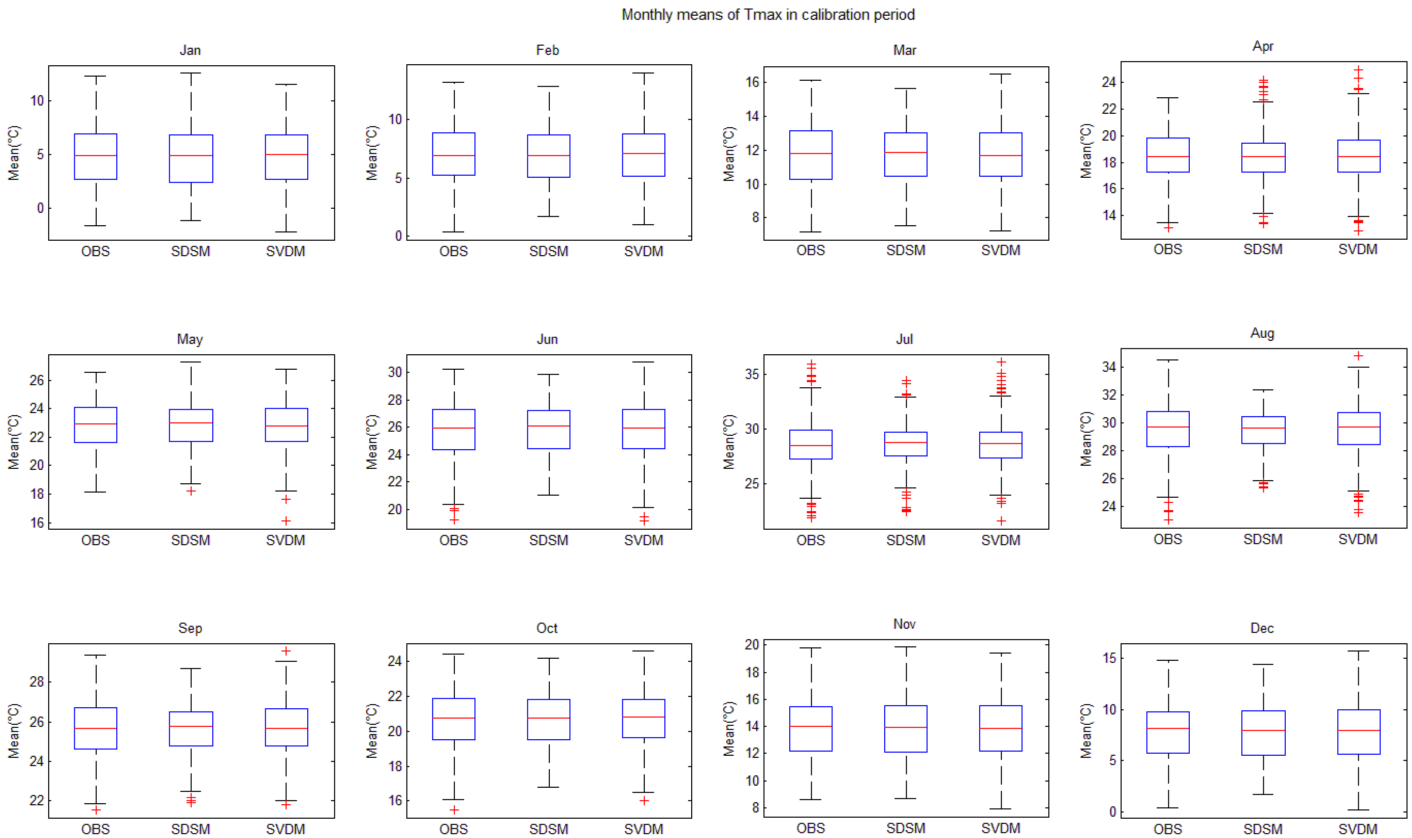

Figure 5.1 Boxplots of monthly means of Tmax computed from the observations and the simulated results by the SDSM and the multi-site SD method (SVDM) for the calibration period (1985-2001)

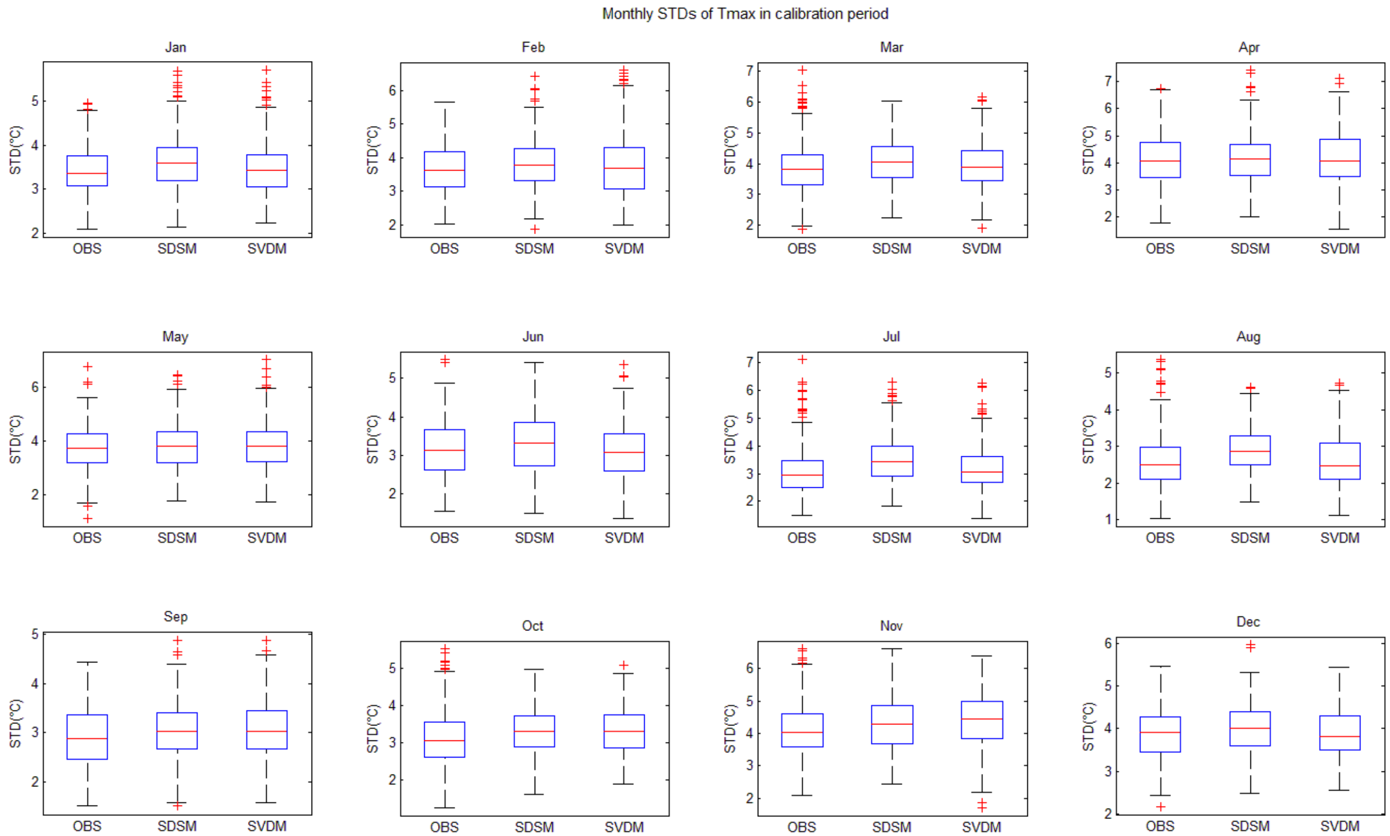

Figure 5.2 Boxplots of monthly STDs of Tmax computed from the observations and the simulated results by the SDSM and the multi-site SD method (SVDM) for the calibration period (1985-2001)

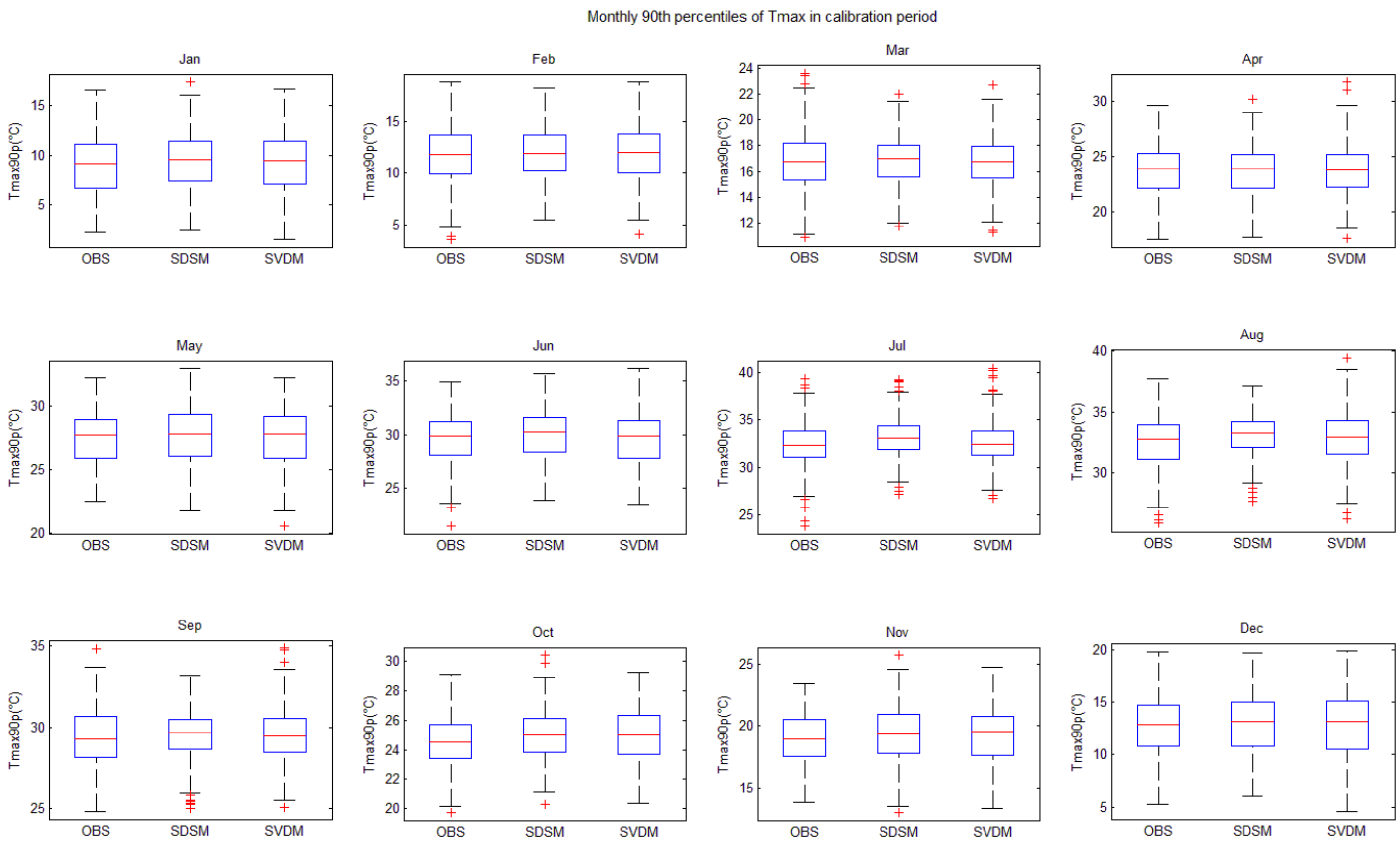

Figure 5.3 Boxplots of monthly Tmax90ps of Tmax computed from the observations and the simulated results by the SDSM and the multi-site SD method (SVDM) for the calibration period (1985-2001)

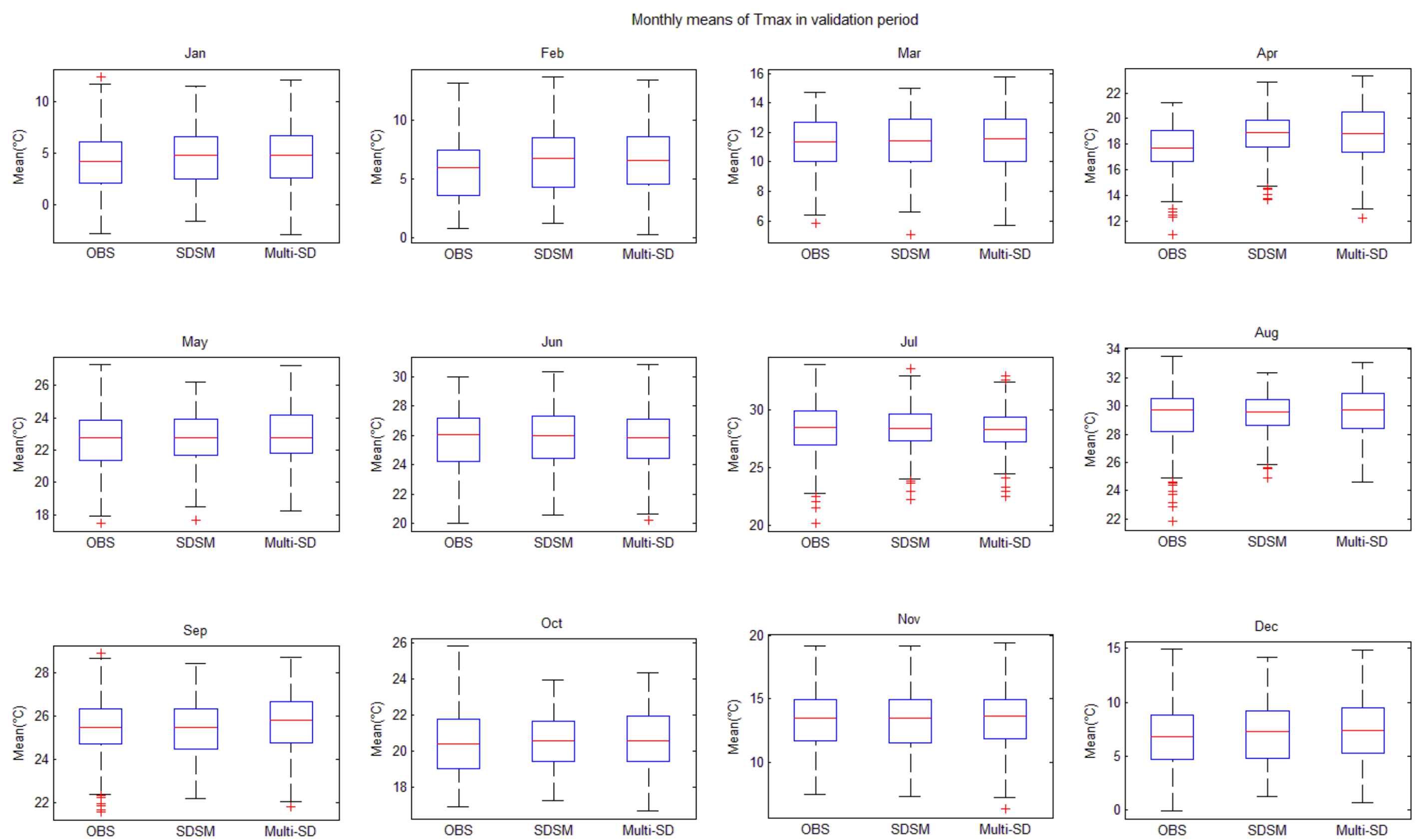

Figure 5.4 Boxplots of monthly means of Tmax computed from the observations and the simulated results by the SDSM and the multi-site SD method (SVDM) for the validation period (1973-1984)

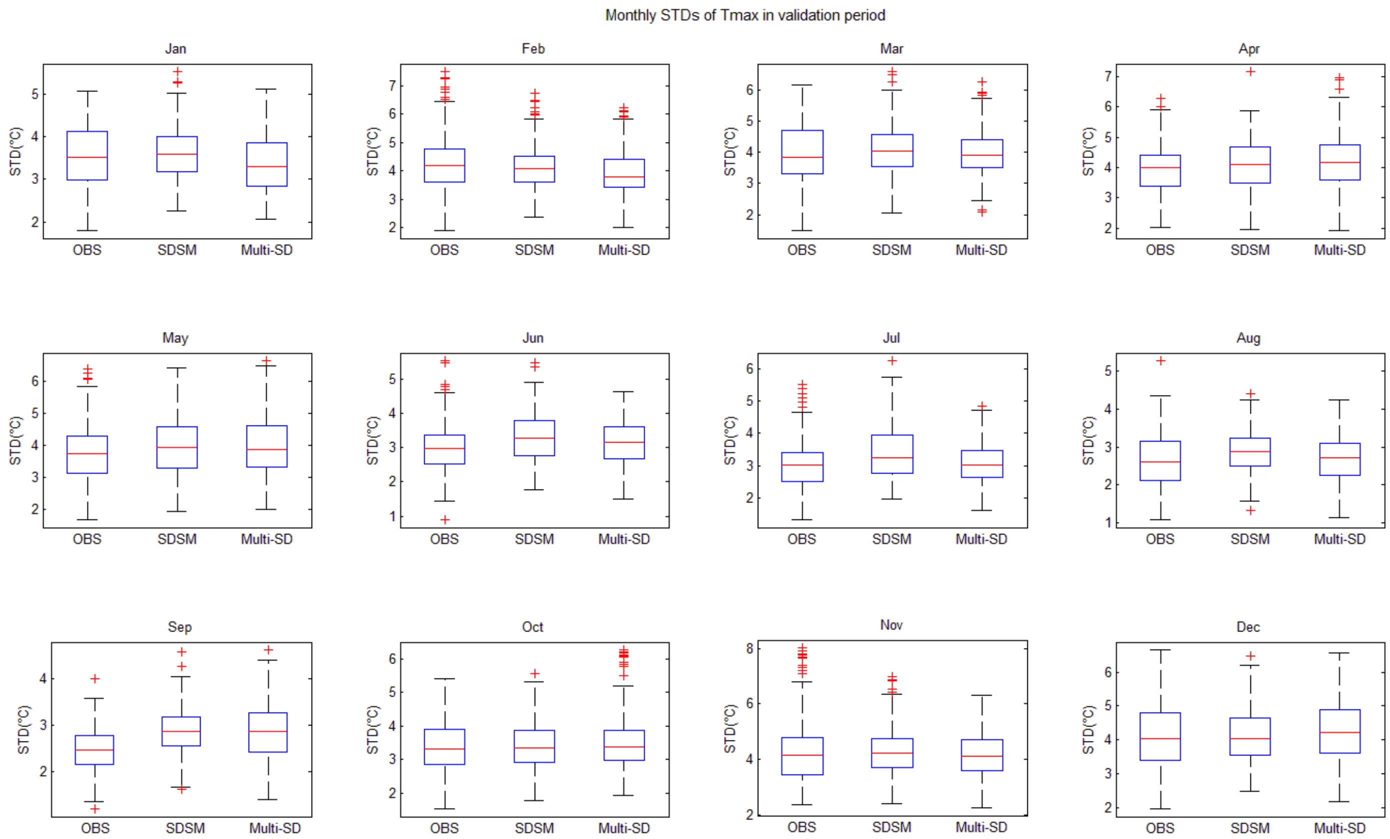

Figure 5.5 Boxplots of monthly STDs of Tmax computed from the observations and the simulated results by the SDSM and the multi-site SD method (SVDM) for the validation period (1973-1984)

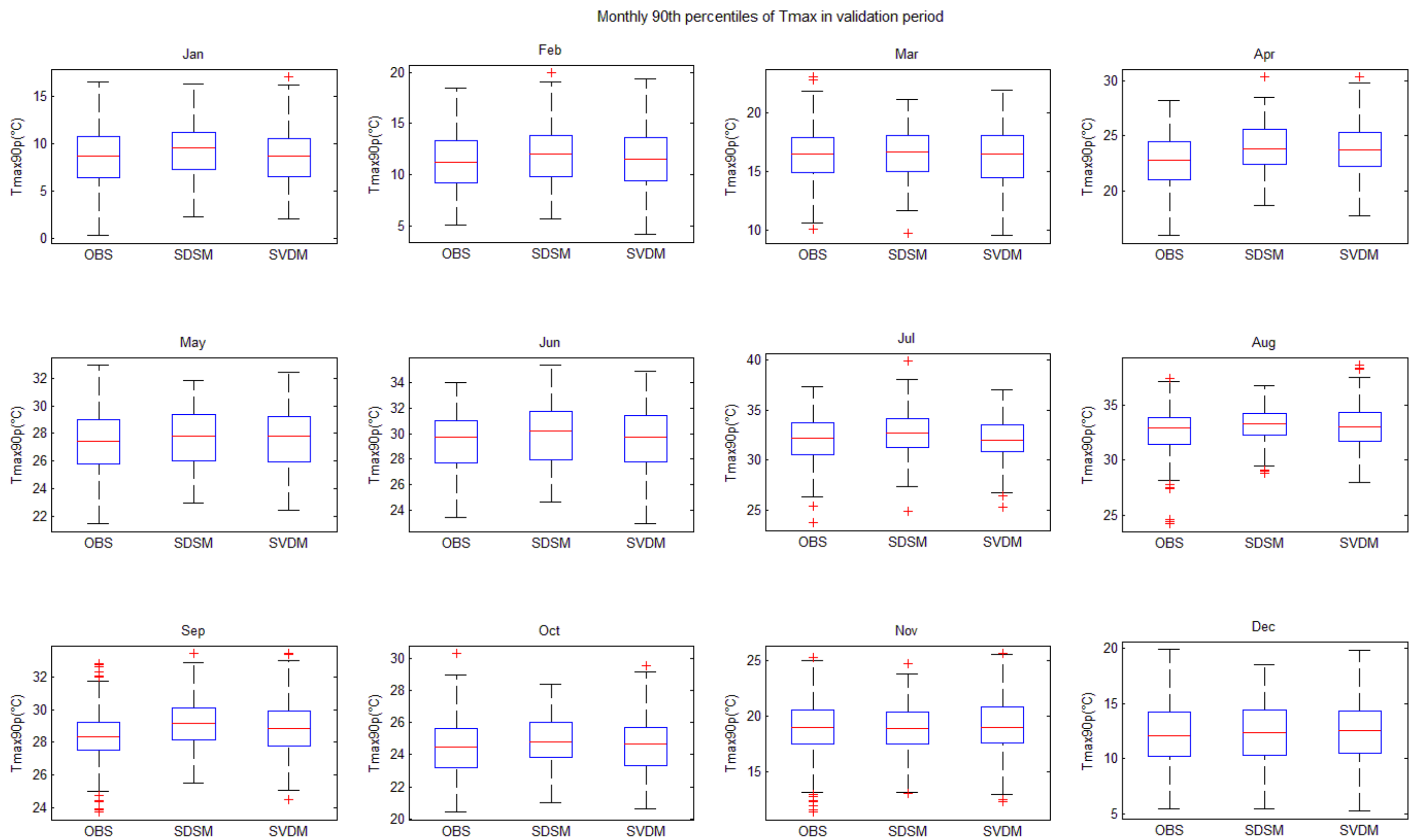

Figure 5.6 Boxplots of monthly Tmax90ps of Tmax computed from the observations and the simulated results by the SDSM and the multi-site SD method (SVDM) for the validation period (1973-1984)

Tmax	Calibration period (1985-2001)						Validation period (1973-1984)					
	Mean		STD		Tmax90p		Mean		STD		Tmax90p	
Month	SDSM	Multi-SD	SDSM	Multi-SD	SDSM	Multi-SD	SDSM	Multi-SD	SDSM	Multi-SD	SDSM	Multi-SD
January	0.73	0.73	0.51	0.47	1.11	1.06	1.18	1.24	0.53	0.50	1.66	1.65
February	0.89	1.45	0.53	0.76	1.55	2.08	1.16	1.84	0.70	0.97	1.82	2.36
March	0.98	0.98	0.61	0.63	1.47	1.46	0.65	0.65	0.61	0.59	1.36	1.28
April	0.89	1.23	0.54	0.69	1.27	1.44	1.37	1.59	0.58	0.57	1.89	2.16
May	0.84	0.82	0.47	0.44	1.15	1.10	0.89	0.87	0.63	0.61	1.24	1.19
June	0.96	1.08	0.43	0.44	1.22	1.34	0.85	0.90	0.53	0.53	1.25	1.26
July	1.18	1.18	0.70	0.66	1.40	1.37	1.27	1.26	0.65	0.62	1.52	1.50
August	1.10	1.05	0.70	0.67	1.45	1.39	1.10	1.10	0.59	0.57	1.51	1.47
September	0.89	1.02	0.51	0.55	1.29	1.38	0.56	0.84	0.60	0.64	1.13	1.44
October	0.69	0.67	0.55	0.58	1.02	1.05	1.00	1.06	0.50	0.51	1.28	1.34
November	0.73	1.14	0.58	0.73	1.22	1.44	0.90	1.60	0.62	0.98	1.58	2.27
December	0.77	0.79	0.55	0.52	1.20	1.23	0.84	0.86	0.54	0.51	1.28	1.30
Mean	**0.89**	**1.01**	**0.56**	**0.60**	**1.28**	**1.36**	**0.98**	**1.15**	**0.59**	**0.63**	**1.46**	**1.60**

Table 5.5 RMSEs of monthly means and STDs of Tmax, and monthly Tmax90ps computed from from the observations and the simulated results by the SDSM and the multi-site SD method for all stations during the calibration and validation periods

Tables 5.6 and 5.7 report monthly means and STDs of Tmin and monthly Tmin10ps computed from the observations and the simulated results at Seoul station. As shown in results of Tmax (Tables 5.4 and 5.5), the multi-site SD method estimates basic properties of Tmin accurately compared to the observations in the calibration and validation periods. Also the multi-site SD method provides comparable results to the SDSM.

Tmin	Calibration period (1985-2001)								
	Mean			STD			Tmin10p		
Month	OBS	SDSM	Multi-SD	OBS	SDSM	Multi-SD	OBS	SDSM	Multi-SD
January	-4.20	-4.49	-4.20	3.65	4.03	3.64	-9.00	-9.67	-9.00
February	-2.61	-2.77	-2.61	3.56	3.98	3.81	-7.03	-7.82	-7.33
March	1.64	1.59	1.64	3.04	3.16	3.17	-2.31	-2.48	-2.46
April	7.01	6.95	7.01	3.37	3.56	3.59	2.55	2.38	2.29
May	12.21	12.20	12.21	2.69	2.88	2.79	8.66	8.49	8.59
June	17.06	16.99	17.06	2.26	2.42	2.42	14.10	13.92	13.88
July	21.43	21.45	21.43	2.18	2.33	2.30	18.48	18.36	18.42
August	21.88	21.86	21.88	1.79	2.14	1.97	19.41	19.06	19.23
September	16.83	16.82	16.83	3.04	3.18	3.31	12.75	12.73	12.42
October	10.29	10.23	10.29	3.31	3.48	3.52	5.86	5.72	5.78
November	3.91	3.88	3.91	3.75	4.10	3.93	-0.97	-1.42	-1.15
December	-1.57	-1.70	-1.57	3.51	3.76	3.52	-6.27	-6.50	-6.22

Table 5.6 Monthly means and STDs of Tmin, and monthly Tmin10ps computed from the observations and the simulated results by the SDSM and the multi-site SD method at Seoul station during the calibration period (1985-2001)

Tmin	Validation period (1973-1984)								
	Mean			STD			Tmin10p		
Month	OBS	SDSM	Multi-SD	OBS	SDSM	Multi-SD	OBS	SDSM	Multi-SD
January	-5.12	-4.59	-4.07	3.58	4.07	4.37	-9.80	-9.83	-9.84
February	-3.68	-2.96	-2.40	4.11	4.15	4.55	-9.03	-8.23	-8.23
March	1.00	1.44	2.13	3.27	3.16	3.41	-3.21	-2.61	-2.42
April	6.90	7.25	8.18	3.36	3.47	3.75	2.55	2.83	3.19
May	11.83	12.05	12.31	3.03	3.03	2.94	7.94	8.19	8.48
June	16.78	16.83	16.99	2.33	2.39	2.46	13.60	13.79	13.68
July	21.20	21.27	21.88	2.01	2.22	2.38	18.57	18.40	18.71
August	21.68	21.86	22.93	2.03	2.10	2.15	18.82	19.15	20.09
September	16.30	16.60	16.70	2.81	2.91	2.92	12.68	12.90	12.86
October	9.87	10.06	10.15	3.73	3.56	3.67	4.74	5.42	5.47
November	3.43	3.64	4.42	4.08	4.04	4.24	-1.91	-1.62	-1.04
December	-2.48	-1.96	-1.72	3.99	3.85	3.87	-7.88	-7.01	-6.64

Table 5.7 Monthly means and STDs of Tmin, and monthly Tmin10ps computed from the observations and the simulated results by the SDSM and the multi-site SD method at Seoul station during the validation period (1973-1984)

In order to examine performances of methods over South Korea, monthly means and STDs of Tmin and monthly Tmin10ps are computed at all 25 stations. Figures 5.1 to 5.6 display boxplots of Tmin indices computed from the observations and the simulated results by the SDSM and the multi-site SD method. Each boxplot represents monthly Tmin indices aggregated at all 25 stations during the calibration period (Figures 5.7, 5.8 and 5.9) and the validation period (Figures 5.10, 5.11 and 5.12). For both of the SDSM and the multi-site SD method, a very close agreement is found between boxplots of the observed and simulated results in both calibration and validation periods. Furthermore, the accuracy of models is numerically measured by RMSE and Table 5.8 presents RMSE values for monthly Tmin indices at all stations. For instance, the SDSM results in RMSE values that are ranged from 0.72 ℃ to 1.76 ℃ for monthly means of Tmin, from 0.41 ℃ to 0.67 ℃ for monthly STDs of Tmin, and from 1.06 ℃ to 2.04 ℃ for monthly Tmin10ps in the validation period. The multi-site SD method results in RMSE values that are ranged from 0.72 ℃ to 2.02 ℃ for monthly means of Tmin, from 0.42 ℃ to 0.78 ℃

for monthly STDs of Tmin, and from 1.01 ℃ to 2.66 ℃ for monthly Tmin10ps in the validation period. For the all three Tmin indices, the SDSM provides slightly lower RMSE values than the multi-site SD method in the calibration and validation periods.

Similar to results obtained in Tmax, the multi-site SD method successfully estimate basic statistical properties of Tmax compared to the observations in all stations over South Korea. Furthermore, the multi-site SD method similarly performs well on predicting statistical properties of Tmax as compared to the SDSM.

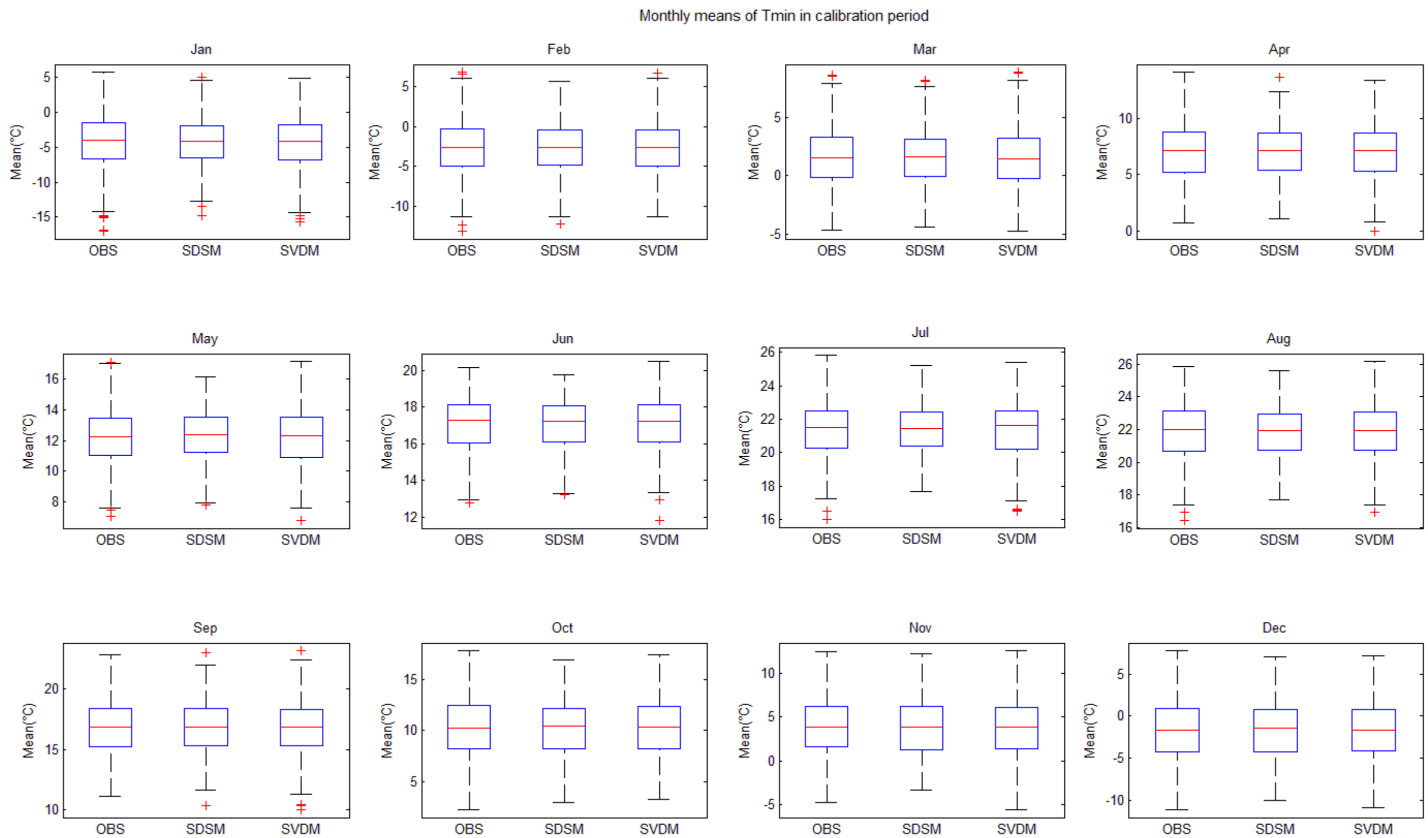

Figure 5.7 Boxplots of monthly Means of Tmin computed from the observations and the simulated results by the SDSM and the multi-site SD method (SVDM) for the calibration period (1985-2001)

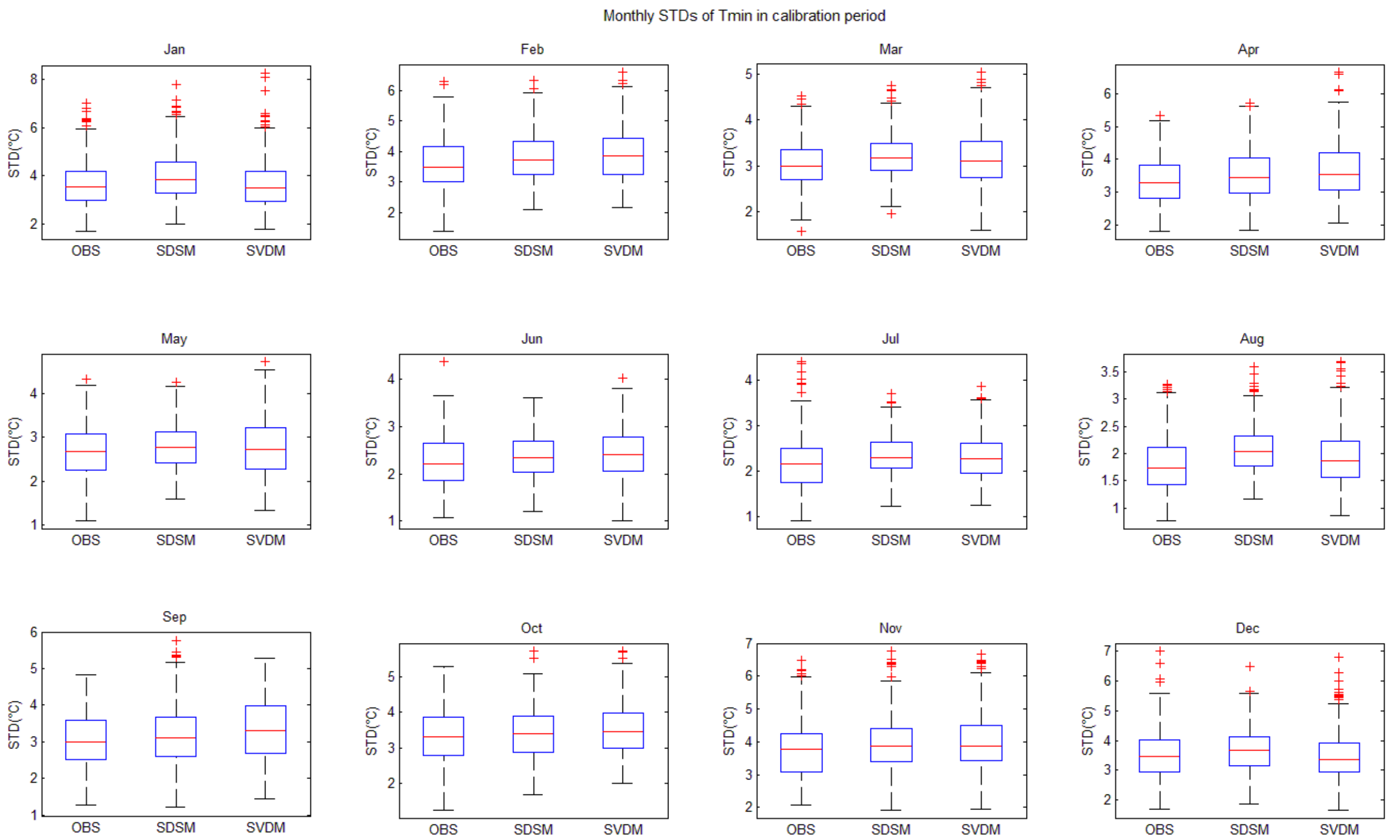

Figure 5.8 Boxplots of monthly STDs of Tmin computed from the observations and the simulated results by the SDSM and the multi-site SD method (SVDM) for the calibration period (1985-2001)

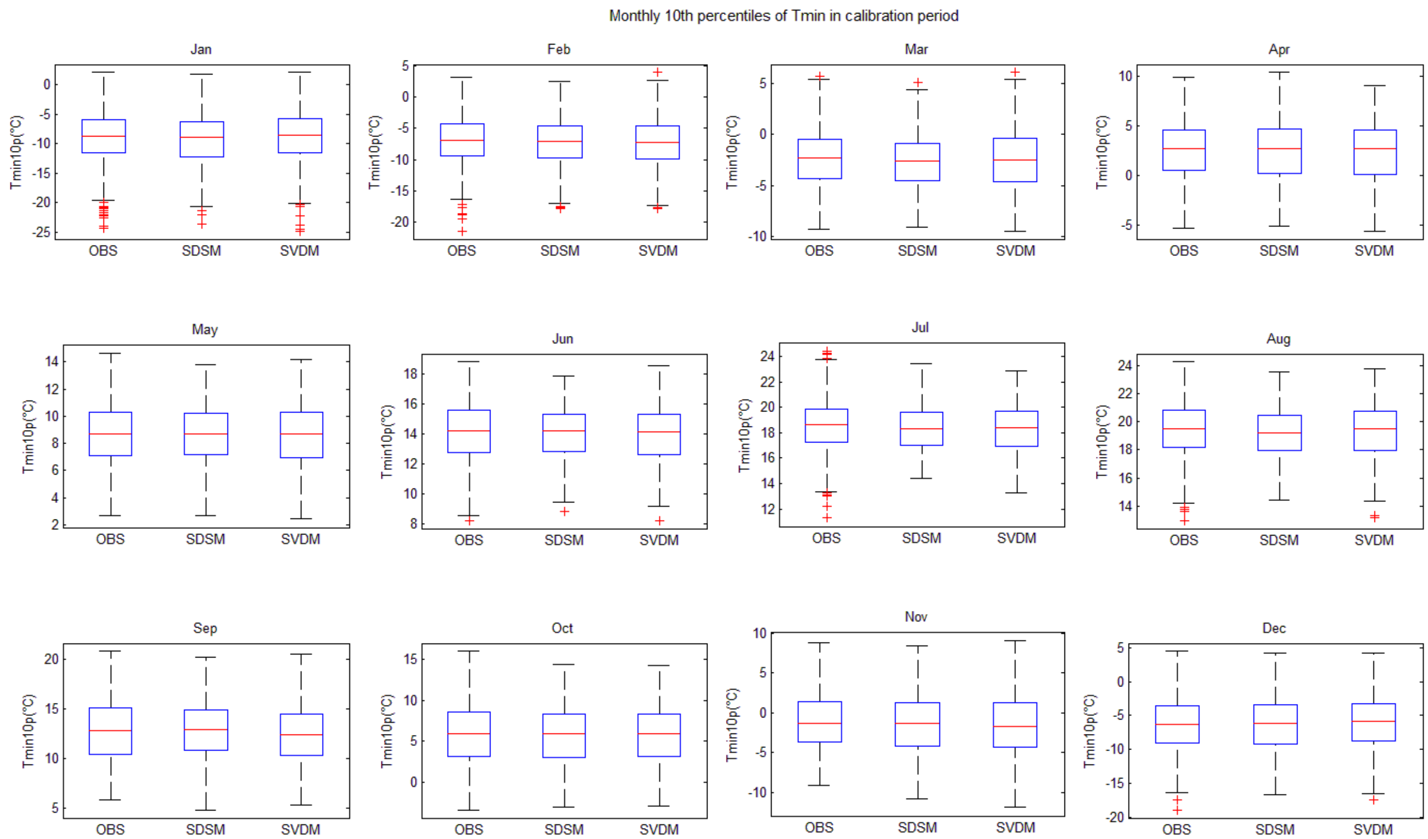

Figure 5.9 Boxplots of monthly Tmin10ps computed from the observations and the simulated results by the SDSM and the multi-site SD method (SVDM) for the calibration period (1985-2001)

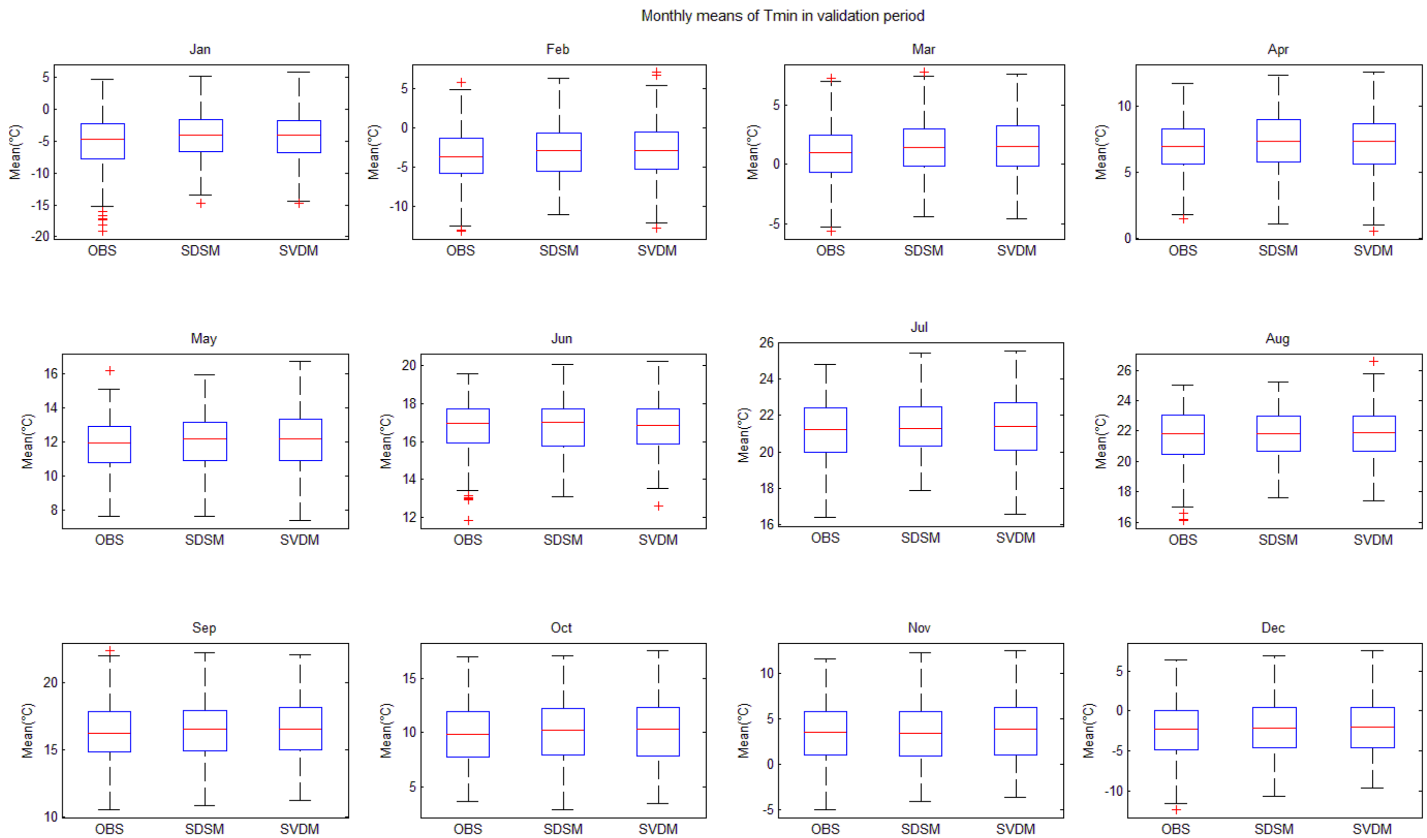

Figure 5.10 Boxplots of monthly Means of Tmin computed from the observations and the simulated results by the SDSM and the multi-site SD method (SVDM) for the validation period (1973-1984)

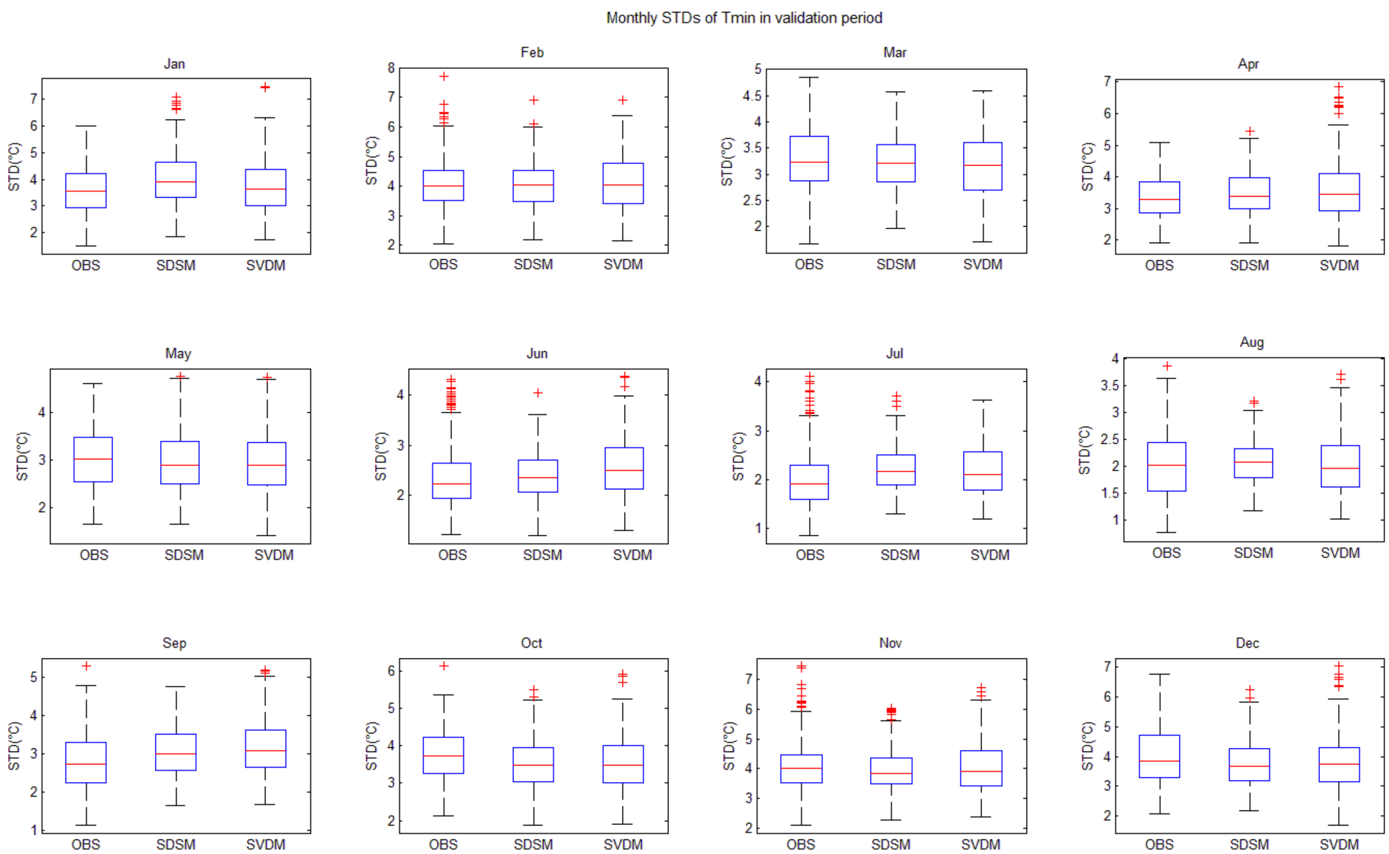

Figure 5.11 Boxplots of monthly STDs of Tmin computed from the observations and the simulated results by the SDSM and the multi-site SD method (SVDM) for the validation period (1973-1984)

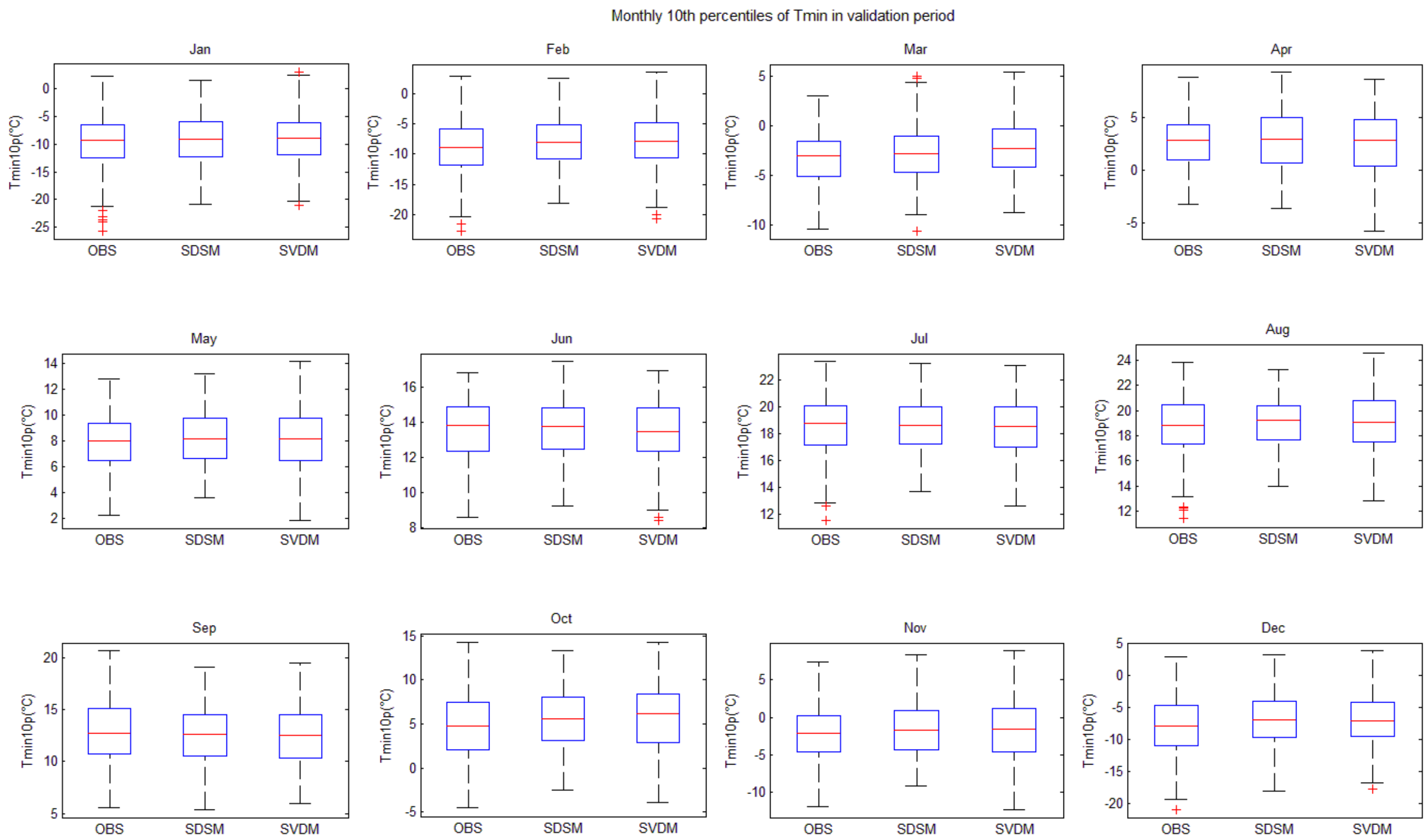

Figure 5.12 Boxplots of monthly Tmin10ps computed from the observations and the simulated results by the SDSM and the multi-site SD method (SVDM) for the validation period (1973-1984)

Tmin	Calibration period (1985-2001)						Validation period (1973-1984)					
	Mean		STD		Tmin10p		Mean		STD		Tmin10p	
Month	SDSM	Multi-SD	SDSM	Multi-SD	SDSM	Multi-SD	SDSM	Multi-SD	SDSM	Multi-SD	SDSM	Multi-SD
January	1.02	1.03	0.61	0.54	1.42	1.44	1.76	1.76	0.67	0.60	1.99	2.00
February	0.88	1.65	0.61	0.80	1.37	1.98	1.14	2.02	0.64	0.76	1.90	2.66
March	0.75	0.75	0.41	0.40	1.03	1.04	0.86	0.87	0.49	0.51	1.19	1.23
April	0.65	1.23	0.43	0.63	0.96	1.39	0.92	1.09	0.52	0.56	1.22	1.19
May	0.70	0.70	0.40	0.44	0.96	0.98	0.72	0.72	0.47	0.45	1.06	1.01
June	0.61	0.88	0.37	0.47	0.89	1.16	0.76	0.94	0.41	0.56	1.11	1.21
July	0.68	0.69	0.47	0.48	1.16	1.18	0.78	0.82	0.42	0.44	1.04	1.06
August	0.71	0.74	0.47	0.46	0.96	0.96	0.76	0.80	0.42	0.42	1.11	1.16
September	0.71	1.14	0.37	0.62	0.94	1.49	0.74	1.41	0.45	0.59	1.07	1.57
October	0.74	0.72	0.44	0.49	1.12	1.11	0.84	0.85	0.53	0.50	1.74	1.68
November	0.81	1.36	0.54	0.83	1.12	1.39	1.09	1.66	0.59	0.78	1.24	1.75
December	0.83	0.82	0.56	0.54	1.22	1.24	1.24	1.23	0.62	0.57	2.04	1.89
MEAN	**0.76**	**0.98**	**0.47**	**0.56**	**1.10**	**1.28**	**0.97**	**1.18**	**0.52**	**0.56**	**1.39**	**1.53**

Table 5.8 RMSEs of monthly Means and STDs of Tmin and monthly Tmin10ps computed from the observations and the simulated results by the SDSM and the multi-site SD method for all stations during both the calibration and validation periods

5.3.2 Temporal Dependency

The ability of the SDSM and the multi-site SD method to capture temporal dependency is evaluated by the autocorrelation coefficients of lags from one to three. Table 5.9 shows autocorrelations for Tmax and Tmin computed from the observations and the simulated results by the SDSM and the multi-site SD at Seoul station. The autocorrelation values simulated by the multi-site SD are close to those of the observation. The results obtained from the SDSM also show similar values to the observation; however the SDSM underestimates the autocorrelations compared to the observation and the multi-site SD method.

In order to examine temporal dependency over South Korea, the autocorrelation values are computed for all 25 stations and the results of Tmax and Tmin are presented in Figures 5.13 and 5.14 respectively. Each graph represents the autocorrelations at all 25 stations. Red squares and blue circles indicate the observed versus simulated autocorrelations for the SDSM and the multi-site SD method respectively. If the simulated autocorrelation is similar to the observed one, the data point lies closer to the diagonal line. Similar to results shown in Seoul station, the autocorrelations computed from the multi-site SD match well with the observation. There is a discrepancy between the observations and the results from the SDSM. The SDSM underestimates the autocorrelations at all 25 stations compared to both the observation and the multi-site SD method.

	Tmax			Tmin		
Serial Autocorrelation	SDSM	Multi-SD	OBS	SDSM	Multi-SD	OBS
lag1_Calibration	0.91	0.95	0.96	0.92	0.96	0.97
lag2_Calibration	0.89	0.91	0.92	0.91	0.92	0.94
lag3_Calibration	0.88	0.89	0.90	0.90	0.91	0.93
lag1_Validation	0.91	0.95	0.96	0.93	0.96	0.97
lag2_Validation	0.90	0.91	0.92	0.91	0.93	0.95
lag3_Validation	0.89	0.90	0.90	0.91	0.91	0.93

Table 5.9 Serial autocorrelation of lag 1 to 3 for Tmax and Tmin computed from the observations and the simulated results by the SDSM and the multi-site SD method at Seoul station for the calibration and validation periods

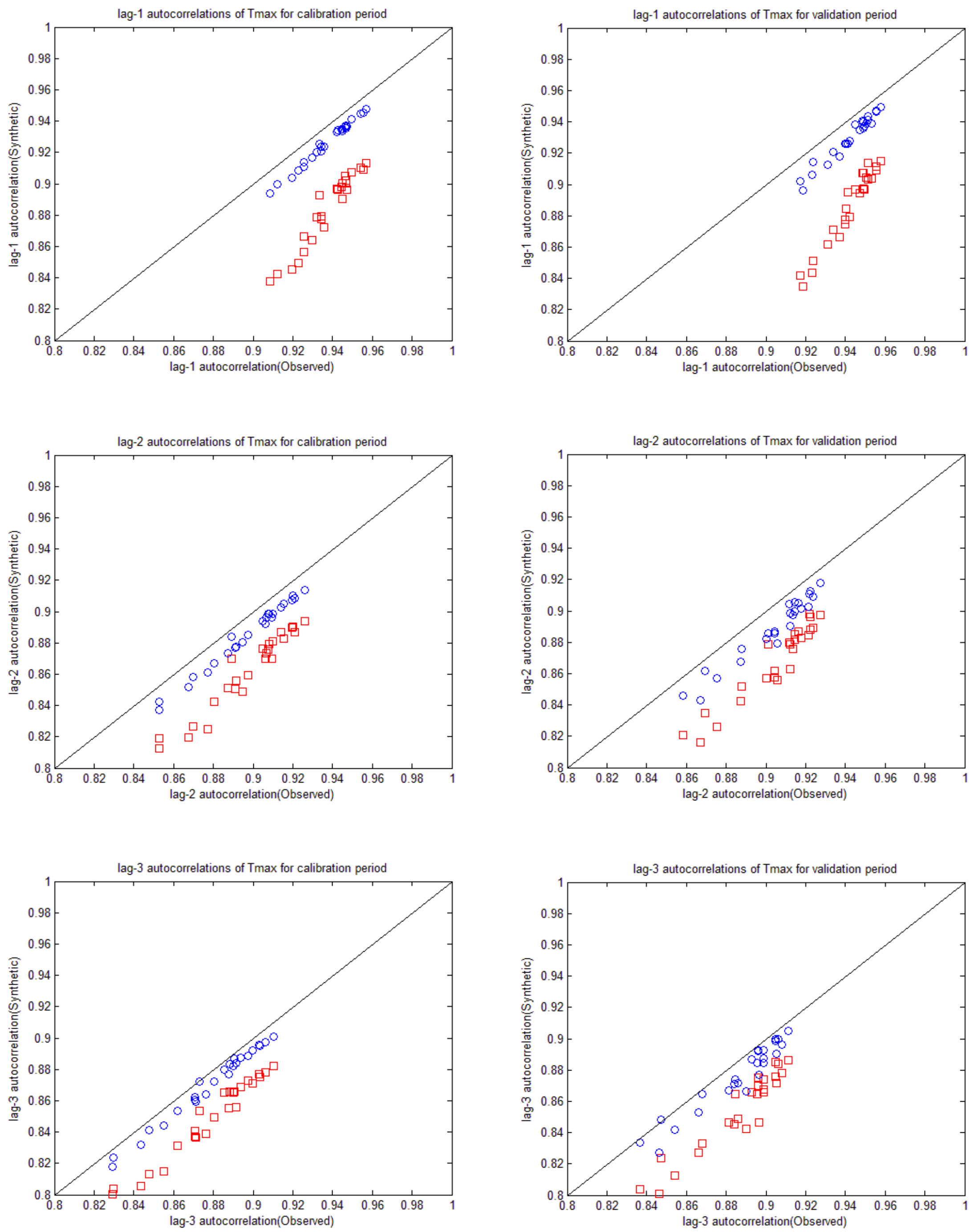

Figure 5.13 Lag 1 to 3 autocorrelations of Tmax computed from the observations and the simulated results by the SDSM (red square) and the multi-site SD method (blue circle) for the calibration period (1985-2001) (right) and the validation period (1973-1984) (left)

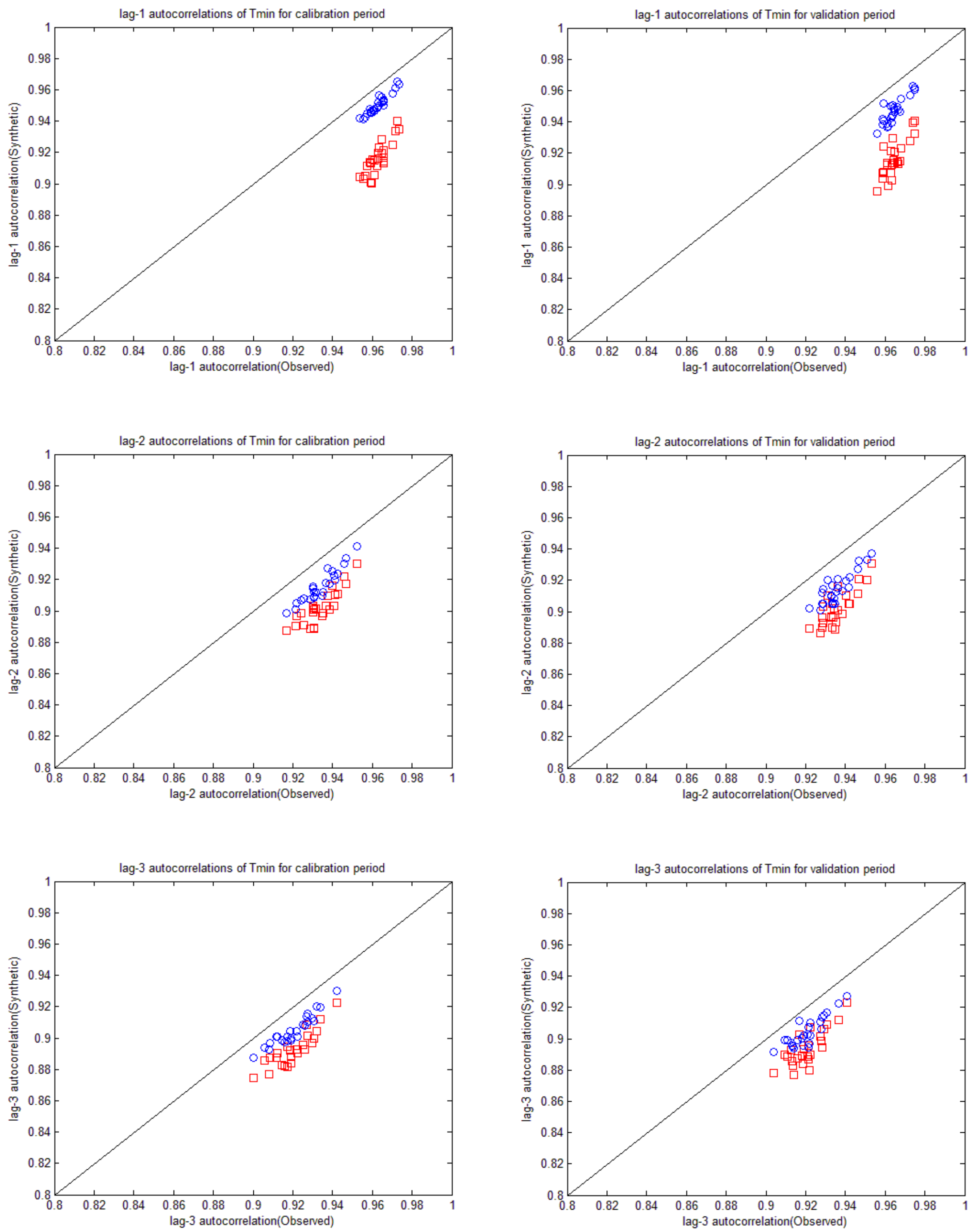

Figure 5.14 Lag 1 to 3 autocorrelations of Tmin computed from the observations and the simulated results by the SDSM (red square) and the multi-site SD method (blue circle) for the calibration period (1985-2001) (right) and the validation period (1973-1984) (left)

5.3.3 Spatial Dependency

Inter-station correlations of Tmax and Tmin are used to examine the spatial dependency in temperature data. Figures 5.15 to 5.19 show the inter-stations correlations of the observations and the simulated results by the SDSM and the multi-site SD method. Each graph represents the inter-station correlations of the 300 pairs of stations in each month. Red squares and blue circles represent the observed versus simulated the inter-station correlations for the SDSM and the multi-site SD method respectively. If the simulated correlations are similar to the observed one then the data points lie closer to the diagonal line.

While the data points of the multi-site SD method lie on the diagonal line for Tmax and Tmin, the data points of the SDSM lie far below the diagonal line. It is clearly shown in Figures 5.15 to 5.19 that the SDSM under-estimates the inter-station correlations but the multi-site SD method accurately predicts the correlations in pairs of stations. In the other words, the SDSM significantly underestimates the spatial dependency in the observed Tmax and Tmin. However, the multi-site SD method takes into account the realistic spatial dependency observed over South Korea.

Overall in this chapter, the results demonstrate that the SDSM performs reasonably well on reproducing statistical properties of Tmax and Tmin, and the temporal dependency, but it misses the realistic spatial dependency. Ignoring the spatial dependency in weather data influences the reliability of impact assessment studies. Therefore, it is better to use the multi-site SD method to account the spatial dependency in stations.

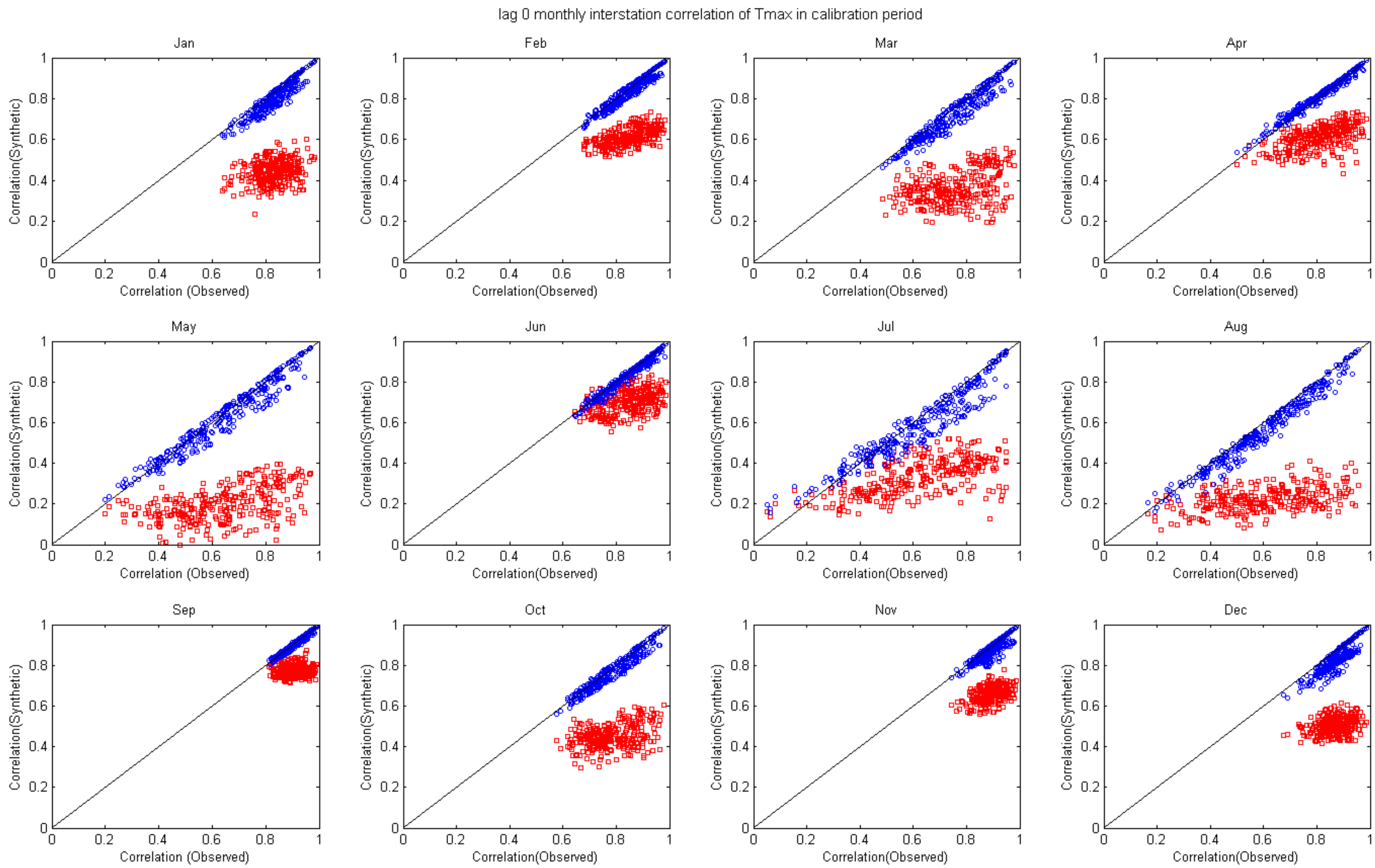

Figure 5.15 Observed versus simulated monthly inter-station correlations of Tmax by the SDSM (red square) and the multi-site SD method (blue circle) for the calibration period (1985-2001)

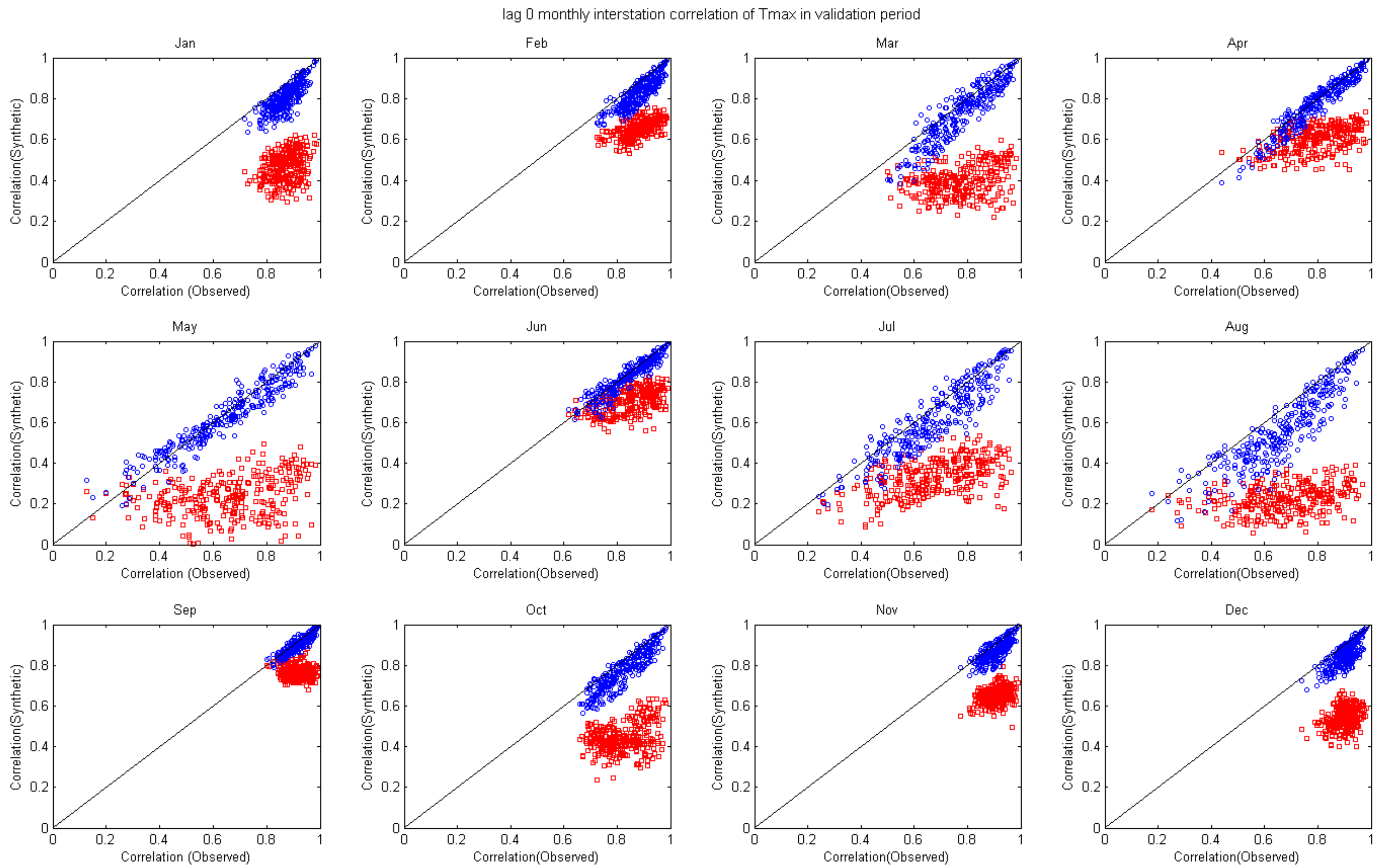

Figure 5.16 Observed versus simulated monthly inter-station correlations of Tmax by the SDSM (red square) and the multi-site SD method (blue circle) for the validation period (1973-1984)

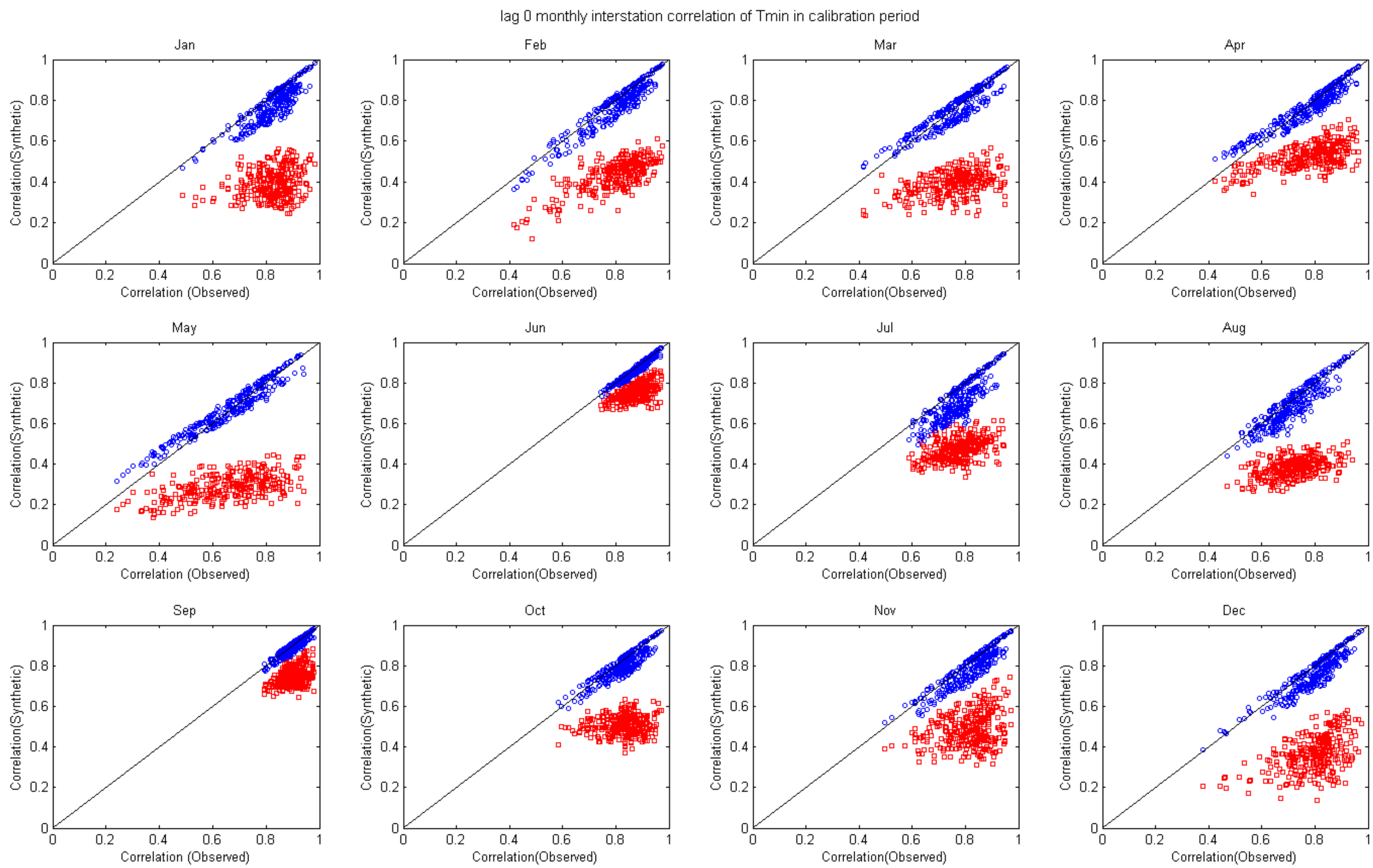

Figure 5.17 Observed versus simulated monthly inter-station correlations of Tmin by the SDSM (red square) and the multi-site SD method (blue circle) for the calibration period (1985-2001)

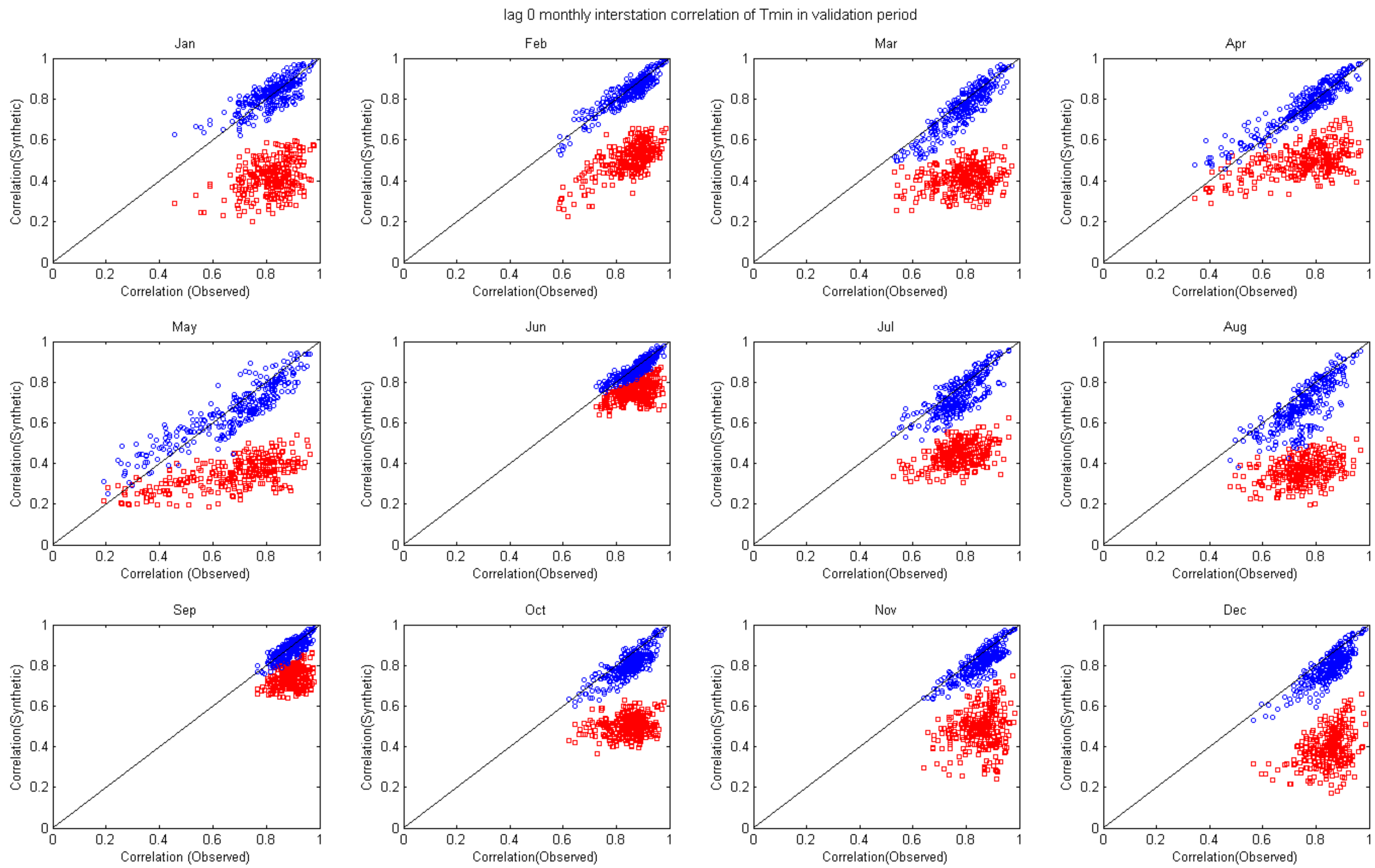

Figure 5.18 Observed versus simulated monthly inter-station correlations of Tmin by the SDSM (red square) and the multi-site SD method (blue circle) for the validation period (1973-1984)

6. PREDICTION OF FUTURE TEMPERATURE EXTREMES

This chapter proivdes the prediction of Tmax and Tmin using the multi-site SD method for the future period 2010-2100. The prediction is based on the A1B and A2 emission scenarios provided from the CGCM3.

Similar to the generation of the synthetic current temperature extremes, the synthetic future temperature extremes are computed by adding the deterministic components to the stochastic components. However, the regression models for future prediction require replacing atmospheric predictors of the NCEP into predictor of the CGCM3. The deterministic components are computed from the regression models using the GGCM3 predictors. For the stochastic components, the residual matrix simulated to generate the current temperature is used.

6.1 Prediction of Future Tmax

The following results are based on 100 simulation of daily Tmax and Tmin. The changes in temperature chrateristics are observed by four indices: monthly means and standard deviations (STDs) of Tmax and Tmin, monthly 90th percentiles of Tmax (Tmax90ps), and monthly10th percentiles of Tmin (Tmin10ps).

Figure 6.1 shows monthly means and STDs of Tmax and monthly Tmax90ps during the period 2010-2100 at Seoul station compared to the observation (1973-2001). From the figures, the increasing trends in all three indices are observed under both the A1B and A2 scenarios while the trends are no obvious for monthly STDs of Tmax.

In order to predict future temperature over South Korea, the indices are computed for 25 weather stations. Figure 6.1 to 6.3 display boxplots of Tmax indices in four months: January, April, July and October, representing the four different seasons of a year. Each boxplot represents monthly Tmax indices aggregated at all 25 stations. The positive trends are very obvious for monthly means of Tmax and monthly Tmax90ps. For monthly

STDs of Tmax, the simulated future monthly STDs are larger than the current values but no significant increases are detected in all four months.

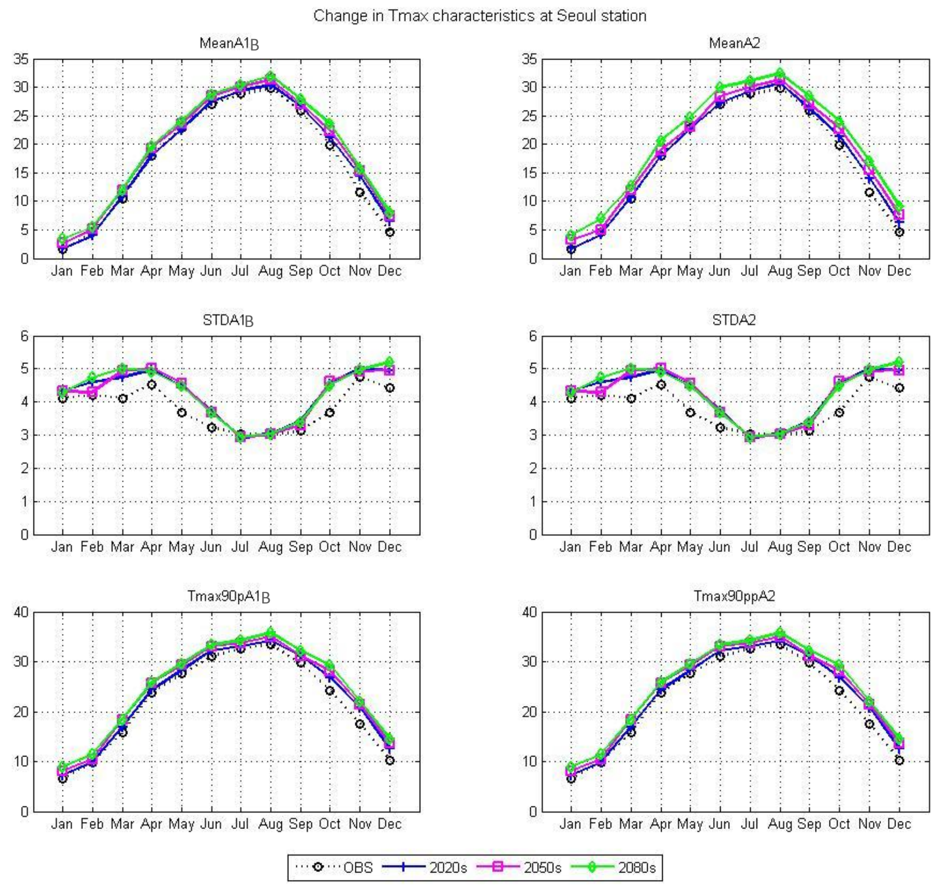

Figure 6.1 Prediction of monthly means and STDs of Tmax and monthly Tmax90ps at Seoul station for the preriod 2010-2100

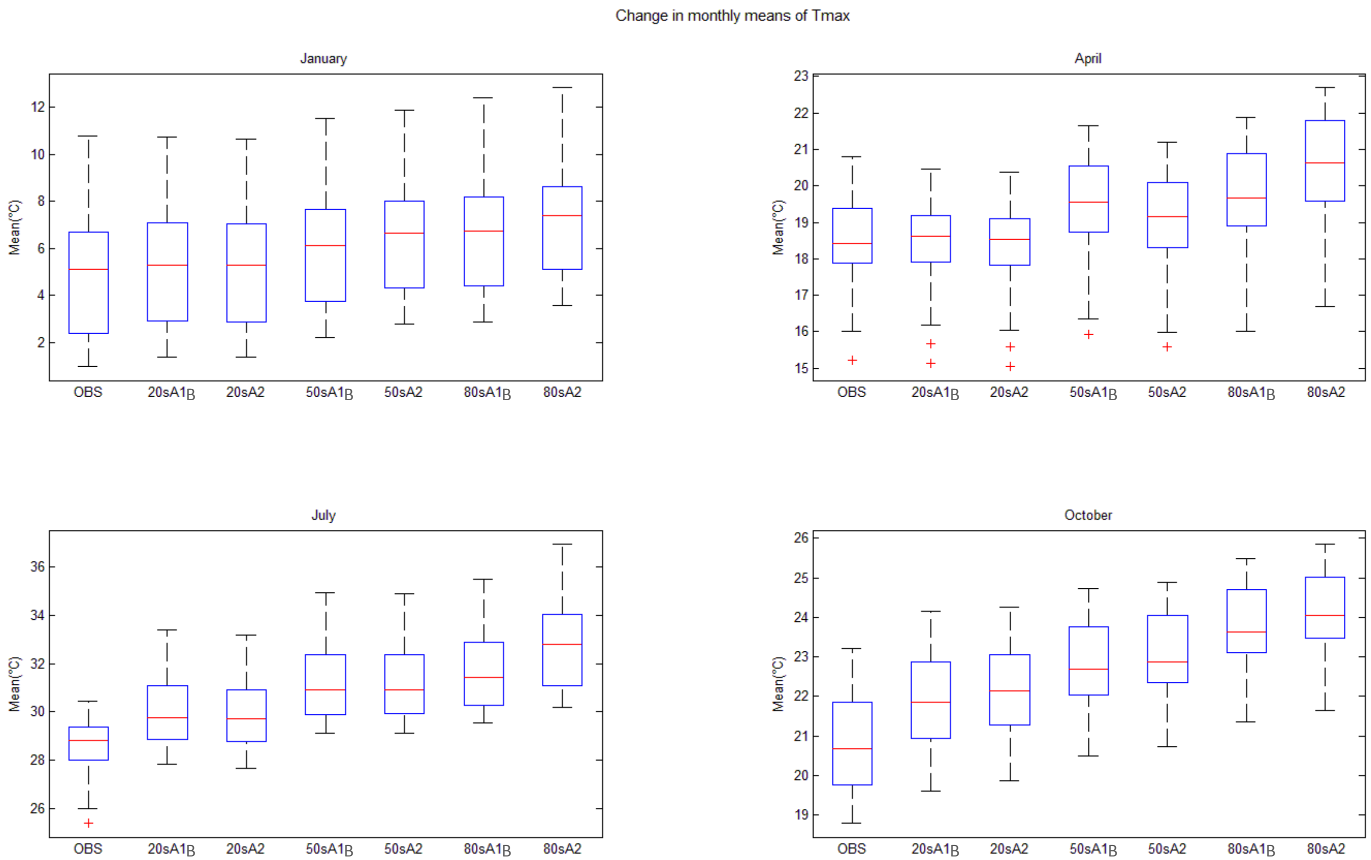

Figure 6.2 Prediction of monthly means of Tmax for the preriod 2010-2100 at all stations in January, April, Julay and October

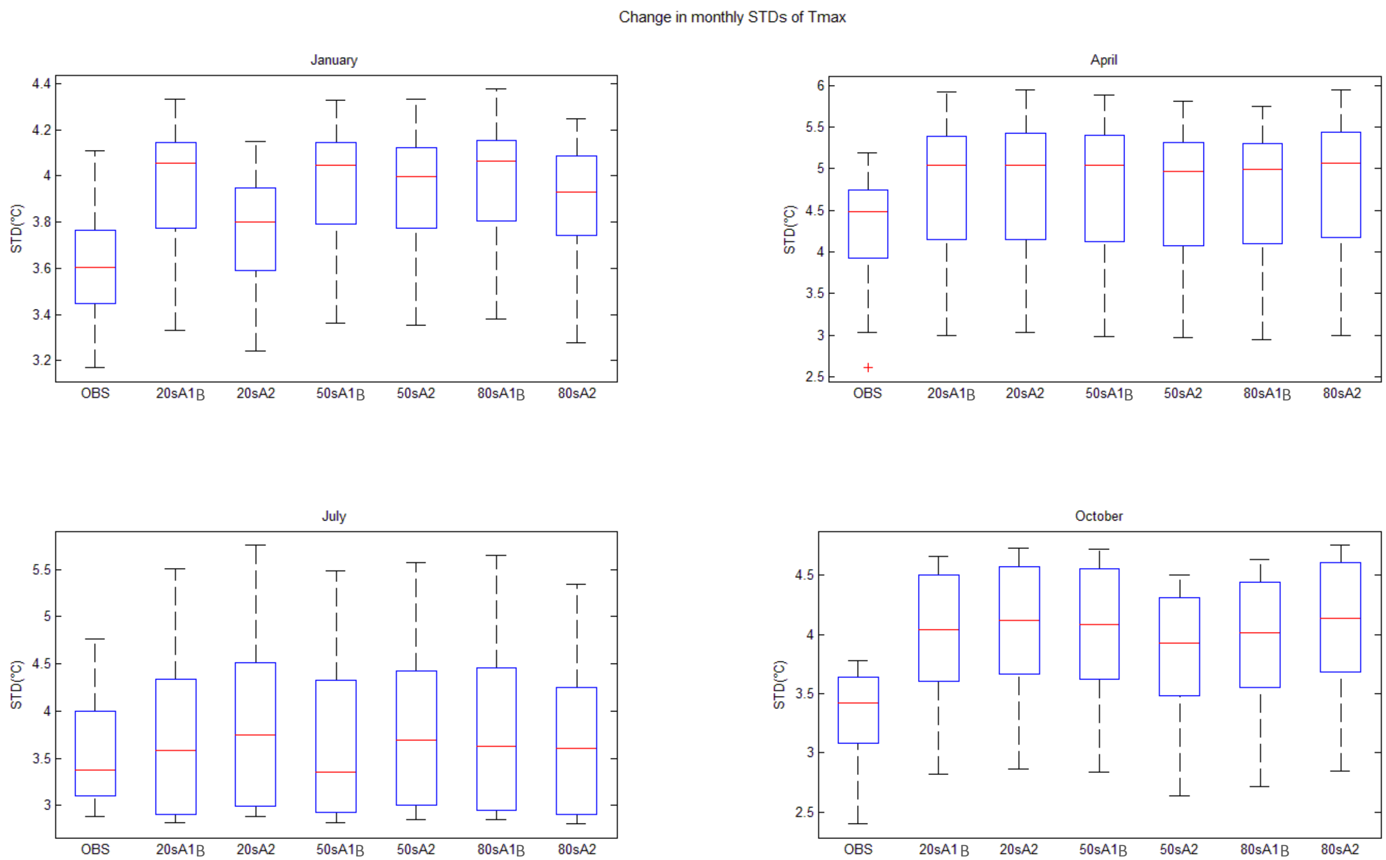

Figure 6.3 Prediction of monthly STDs of Tmax for the preriod 2010-2100 at all stations in January, April, Julay and October

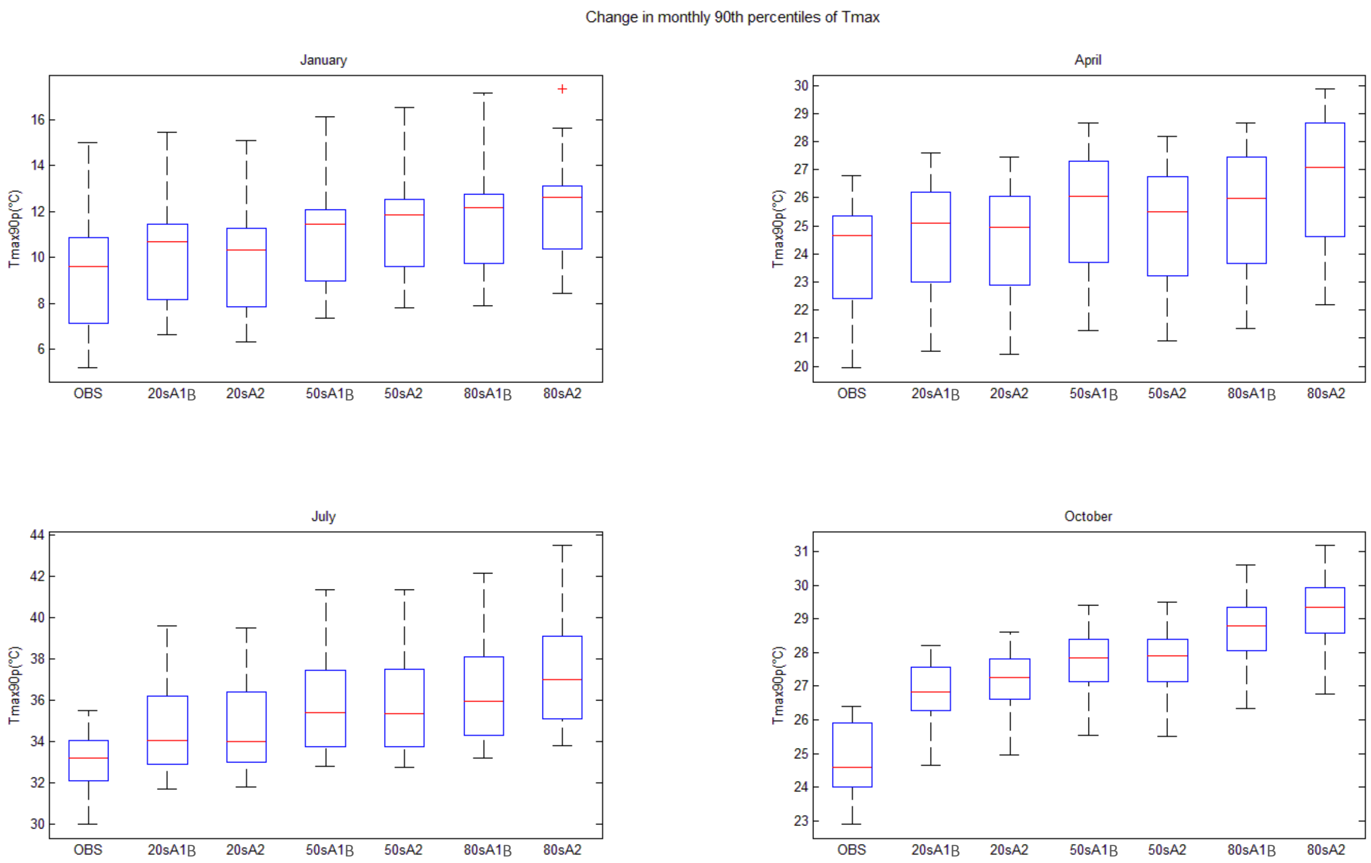

Figure 6.4 Prediction of monthly Tmax90ps for the preriod 2010-2100 at all stations in January, April, Julay and October

6.1 Prediction of Future Tmin

Figure 6.5 shows monthly means and STDs of Tmin and monthly Tmin10ps during the period 2010-2100 at Seoul station compared to the observation (1973-2001). Similar to the results obtained from monthly means of Tmax, the increasing trends are found in all three indices under both of the A1B and A2 scenarios while the trends are no obvious for monthly STDs of Tmin.

In order to predict future temperature over South Korea, Figure 6.1 to 6.3 display boxplots of Tmin indices at 25 stations in four months: January, April, July and October. The significant positive trends are detected for monthly means of Tmin and monthly Tmin10ps. Yet, the increasing trends in monthly STDs of Tmin are not obvious in all four months.

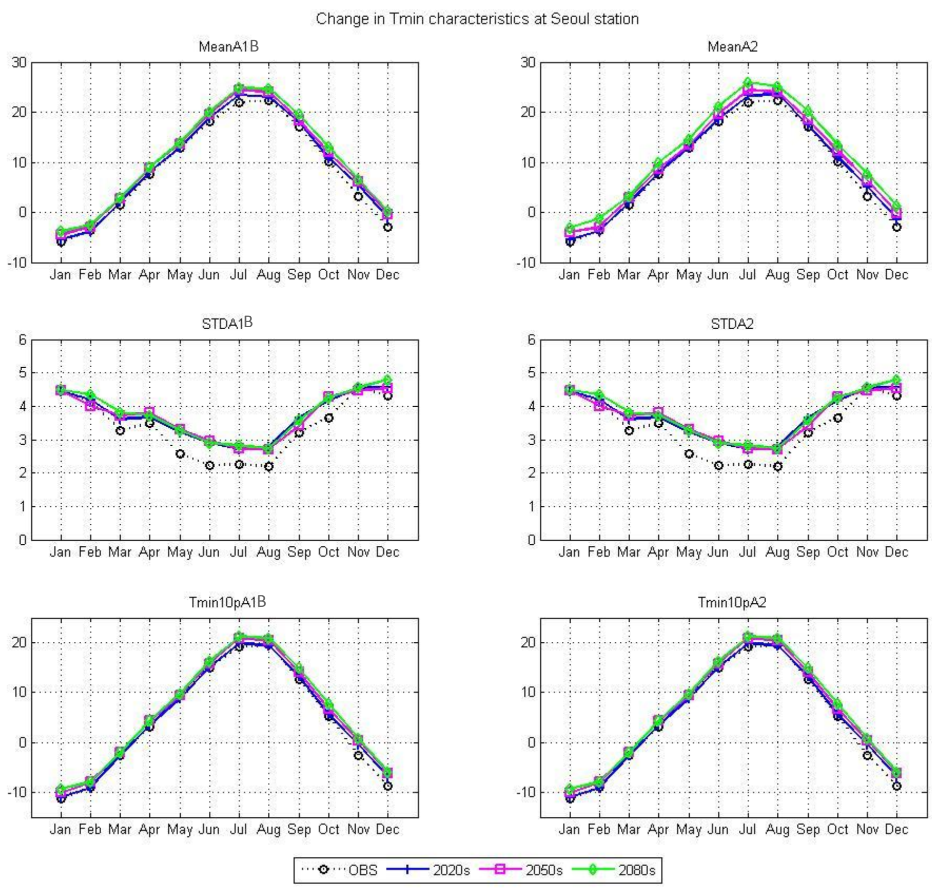

Figure 6.5 Prediction of monthly means and STDs of Tmin and monthly Tmin10ps at Seoul station for the preriod 2001-2100

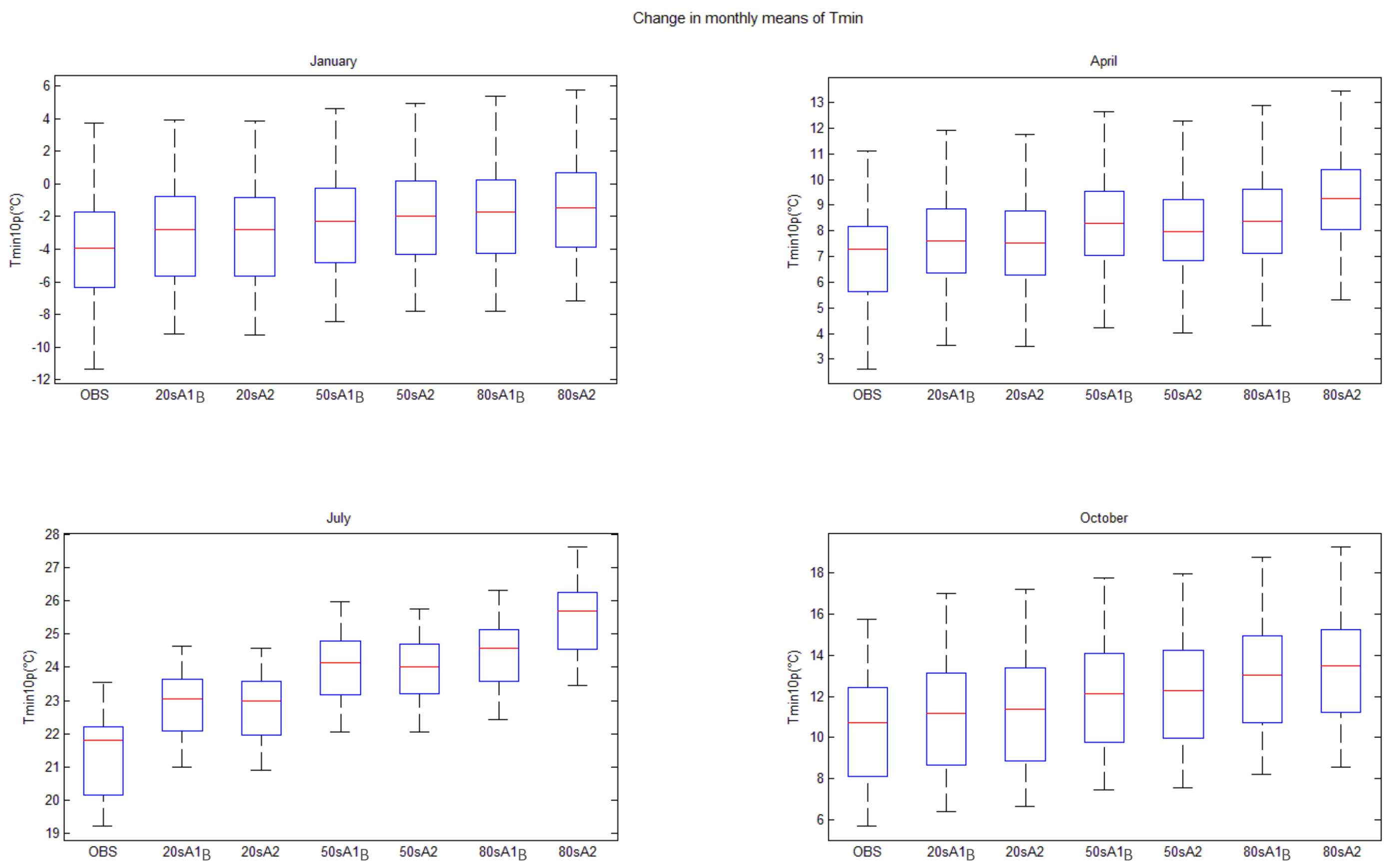

Figure 6.6 Prediction of monthly means of Tmin for the preriod 2010-2100 at all stations in January, April, Julay and October

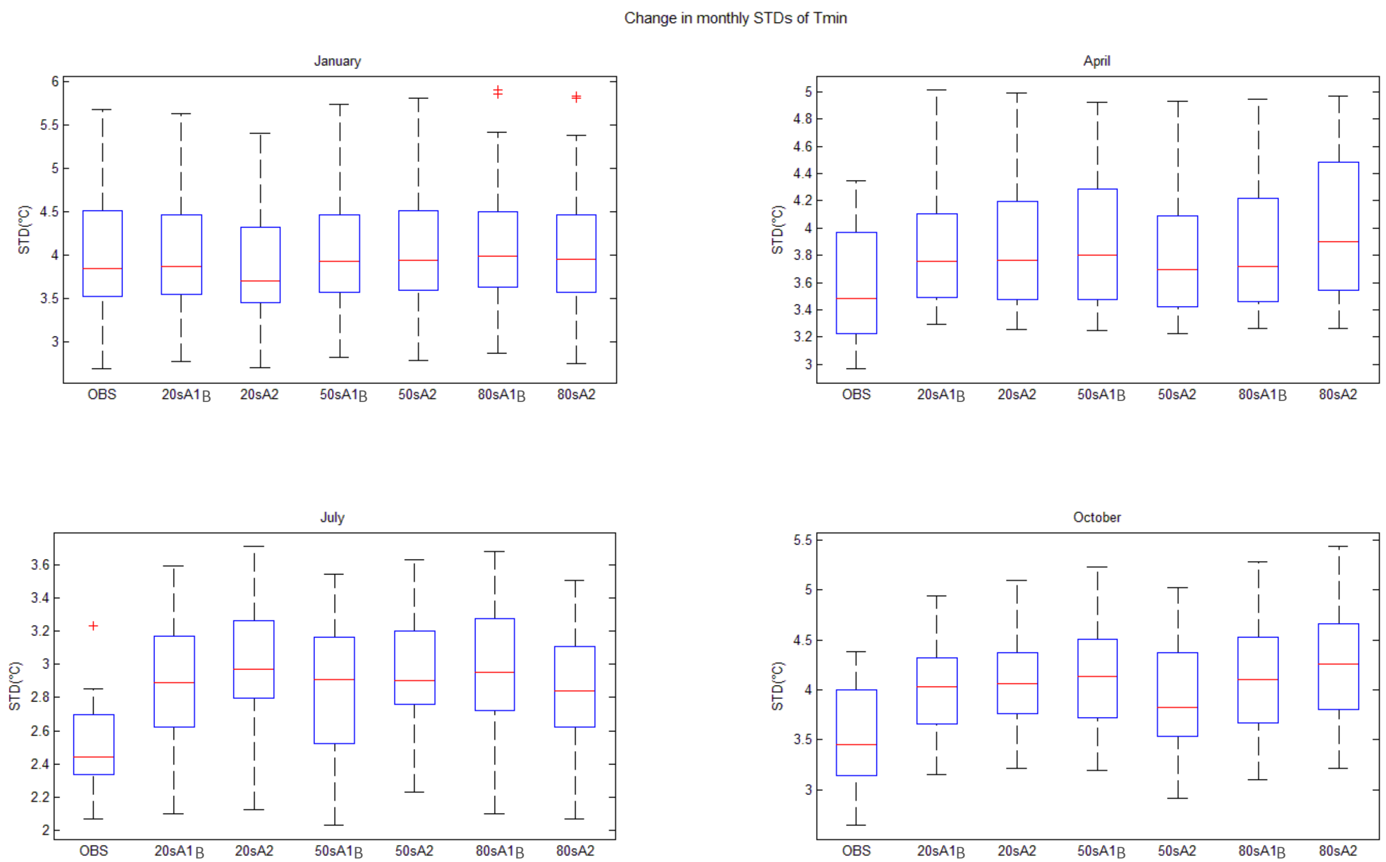

Figure 6.7 Prediction of monthly STDs of Tmin for the preriod 2010-2100 at all stations in January, April, Julay and October

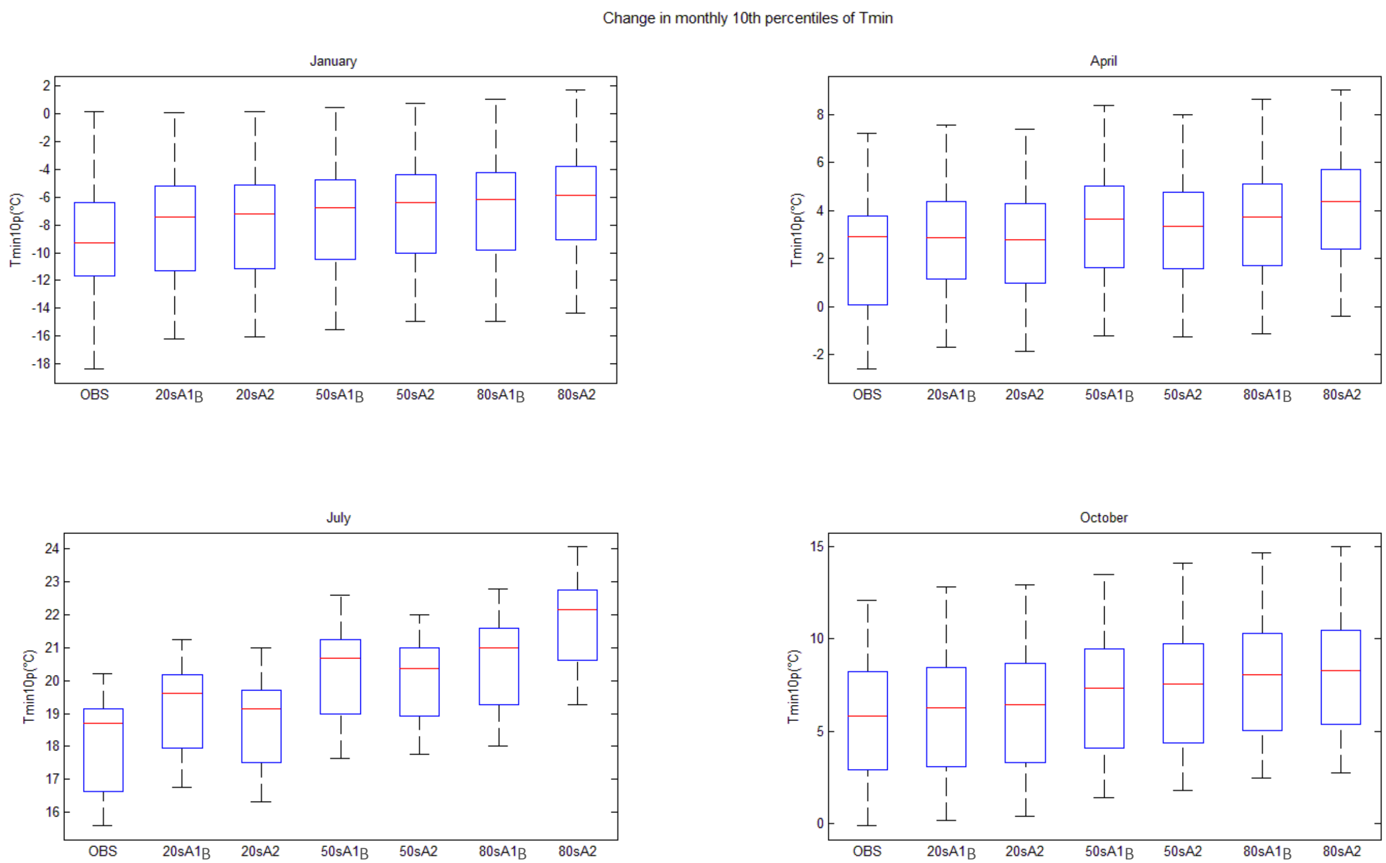

Figure 6.8 Prediction of monthly Tmin10ps for the preriod 2010-2100 at all stations in January, April, Julay and October

Overall in this chapter, the remarkably positive trends of monthly means of Tmax and Tmin, monthly 90th percentiles of Tmax and monthly 10th percentiles of Tmin were found during the period 2010-2100 at most of 25 weather stations over the country. These results indicated that South Korea region could likely experience hotter summer and warmer winter for the next century based on both A1B and A2 climate scenarios.

7. CONCLUSIONS AND RECOMMENDATIONS FOR FURTHER STUDIES

7.1 Conclusions

The following conclusions can be drawn from this study:

1. Evidences of temperature changes were detected by a detailed statistical analysis of the trends in a total of 18 temperature indices, which were computed using the daily extreme temperature data available from a network of 25 stations in South Korea for the 1973-2009 period. The slopes of the trends were computed by the least squares fitting. The statistical significances of the trends were analyzed using the Mann-Kendall test. The significant changes in Tmax and Tmin characteristics were found for most of the stations. In particular, the significant positive trends were identified for the annual means of Tmax and Tmin at the 95% confidence level. In addition, the number of cold events tends to decrease while the number of warm events tends to increase at many stations.
2. The present study was the first study that provided a detailed comparison between the performance of a SVD-based multi-site SD method and the performance of the popular single-site SDSM. On the basis of this comparison, the strength and weakness of each of these two methods could be identified. This could allow a selection of the best method for high-quality climate impact assessment studies..
3. Results of this comparative study using the observed daily extreme temperature data and NCEP re-analysis data for South Korea have indicated the superior performance of the SVD-based multi-site SD method in terms of the accurate reproduction of the basic statistical properties, the temporal correlation at each site, and the between-site spatial correlations of the daily extreme temperature series. In particular, the popular single-site SDSM was not able to capture the spatial dependence of temperature extremes between different sites.
4. Result of the predictions of daily temperature extremes using the SVD-based multi-site SD method under the A1B and A2 climate scenarios given by the CGCM3 have indicated significant changes in the characteristics of daily

temperature extremes in South Korea for the 2010-2100 period. In particular, the increasing trends were found for monthly means of Tmax and Tmin, monthly 90th percentiles of Tmax and monthly 10th percentiles of Tmin during this period in the future.

7.2 Recommendations for Further Research

For further studies, it is recommended that

1. The performance of the proposed SVD-based multi-site SD method could be compared with those of other existing multi-site SD techniques such as the multi-site Artificial Neural Network procedure in order to determine the best method for climate change impact assessment studies.
2. The predictions of daily temperature extremes for future periods should be performed using the climate change scenarios given by other GCMs such as the UK HadCM3 or the German ECHAM5 in order to assess the reliability and uncertainty of these predictions.
3. Similar studies using data from different climatic conditions should be performed in order to assess the accuracy and reliability of these downscaling procedures.

REFERENCES:

Achen, C.H. 2000. Why Lagged Dependent Variable can Suppress the Explanatory Power of Other Independent Variables. Working paper, Society of Political Meteodology, St Louis, W.A., Accessed from http://www.polmeth.wustl.edu/media/Paper/achen00.pdf.

Alexander L.V., Zhang, X., Peterson, T.C, Caesar, J., Gleason, B., Klein Tank, A.M.G., Haylock, M., Collins, D.,Trewin, B., Rahimzadeh, F., Tagipour, A., Ambenje, P., Rupa Kumar, K., Revadekar, J. and Griffiths, G. 2006. Global Observed Changes in Daily Climate Extremes of Temperature and Precipitation. *J. Geophys. Res,* 111, D05109.

Bardossy, A. and Plate, E.J. 1992. A Bardossy and E.J Plate, Space-time Model for Daily Rainfall using Atmospheric Circulation Patterns. *Water Resources Research*, 28, 1247–1259.

Buerger, G. and Chen, Y. 2005. Regression-based downscaling of spatial variability for hydrologic applications. *J. Hydrology***,** 311, 299-317.

Busuioc, A., Tomozeiu, R. and Cacciamani, C. 2008. Statistical Downscaling Model based on Canonical Correlation Analysis for Sinter Extreme Precipitation Events in the Emilia–Romagna region. *Int J Climatol*, 28, 449–464.

Cannon, A.J. 2008. Probabilistic Multisite Precipitation Downscaling by an Expanded Bernoulli–Gamma Density Network. *J. Hydrometeorology*, 9, 1284-1300.

Cavadias, G.S. 1985. A Multivariate Seasonal Model for Streamflow Simulation*: Symposium on the research of hydrology in Quebe*c, 23, May 1985, Montreal, Quebec.

Chaleeraktrakoon, C. 1995. Stochastic modelling and simulation of streamflow processes: Ph.D. thesis, *Department of Civil Engineering and Applied Mechanics*, McGill University, Montreal, Quebec, Canada, 236 pp.

Chandler, R.E. and Wheater, H.S. 2002. Analysis of Rainfall Variability using Generalized Linear Models: A case study from the west of Ireland, *Water Resources. Research , 38*(10), 1192.

Charles, S.P., Bates, B.C., Smith, I.N. and Hughes, J.P. 2004. Statistical Downscaling of Daily Precipitation from Observed and Modelled Atmospheric Fields. *Hydrological Processes,* 18(8), 1373-1394.

Choi, Y., Jung, H.S., Nam, K.Y. and Kwon, W.T. 2003. Adjusting Urban Bias in the Regional Mean Surface Temperature Series of South Korea, 1968-99. *Int J Climatol*, 23, 577-591.

Choi, Y. 2004. Trends on Temperature and Precipitation Extreme Events in Korea. *Journal of the Korean Geographical Society,* 39, 711–721.

Chong, I.G. and Jun, C.H. 2005. Performance of Some Variable Selection Methods when Multicollinearity is Present. *Chemometr. Intell. Lab*., 78,103-112.

Church, J. and White, N. 2006. A 20th Century Acceleration in Global Sea Level Rise. *Geophys. Res. Lett.*, 33, L01602, doi:10.1029/2005GL024826.

Crane, R.G. and Hewitson, B.C. 1998. CO_2 Precipitation Changes for the Susquehanna basin: Downscaling from the GENESIS General Circulation Model. *International Journal of Climatology*, 18, 65–76.

Dibike, Y., Gachon, P., St-Hilaire, A., Ouarda, T.B.M.J. and Nguyen, V.T.V. 2008. Uncertainty Analysis of Statistically Downscaled Temperature and Precipitation Regimes in Northern Canada. *Theor Appl Climatol*, 91(1-4), 149-170.

Easterling, D.R., Evans, J. L., Groisman, P. Y., Karl, T. R., Kunkel, K. E. and Ambenje, P. 2000. Observed Variability and Trends in Extreme Climate events: A brief review. *Bull.Am. Meteorol*. Soc. 81, 417–425.

EPA. 2007. Inventory of U.S. Greenhouse Gas Emissions and Sinks 1990-2005. US EPA, Washington, D.C. U.S.A..

Frich, P., Alexander, L. V., Della-Marta, P., Gleason, B., Haylock, M., Tank, A. M.G.K. and Peterson, T. 2002. Observed Coherent Changes in Climatic Extremes during the Second Half of the Twentieth Century. *Climate Res.*,19, 193-212.

Golun, G.H., and Reinsch, C., 1970. Singular Value Decomposition and Least Squares Solutions. *Numerische. Mathematik.*, 14, 403-420.

Goodess C.M., Hulme, M. and Osborn, T. 2001. The Identification and Evaluation of Suitable Scenario Development Methods for the Estimation of Future Probabilities of Extreme Weather Events. *Tyndall Centre Working Paper 6.*

Harpham, C. and Wilby, R.L. 2005. Multi-site Downscaling of Heavy Daily Precipitation Occurrence and Amounts. *J. Hydrology* , 312, 235-255.

Held, I.M., and Soden, B.J. 2000. Water Vapor Feedback and Global Warming. *Annu.Rev. Energy Environ*., 25, 441-475.

Hessami, M., Gachon, P., Ouarda. T.B.M.J. and St-Hilaire, A. 2008. Automated regression-based Statistical Downscaling Tool. *Environmental Modelling & Software*, 23, 813-834.

Im, E. S., Jung, I. W. and Bae, D. H. 2011. The Temporal and Spatial Structures of Recent and Future trends in Extreme Indices over Korea from a Regional Climate Projection. *Int J Climatol*, 31,72-86

IPCC. 2001. IPCC Third Assessment Report of the Intergovernmental Panel on Climate Change. *Climate Change 2001*: *The Scientific Basis.* Cambridge University Press, Cambridge, U.K..

IPCC. 2007. IPCC Fourth Assessment Report of the Intergovernmental Panel on Climate Change. *Climate Change 2007*: *The Scientific Basis.* Cambridge University Press, Cambridge, U.K..

Jung, H. S., Choi, Y., Oh, J. H. and Lim, G. H. 2002. Recent Trends in Temperature and Precipitation over South Korea. *Int J Climatol*, 22, 1327-1337.

Kalnay, E., Kanamitsu, M., Kistler, R., Collins, W., Deaven, D., Gandin, L., Iredell, M., Saha, S., White, G., Woollen, J., Zhu, Y., Chelliah, M., Ebisuzaki, W., Higgins, W., Janowiak, J., Mo, K. C., Ropelewski, C., Wang, J., Leetmaa, A., Reynolds, R., Jenne, R. and Joseph, D. 1996. The NCEP/NCAR 40-year Reanalysis Project. *B. Am. Meteorol. Soc.*, 77, 437-471.

Katz, R.W. and Brown, B.G., 1992. Extreme Events in a Changing Climate: Variability is More Important than Averages. *Clim. Change*, 21, 289–302.

Kendall, M.G. 1975. Rank Correlation Methods, Charles Griffin & Co., London, p.202

Klein, Tank A.M.G. and Können G.P. 2003. Trends in Indices of Daily Temperature and Precipitation Extremes in Europe, 1946-99. *J. Climat*e, 16, 3560-3571.

Kilsby, C. G., Jones P. D., Urton, A., Ford, A. C., Fowler, H. J., Harpham, C., James, P., Smith, A. and Wilby, R. L. 2007. A Daily Weather Generator for Use in Climate Change Studies. *Environmental Modelling and Software*, 22(12), 1705-1719.

Khalili,M., Leconte, R. and Brissette, F. 2006. Efficient Watershed Modeling using a Multi-site Weather Generator for Meteorological Data. *Geo-Environment and Landscape Evolution II. Transaction of Wessex Institute of Technology*, UK, D. 89, pp. 273-281.

Khalili, M., and Nguyen, V-T-V. 2012. A Statistical Approach to Multisite Multivariate Downscaling of Daily Extreme Temperature Series for Climate-Related Impact Assessment Studies, Proceedings of the 10th International Conference on Hydroinformatics, July 14-18, 2012, Hamburg, Germany, 8 pages.

Kunkel, K.E., Easterling, D.R., Redmond, K.T. and Hubbard, K.G. 2004. Temporal Trends in Frost-free Season in the United States: 1895-2000. *Geophys, Res. Lett.*, 31, DOI: Artn L03201Doi 10.1029/2003gl018624.

Kwon, W.T. 2005. Current Status and Perspectives of Climate Change Sciences. *Journal of Korean Meteorological Society* , 41, 325–336.

Mann, H.B. 1954. Nonparametric Tests against Trend. *Econometrica*,13, 245-259

Mann, M.E., Bradley, R.S., and Hughes, M.K. 1999. Northern Hemisphere Temperatures during the Past Millennium: Inferences, Uncertainties, and Limitations. *Geophys, Res. Lett.*, 26, 759-762.

Maraun, D., Rust H.W. and Osborn, T.J. 2010. Synoptic Airflow and UK Daily Precipitation Extremes Development and Validation of a Vector Generalised Linear Model. *Extremes*, 13(2), 133-153.

Mokssit, A. 2003. Development of Priority Climate Indices for Africa. *A CCL/CLIVAL workshop of the World Meteorological Organization in Mediterranean Climate: Variability and Trends*, Bolle HF (ed.), *Springer*, Berin, 116-123.

Nguyen, V.T.V. 2002. A state-of-the-art Review of Downscaling Methods for Evaluation Change Impacts on the Hydrologic Cycle. *Water Resource Management and Engineering Series*, Research Report. No. WRME03/1, McGill University, Montreal, Quebec, Canada.

Patz, J.A., Engelberg, D. and Last, J. 2000. The Effects of Changing Weather on Public Health. *Annu Rev Public Health*,21,271–307.

Petit, J.R., Jouzel J., Raynaud D., Barkov N.I., Barnola J.-M., Basile I., Bender M., Chappellaz J., Davis M., Delayque G., Delmotte M., Kotlyakov V.M., Legrand M., Lipenkov V.Y., Lorius C., Pepin L., Ritz C., Saltzman E., and Stievenard M.. 1999. Climate and Atmospheric History of the Past 420,000 years from the Vostok Ice Core, Antarctica. *Nature*, 399, 429-436.

Plummer, N., Salinger, M. J., Nicholls, N., Suppiah, R., Hennessy, K. J., Leighton, R. M., Trewin, B., Page, C. M. and Lough, J. M. 1999. Changes in Climate Extremes over the Australian Region and New Zealand during the Twentieth Century. *Climate Change*, 42, 183-202.

Palutikof, J.P., Goodess, C.M., Watkins, S.J. and Holt, T. 2002. Generating Rainfall and Temperature Scenarios at Multiple Sites: examples from the Mediterranean. *Journal of Climate* 15(24), 3529-3548.

Qian, W.H. and Lin, X. 2004. Regional Trends in Recent Temperature Indices in China. *Climate Res.*, 27, 119-134.

Richardson, C. 1981. Stochastic Simulation of Daily Precipitation, Temperature, and Solar Radiation. *Water Resources Researc*, 17, 182-190.

Semenov, M.A. and Barrow, E. 1997. Use of Stochastic Weather Generator in the Development of Climate Change Scenarios. *Climatic Change*, 35, 397-414.

Srikanthan R. and McMahon T.A. 2001. Stochastic Generation of Annual, Monthly and Daily Climate Data: A review. *Hydrology and Earth System Sciences*, 5(4), 653-656.

Vermeer, M., and Rahmstorf, S. 2010. Global Sea Level Linked to Global Temperature. *Proc. Natl. Acad. Sci. U.S.A.*, doi:10.1073/pnas.0907765106, in press.

Vincent, L.A. 1998. A Technique for the Identification of Inhomogeneities in Canadian Temperature Series. *J. Clim.*, 11, 1094–1104.

Vincent, L. A., Peterson, T. C., Barros, V. R., Marino, M. B., Rusticucci, M., Carrasco, G., Ramirez, E., Alves, L. M., Ambrizzi, T., Berlato, M. A., Grimm, A. M. Marengo, J. A., Molion, L., Moncunill, D. F., Rebello, E., Anunciacao, Y. M. T., Quintana, J., Santos, J. L., Baez, J., Coronel, G., Garcia, J., Trebejo, I.,Bidegain, M.,Haylock, M. R. and Karoly, D. 2005. Observed Trends in Indices of Daily Temperature Extremes in South America 1960-2000. *J. Climat*e, 18, 5011-5023.

Walther, G. R., Post, E., Convey, P., Menzel, A., Parmesan, C., Beebee, T. J., Fromentin, J. M., Hoegh-Guldberg, O. and Bairlein, F. 2002. Ecological Responses to Recent Climate Change. *Nature*, 416, 389-395

Wilby, R.L., Dawson, C.W. and Barrow, E.M. 2002. SDSM- A Decision Support Tool for the Assessment of Regional Climate Change Impacts: *Environmental Modeling and Software*, 17,147-159.

Wilby, R.L., Charles S.P., Zorita, E., Timbal, B., Whetton P. and Mearns, L.O. 2004. Guidelines for Use of Climate Scenarios Developed from Statistical Downscaling Methods. *Supporting Material of the Intergovernmental Panel on Climate Change*, available from the DDC of IPCC TGCIA, 27.

Wilby, R. L. and Wigley, T. M. L. 1997. Downscaling General Circulation Model Output: a review of methods and limitations. *Prog. Phys. Geogr*., 21, 530–548.

Wilks, D. S. 1998. Multisite Generalization of a Daily Stochastic Precipitation Generation Model. *J. Hydrol.*, 210, 178– 191

Wold, S., Sjostrom, M. and Eriksson, L. 2001. PLS-Regression: a Basic Tool of Chemometrics. *Chemometr. Intell. Lab.*, 58, 109-130

Yang, C., Chandler R. E., Isham V. S., and Wheater H. S. 2005. Spatial-temporal Rainfall Simulation using Generalized Linear Models. Water Resour. Res., 41, W11415, doi:10.1029/2004WR003739.

Yarnal, B., Comrie, A. C., Frakes, B. and Brown, D. P. 2001. Developments and Prospects in Synoptic Climatology. *Int J Climatol*, 21, 1923-1950.

Zhai, P. and Pan, X. 2003. Trends in Temperature Extremes during 1951-1999 in China. *Geophys, Res. Lett.*, 30, 1913.

APPENDIX A

DATA DESCRIPTION

Station		Location [1]		CGCM grid		Archived Period	
Number	Name	Latitude	Longitude	X	Y	Start	End
1	Seoul	37°34′08″N	126°58′36″E	34	14	1961	2009
2	Incheon	37°29′00″N	126°38′00″E	34	14	1961	2009
3	Suwon	37°16′00″N	127°01′00″E	34	14	1964	2009
4	Uljin	37°00′00″N	129°24′00″E	35	14	1972	2009
5	Gangneung	37°45′00″N	128°54′00″E	35	14	1961	2009
6	Chuncheon	37°52′00″N	127°44′00″E	35	14	1966	2009
7	Inje	38°04′00″N	128°10′00″E	35	14	1973	2009
8	Hongcheon	37°41′33″N	127°52′48″E	35	14	1973	2009
9	Yeongju	36°52′00″N	128°32′00″E	35	14	1973	2009
10	Sokcho	38°12′15″N	128°34′00″E	35	14	1968	2009
11	Cheongju	36°38′00″N	127°29′00″E	34	14	1967	2009
12	Daegu	35°52′00″N	128°36′00″E	35	14	1961	2009
13	Yeosu	34°44′00″N	127°44′00″E	35	15	1961	2009
14	Ulsan	35°33′00″N	129°19′00″E	35	14	1961	2009
15	Mokpo	34°75′89″N	126°38′00″E	34	15	1961	2009
16	Pohang	36°01′56″N	129°21′54″E	35	14	1961	2009
17	Jeonju	35°49′00″N	127°09′00″E	34	14	1961	2009
18	Busan	35°10′46″N	129°04′32″E	35	15	1961	2009
19	Gwangju	35°10′00″N	126°55′00″E	34	15	1961	2009
20	Chupungnyeng	36°13′00″N	128°00′00″E	35	14	1961	2009
21	Hapcheon	35°25′00″N	127°55′00″E	35	14	1973	2009
22	Jinju	35°12′00″N	128°05′00″E	35	15	1970	2009
23	Jeju	33°30′00″N	126°31′00″E	34	15	1961	2009
24	Seogwipo	33°15′10″N	126°33′40″E	34	15	1961	2009
25	Ulleung	37°30′00″N	130°52′00″E	35	14	1961	2009

Table A.1 Information of 25 weather stations over South Korea

APPENDIX B

ANALYSES OF TEMPERATURE EXTREMS

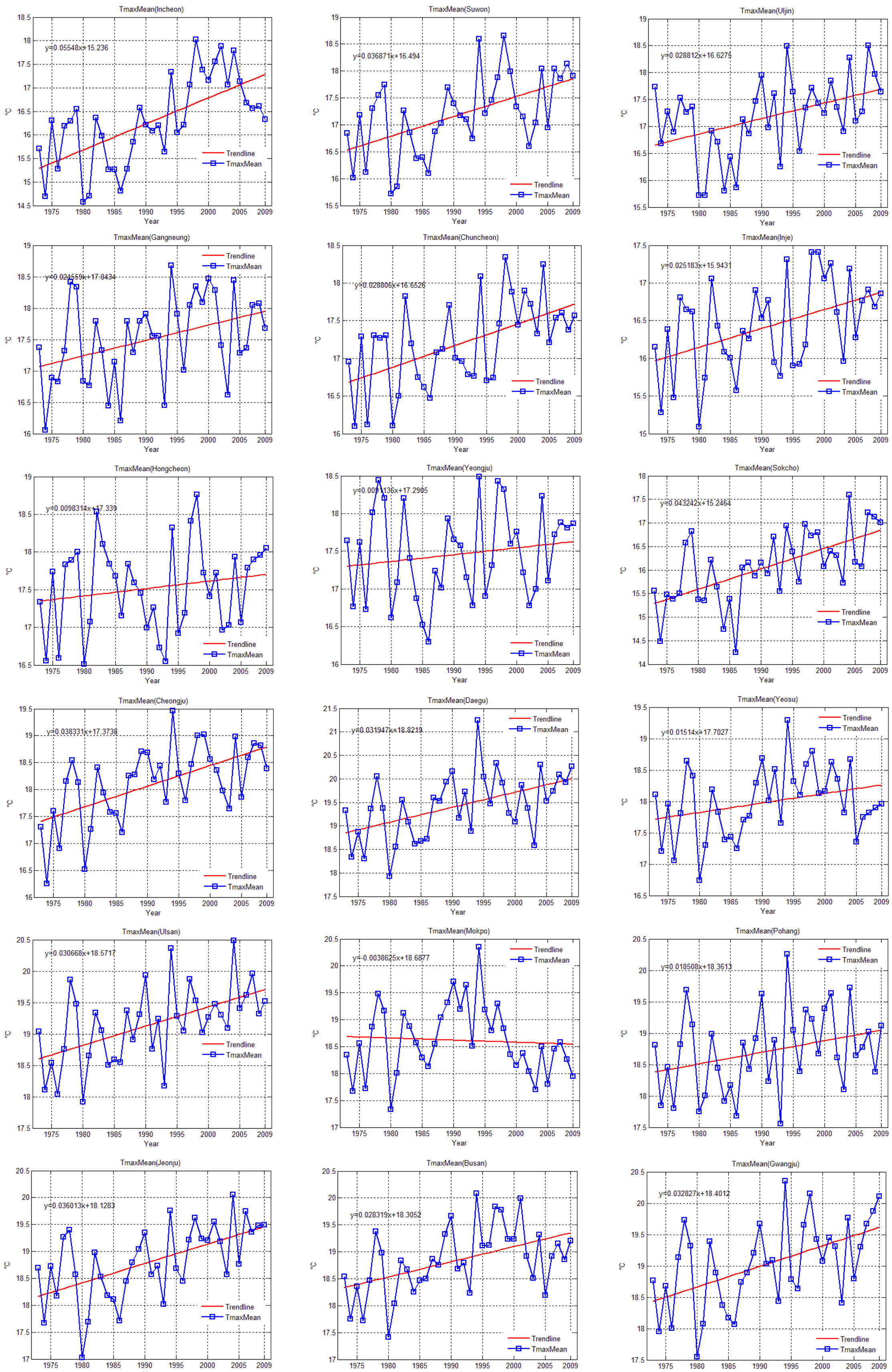
TmaxMean(Incheon)
y=0.05548x+15.236
TmaxMean(Suwon)
y=0.036871x+16.494
TmaxMean(Uljin)
y=0.028812x+16.6275
TmaxMean(Gangneung)
y=0.024559x+17.0434
TmaxMean(Chuncheon)
y=0.028806x+16.6526
TmaxMean(Inje)
y=0.025183x+15.9431
TmaxMean(Hongcheon)
y=0.0098314x+17.339
TmaxMean(Yeongju)
y=0.009136x+17.2905
TmaxMean(Sokcho)
y=0.043242x+15.2464
TmaxMean(Cheongju)
y=0.038331x+17.3738
TmaxMean(Daegu)
y=0.031947x+18.8219
TmaxMean(Yeosu)
y=0.01514x+17.7027
TmaxMean(Ulsan)
y=0.030668x+18.5717
TmaxMean(Mokpo)
y=-0.0038625x+18.6877
TmaxMean(Pohang)
y=0.018508x+18.3613
TmaxMean(Jeonju)
y=0.036013x+18.1283
TmaxMean(Busan)
y=0.028319x+18.3052
TmaxMean(Gwangju)
y=0.032827x+18.4012
Trendline
TmaxMean
Year
°C

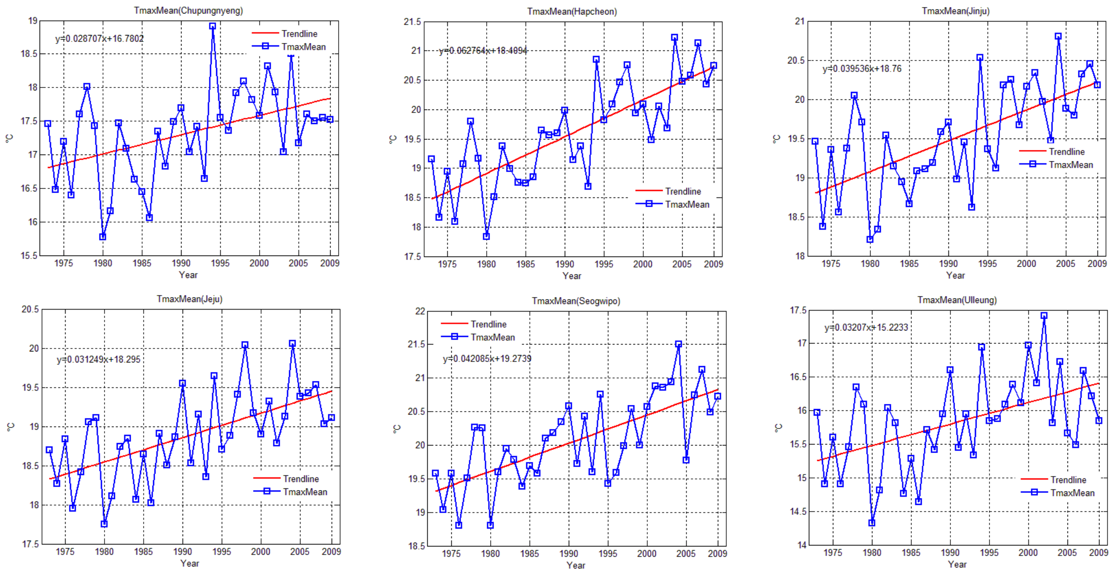

Figure B.1 TmaxMean at 24 stations

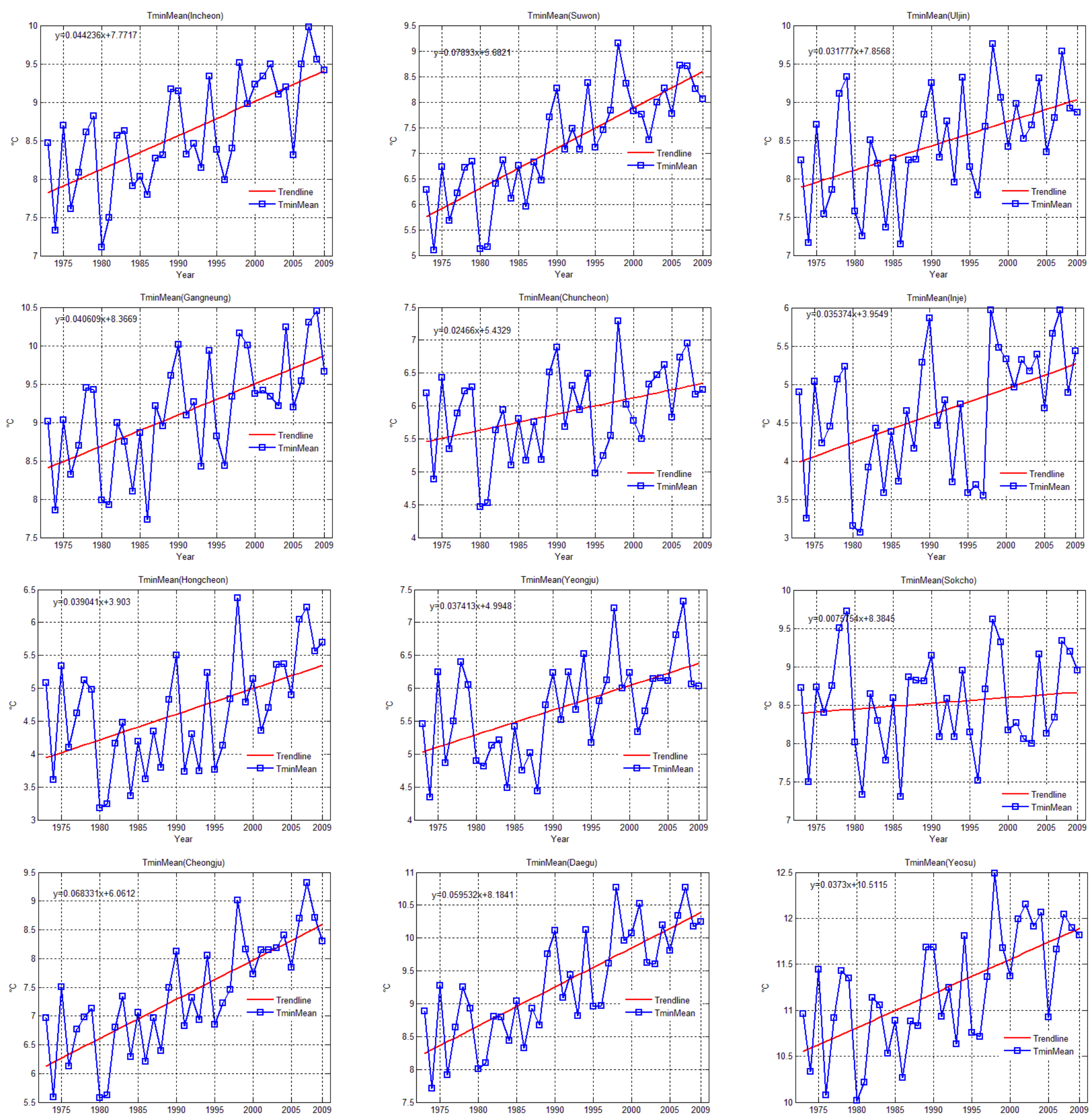

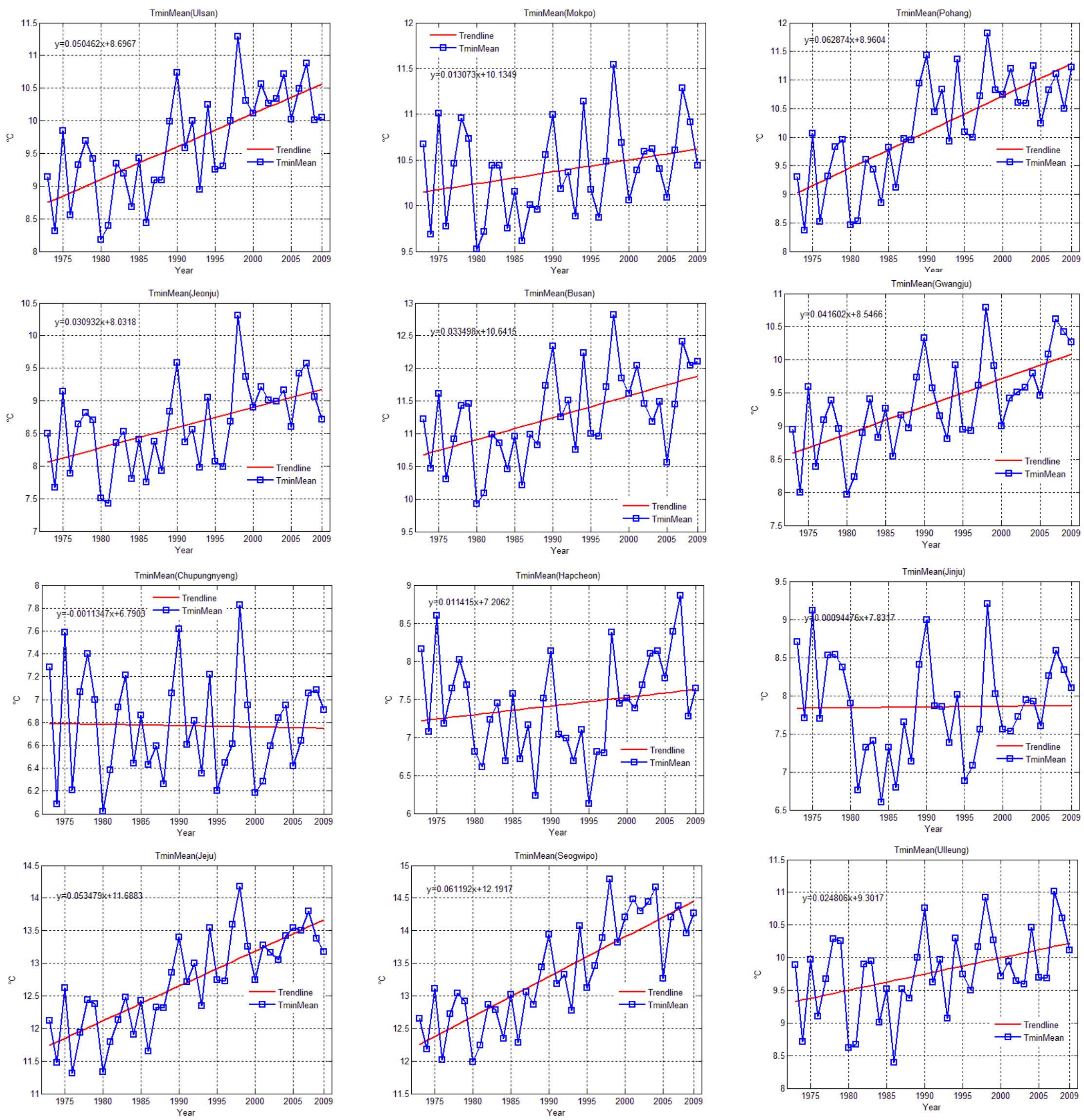

Figure B.2 TminMean at 24 stations

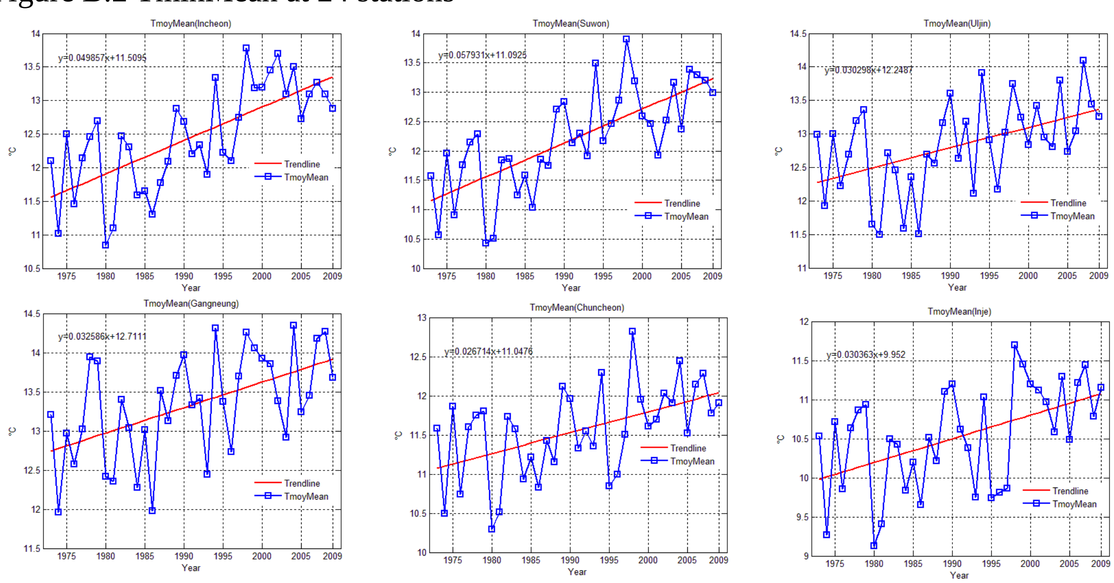

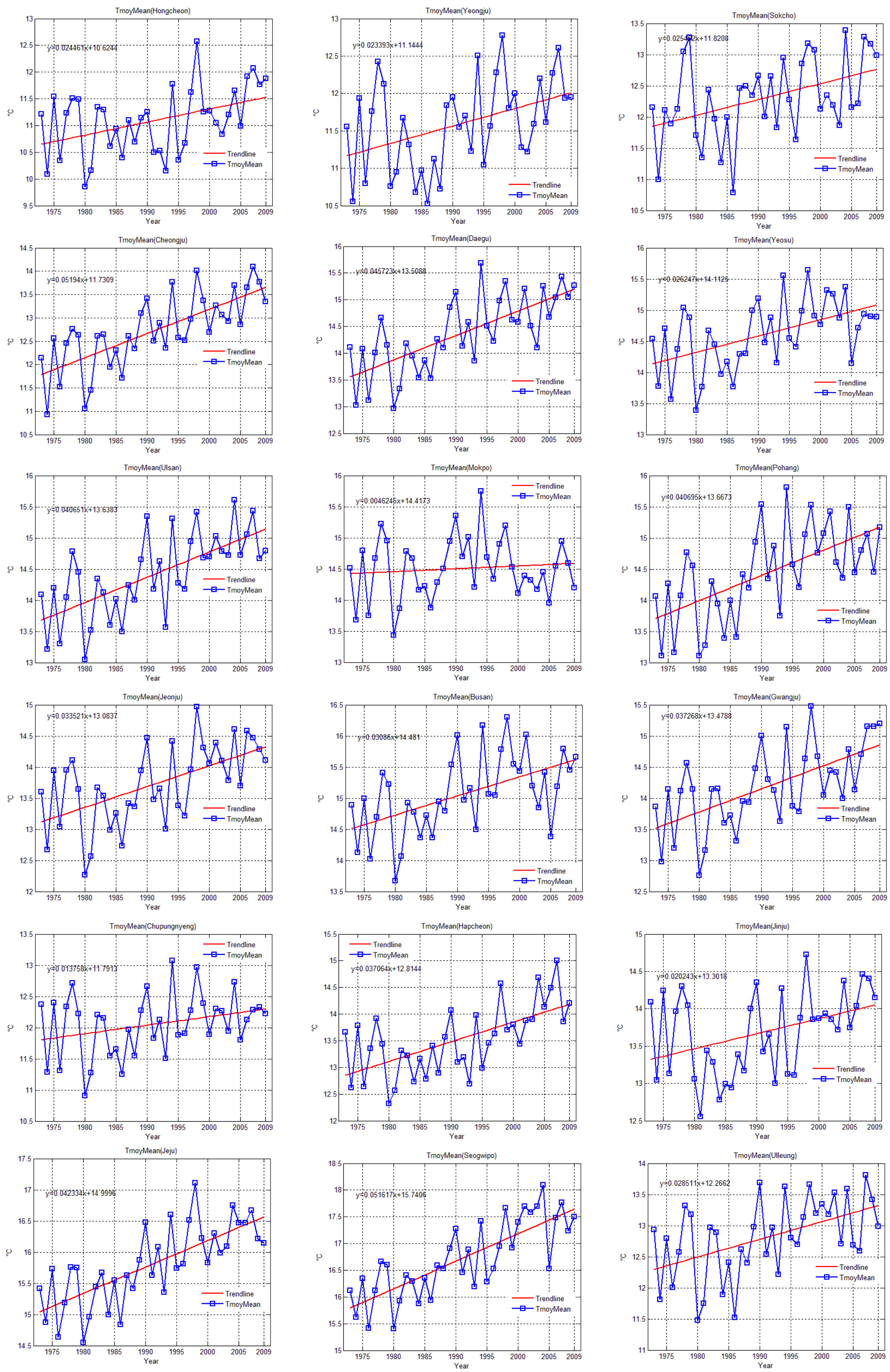

Figure B.3 TmoyMean at 24 stations

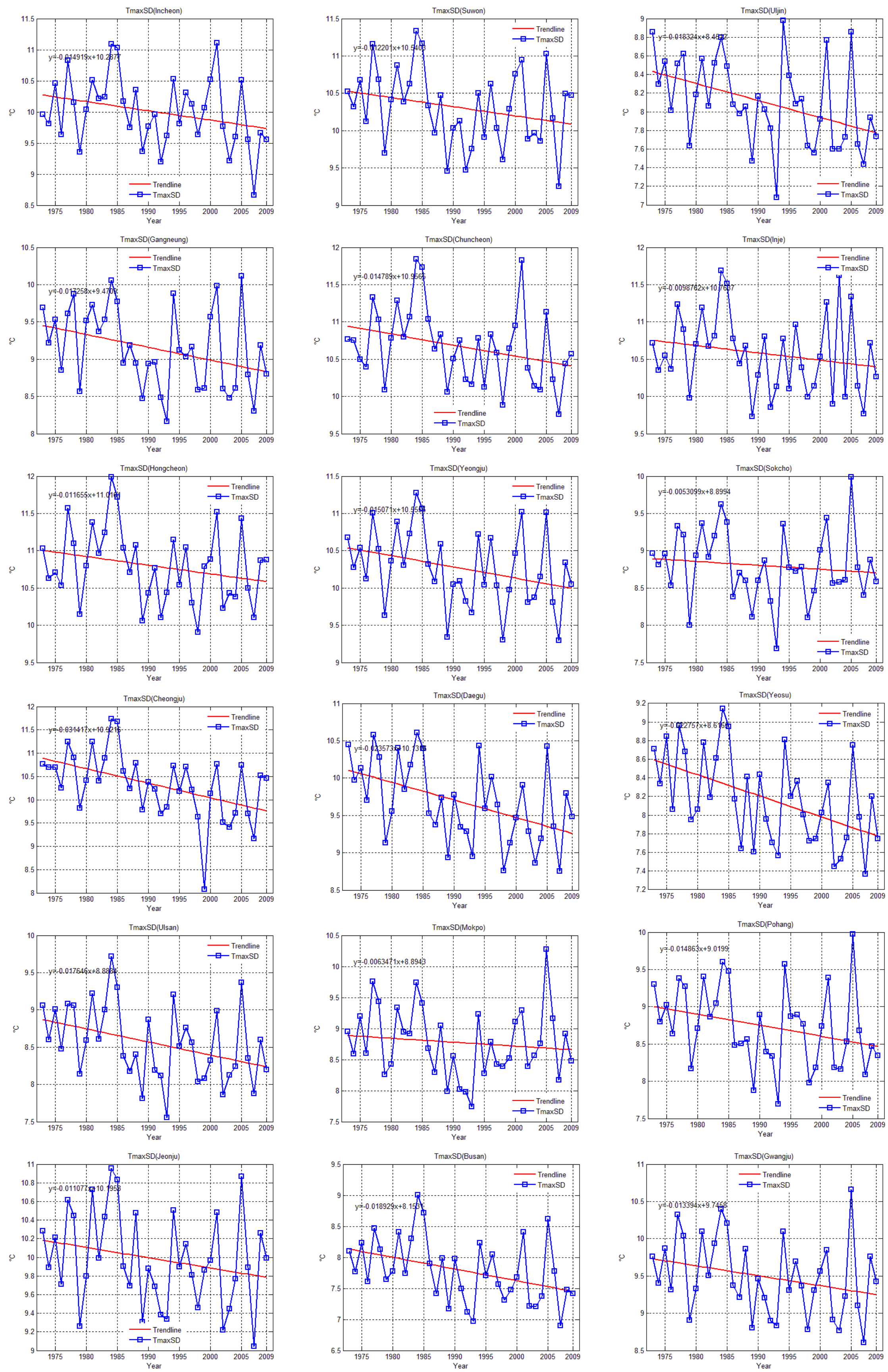
TmaxSD(Incheon)
TmaxSD(Suwon)
TmaxSD(Uljin)
TmaxSD(Gangneung)
TmaxSD(Chuncheon)
TmaxSD(Inje)
TmaxSD(Hongcheon)
TmaxSD(Yeongju)
TmaxSD(Sokcho)
TmaxSD(Cheongju)
TmaxSD(Daegu)
TmaxSD(Yeosu)
TmaxSD(Ulsan)
TmaxSD(Mokpo)
TmaxSD(Pohang)
TmaxSD(Jeonju)
TmaxSD(Busan)
TmaxSD(Gwangju)
Trendline
TmaxSD
Year
°C

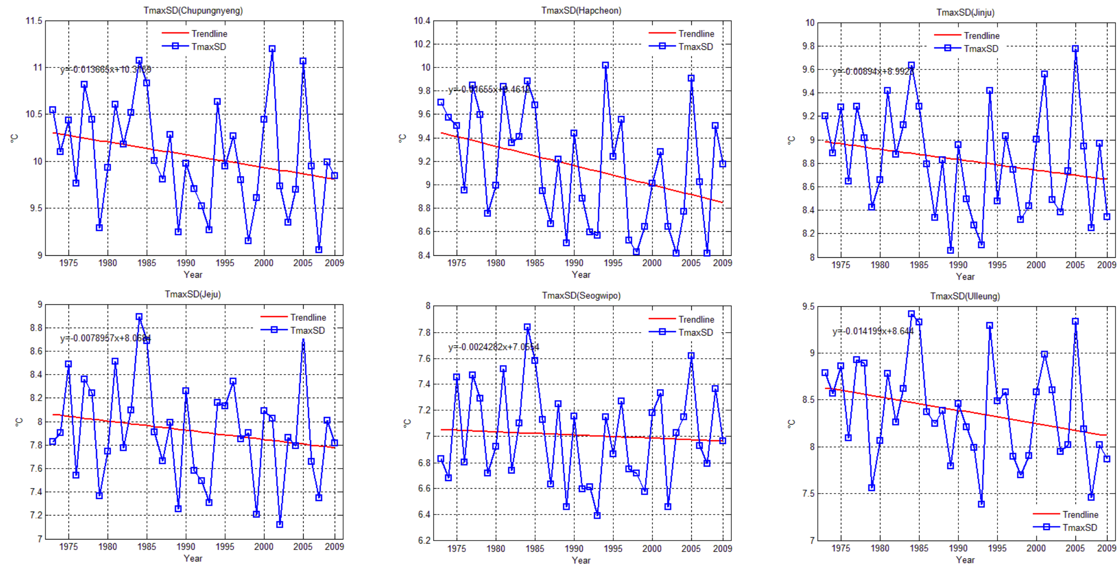

Figure B.4 TmaxSD at 24 stations

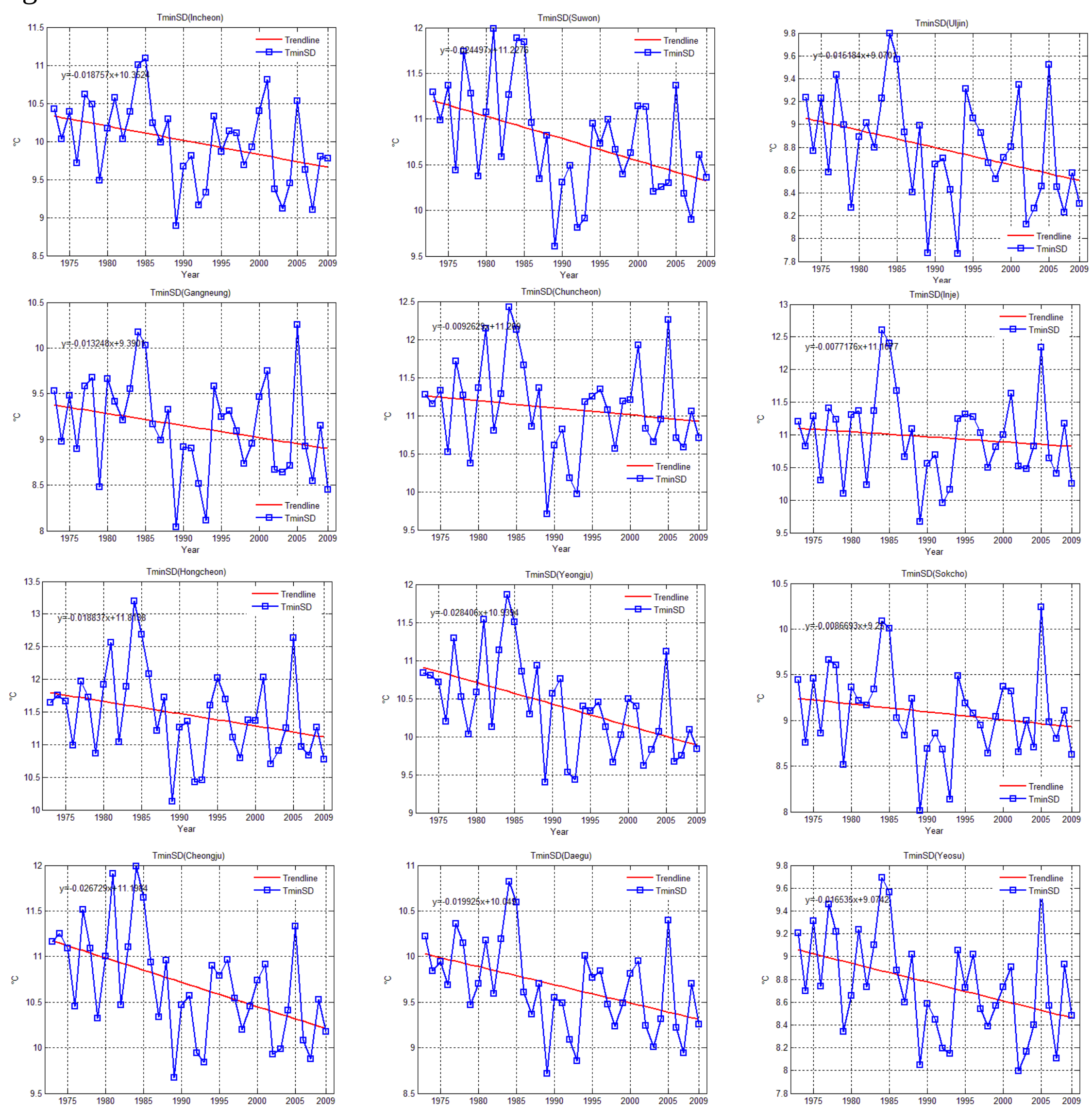

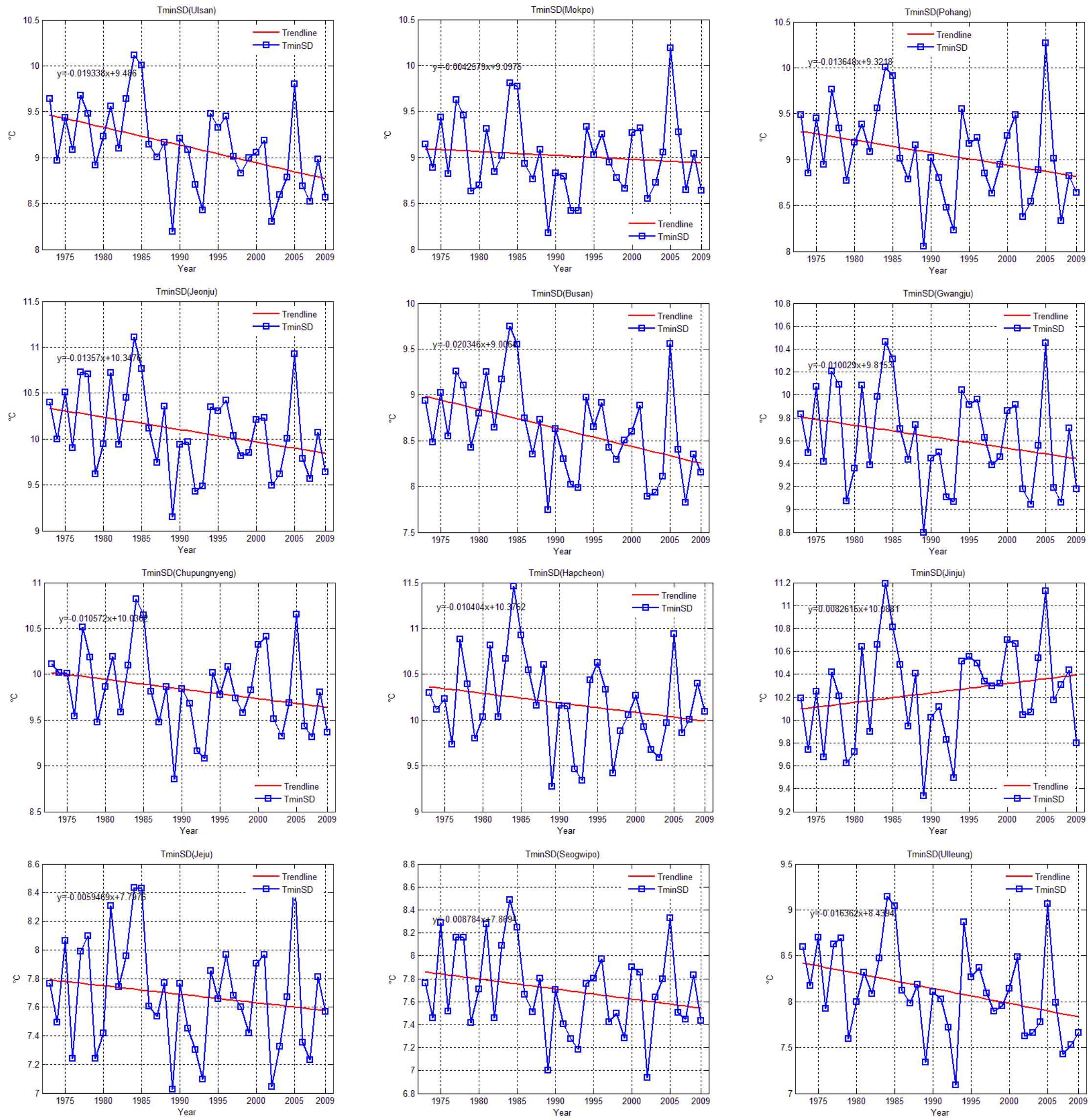

Figure B.5 TminSD at 24 stations

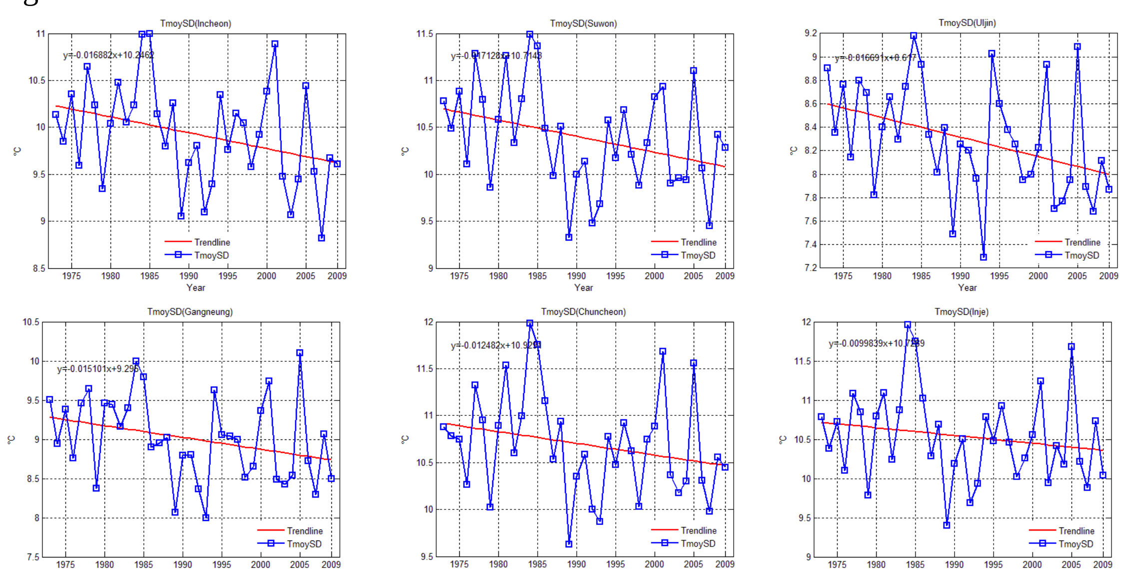

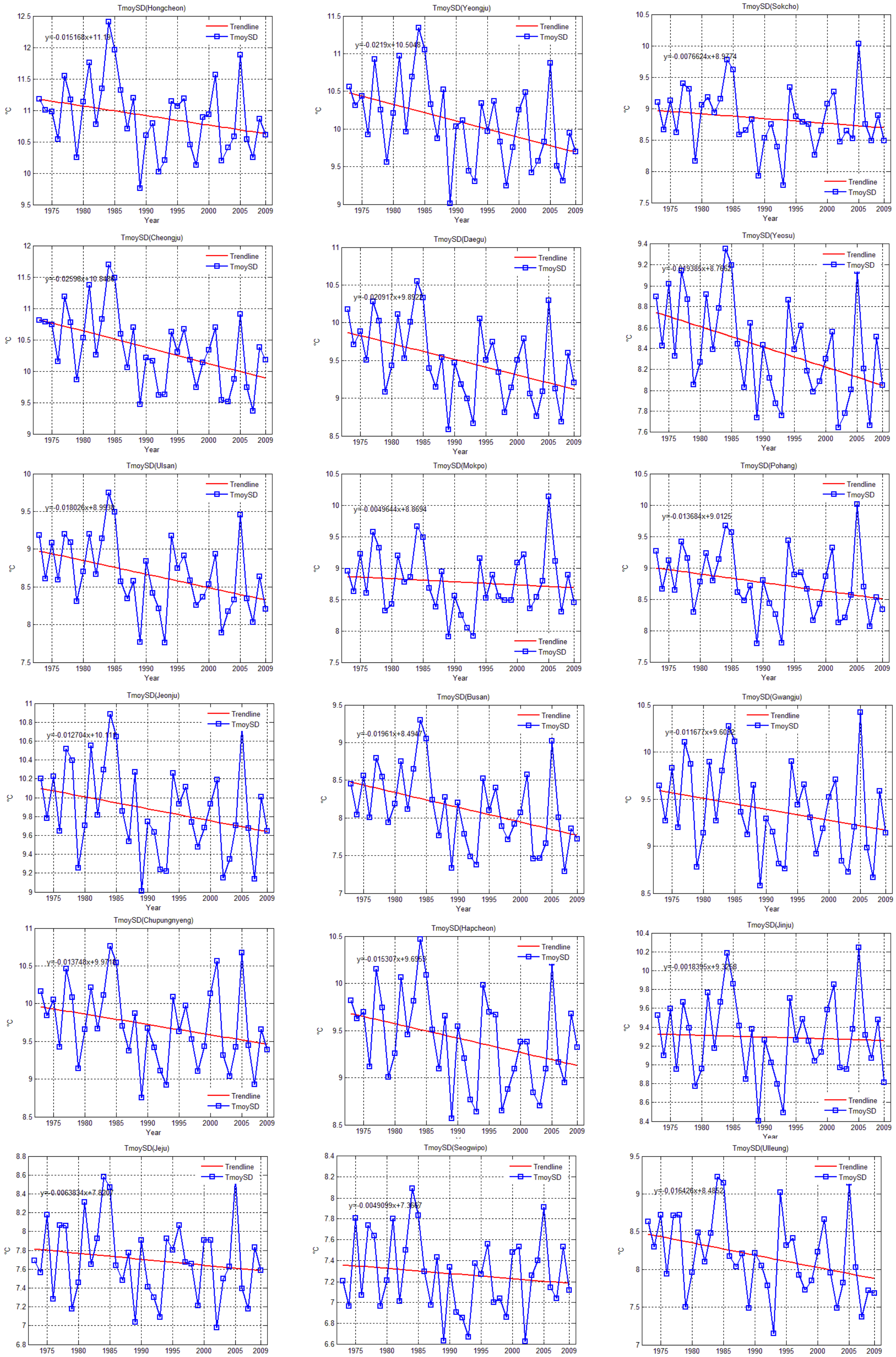

Figure B.6 TmoySD at 24 stations

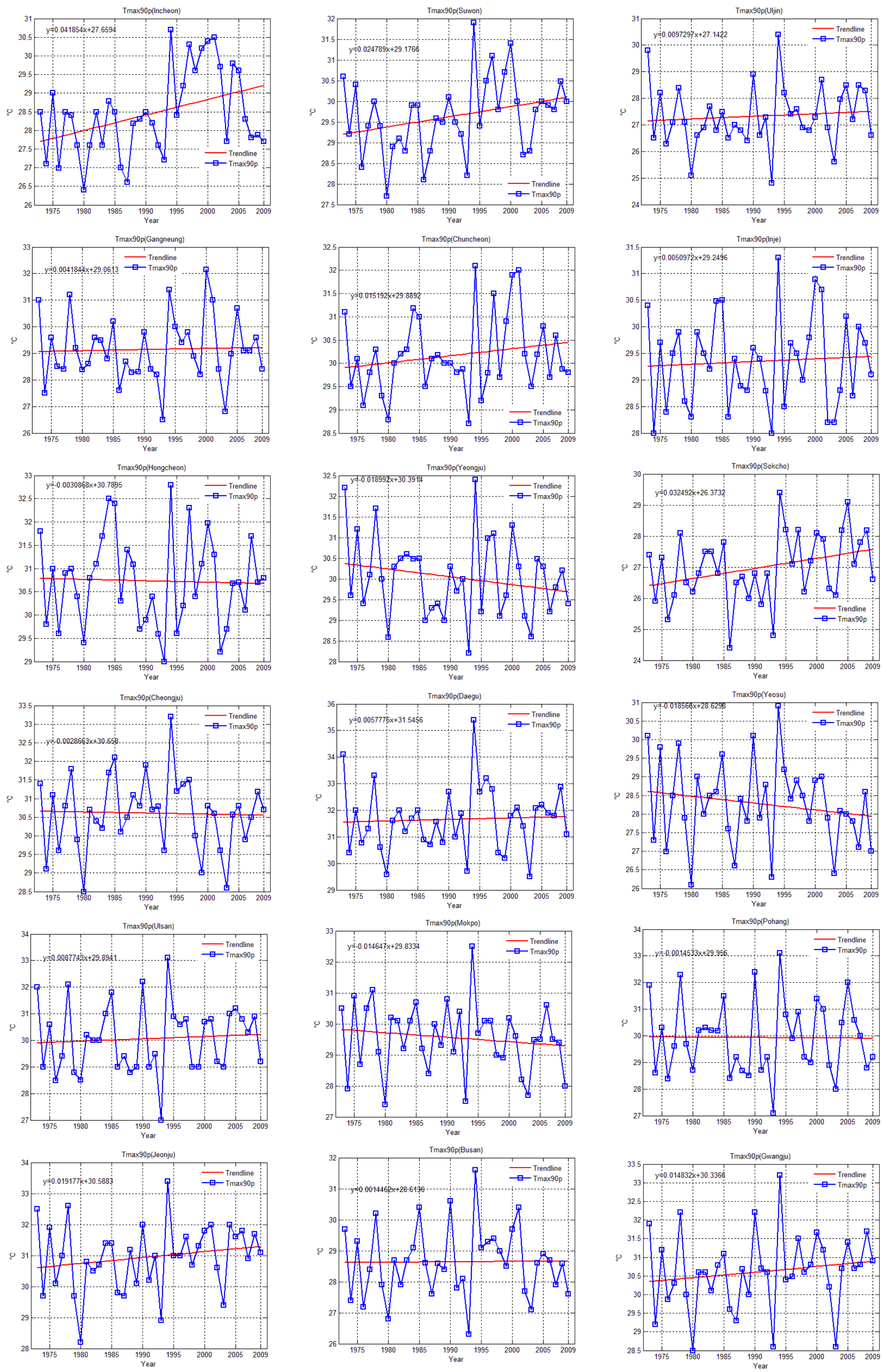
Tmax90p(Incheon)
y=0.041854x+27.6594
Tmax90p(Suwon)
y=0.024789x+29.1766
Tmax90p(Uljin)
y=0.0097297x+27.1422
Tmax90p(Gangneung)
y=0.0041844x+29.0613
Tmax90p(Chuncheon)
y=0.015192x+29.8892
Tmax90p(Inje)
y=0.0050972x+29.2496
Tmax90p(Hongcheon)
y=-0.0030868x+30.7895
Tmax90p(Yeongju)
y=-0.018992x+30.3914
Tmax90p(Sokcho)
y=0.032492x+26.3732
Tmax90p(Cheongju)
y=-0.0028663x+30.658
Tmax90p(Daegu)
y=0.0057775x+31.5456
Tmax90p(Yeosu)
y=-0.018566x+28.6298
Tmax90p(Ulsan)
y=0.0087743x+29.8941
Tmax90p(Mokpo)
y=-0.014647x+29.8334
Tmax90p(Pohang)
y=-0.0014533x+29.956
Tmax90p(Jeonju)
y=0.019177x+30.5883
Tmax90p(Busan)
y=0.0014462x+28.6136
Tmax90p(Gwangju)
y=0.014832x+30.3366
Trendline
Tmax90p
Year
℃

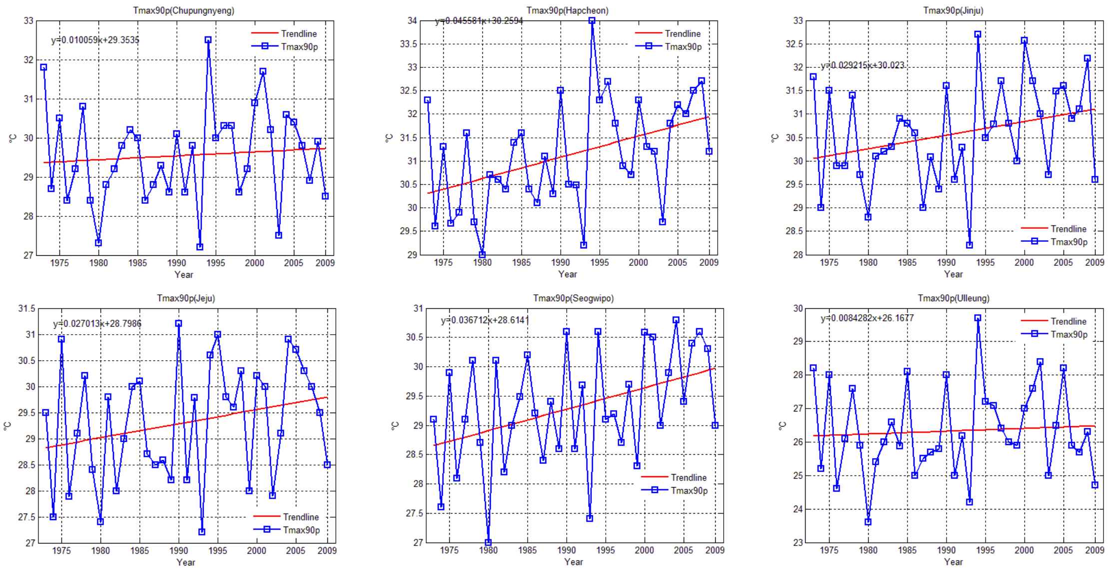

Figure B.7 Annual Tmax90p at 24 stations

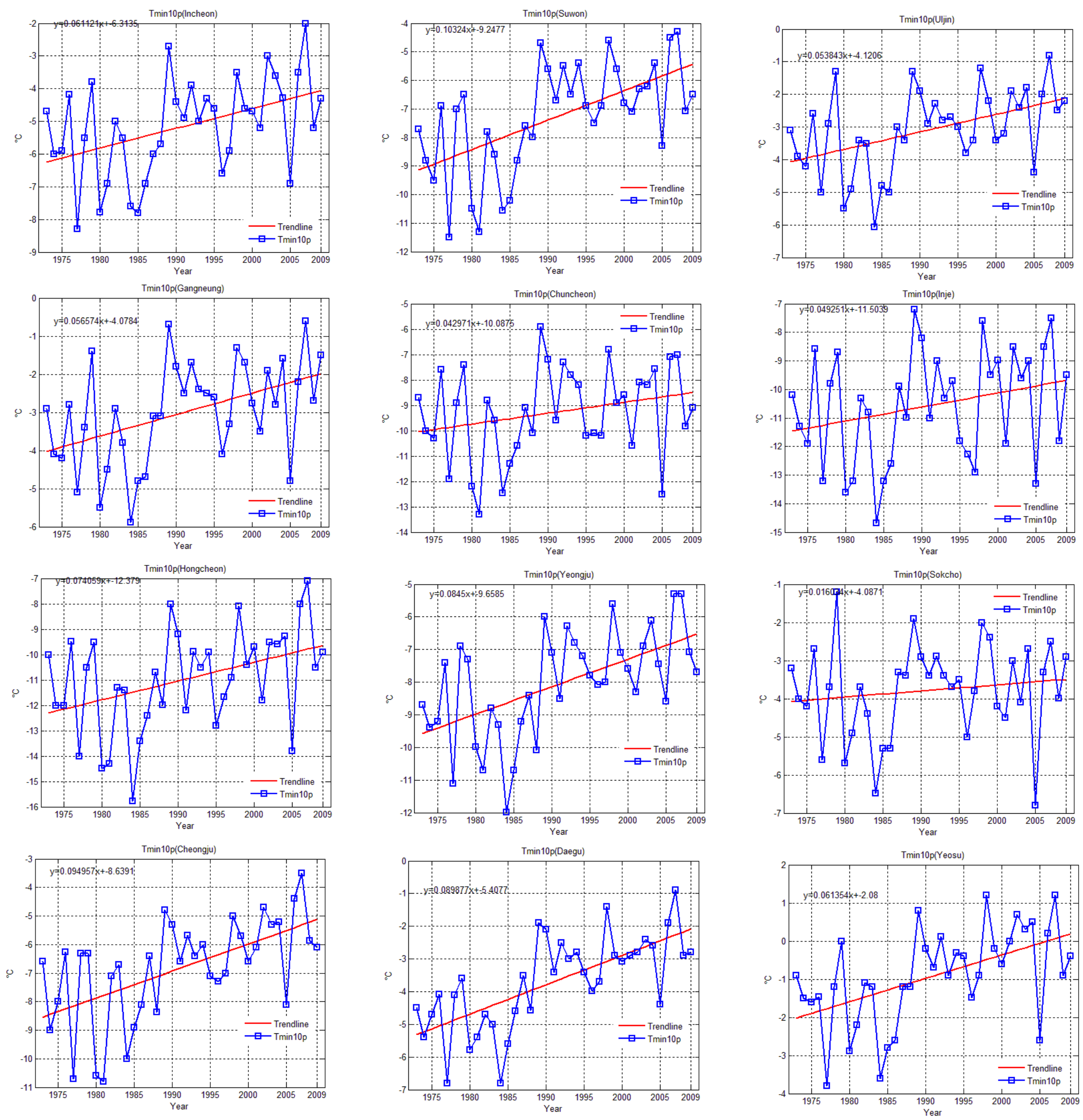

Figure B.8 Annual Tmin10p at 24 stations

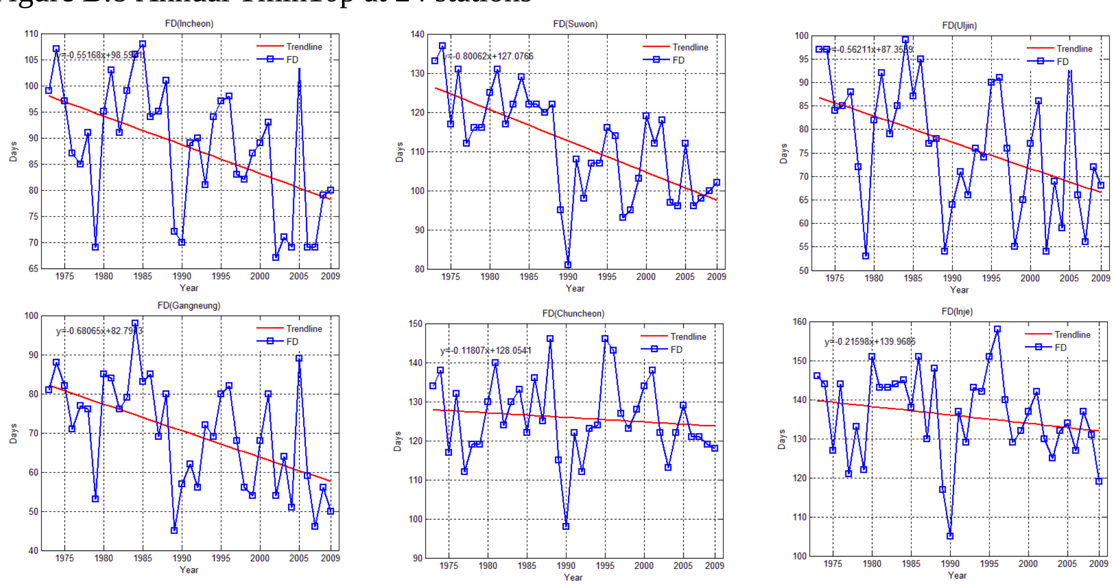

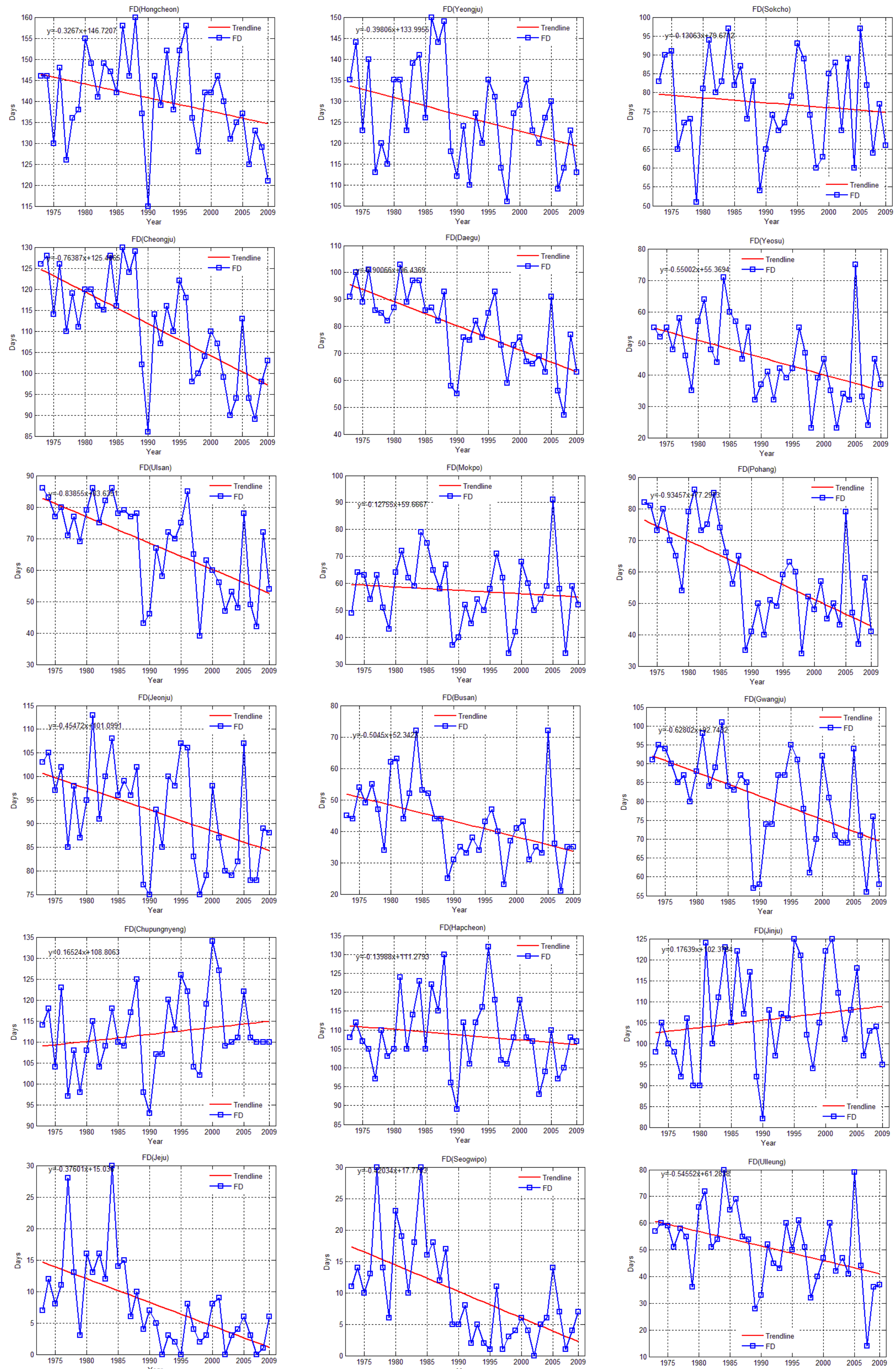

Figure B.9 FD at 24stations

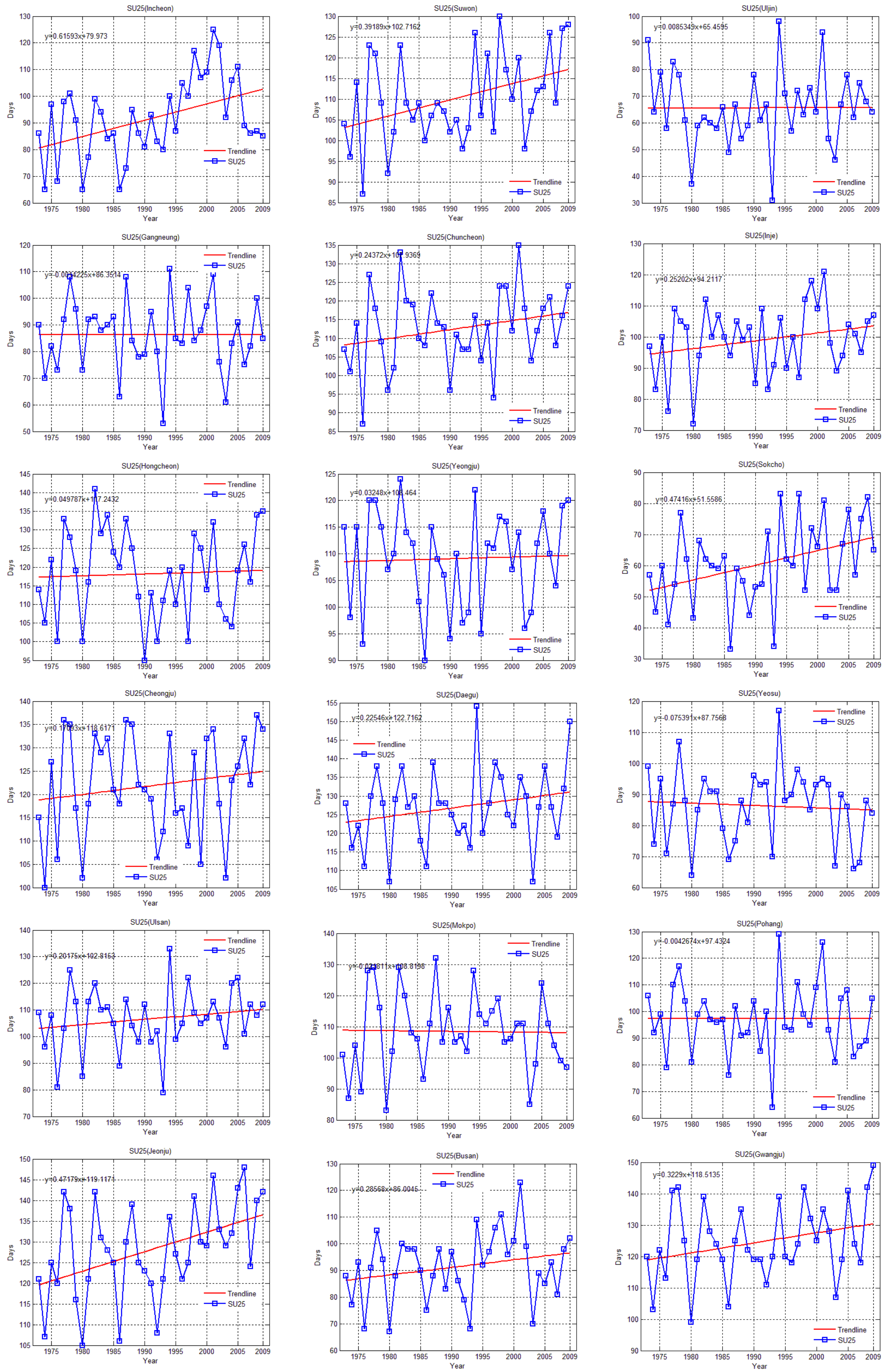
SU25(Incheon)
y=0.61593x+79.973
SU25(Suwon)
y=0.39189x+102.7162
SU25(Uljin)
y=0.0085349x+65.4595
SU25(Gangneung)
SU25(Chuncheon)
SU25(Inje)
y=0.25202x+94.2117
SU25(Hongcheon)
SU25(Yeongju)
SU25(Sokcho)
y=0.47416x+51.5586
SU25(Cheongju)
SU25(Daegu)
y=0.22546x+122.7162
SU25(Yeosu)
y=-0.075391x+87.7568
SU25(Ulsan)
SU25(Mokpo)
SU25(Pohang)
y=-0.0042674x+97.4324
SU25(Jeonju)
SU25(Busan)
y=0.28568x+86.0045
SU25(Gwangju)
y=0.3229x+118.5135
Days
Year
Trendline
SU25

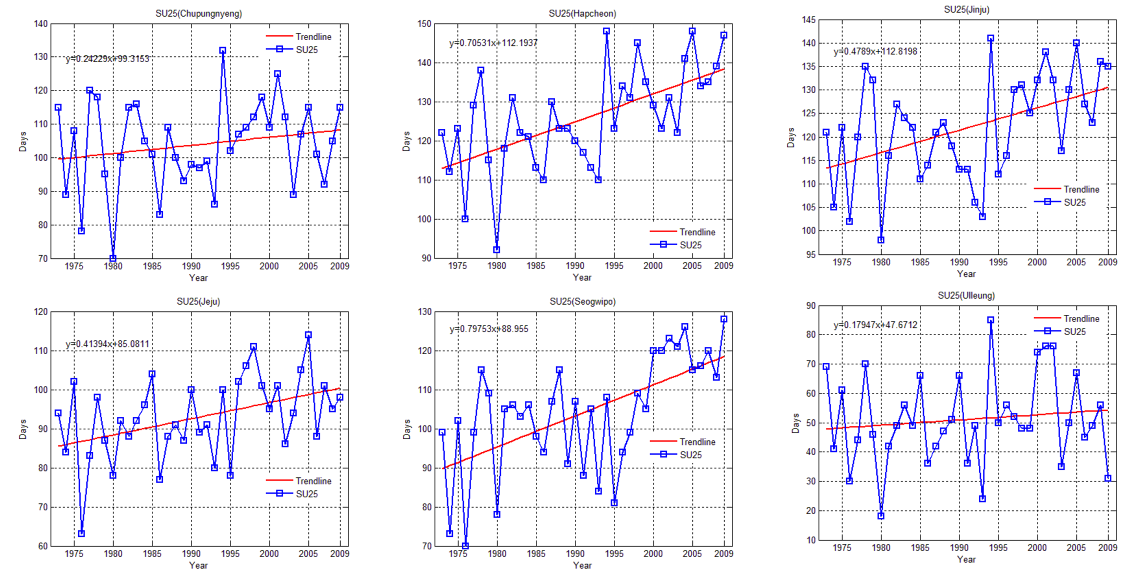

Figure B.10 SU25 at 24 stations

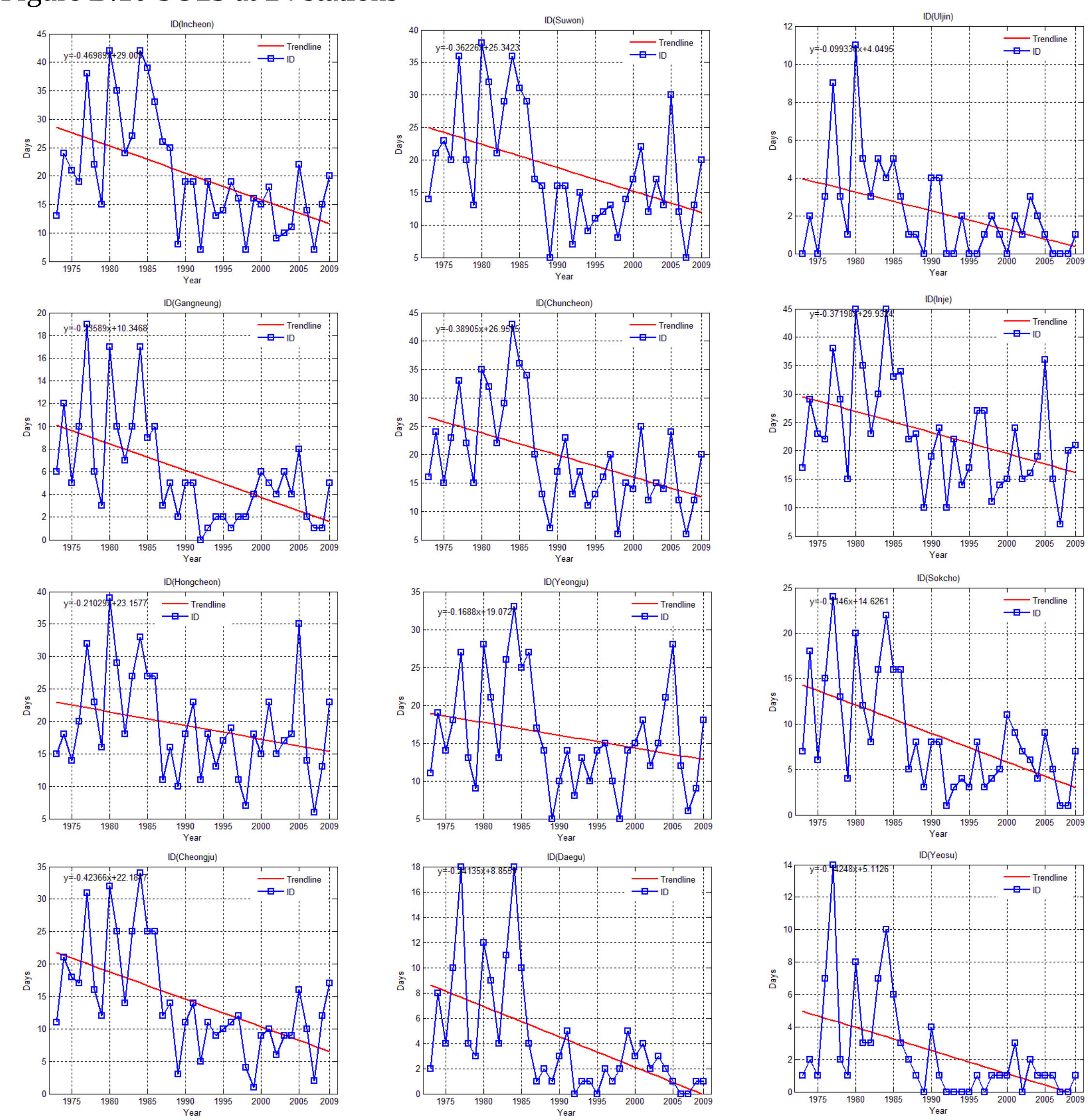

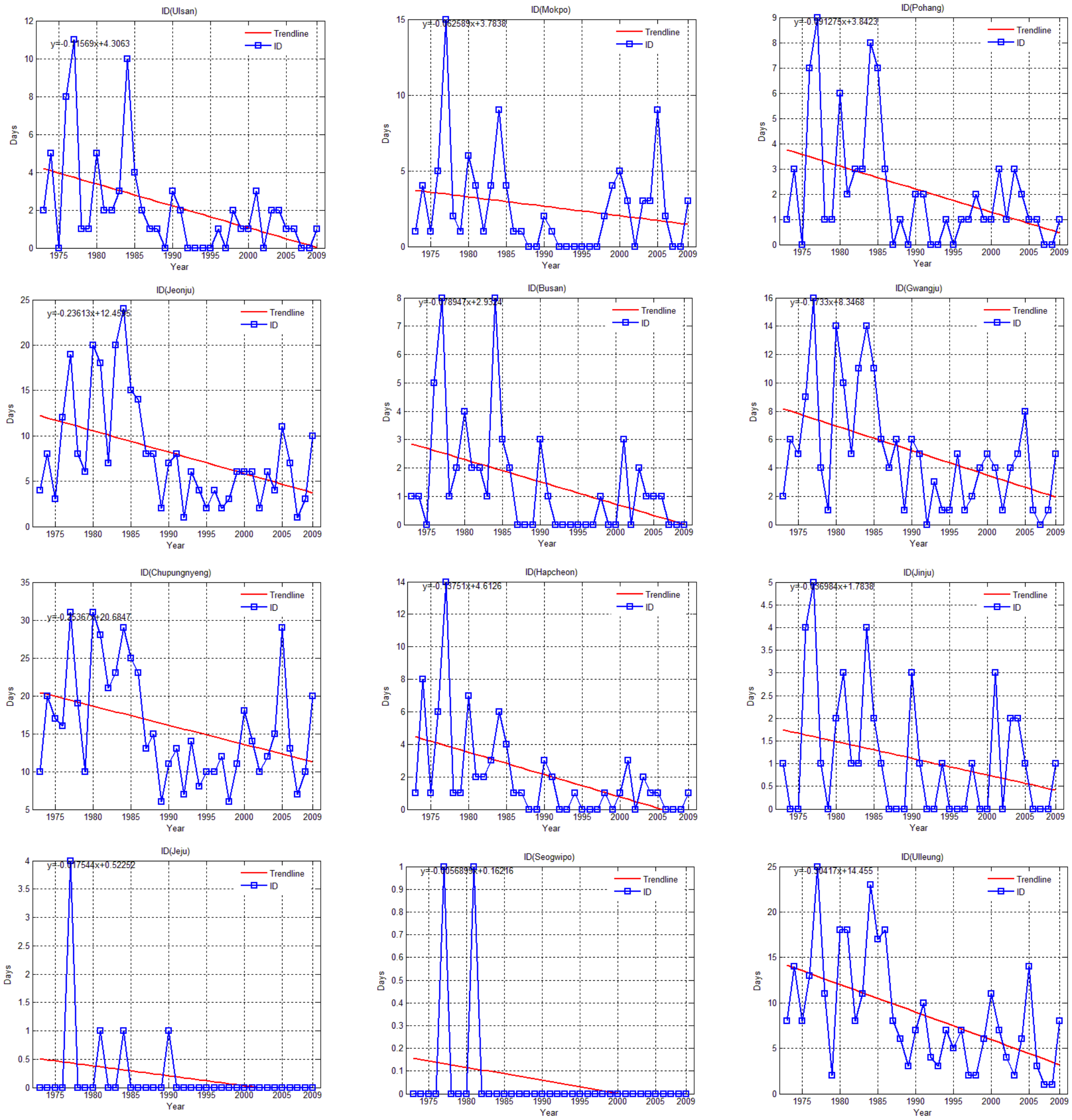

Figure B.11 ID at 24 stations

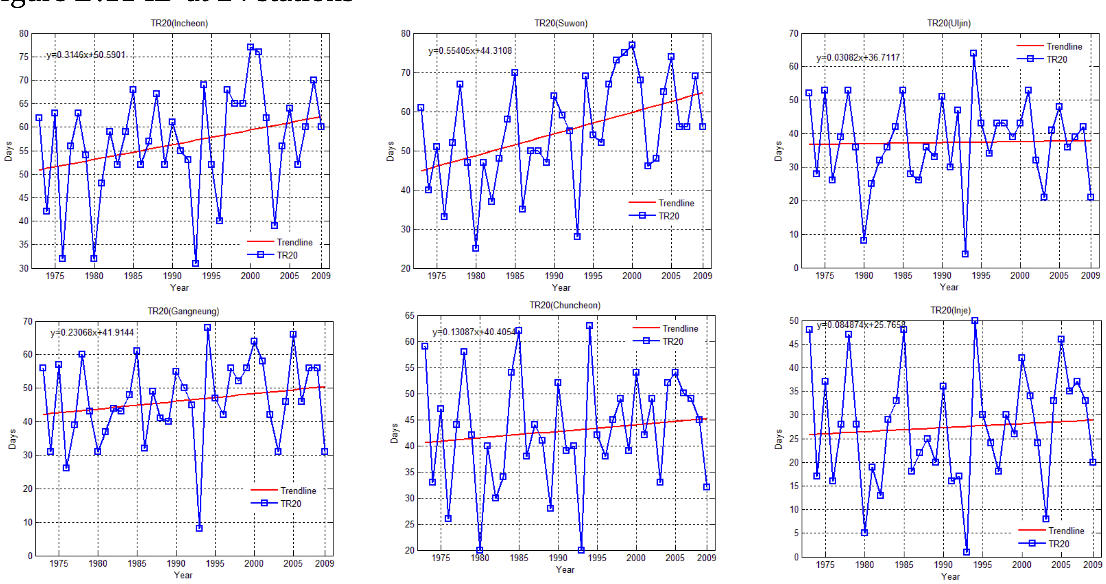

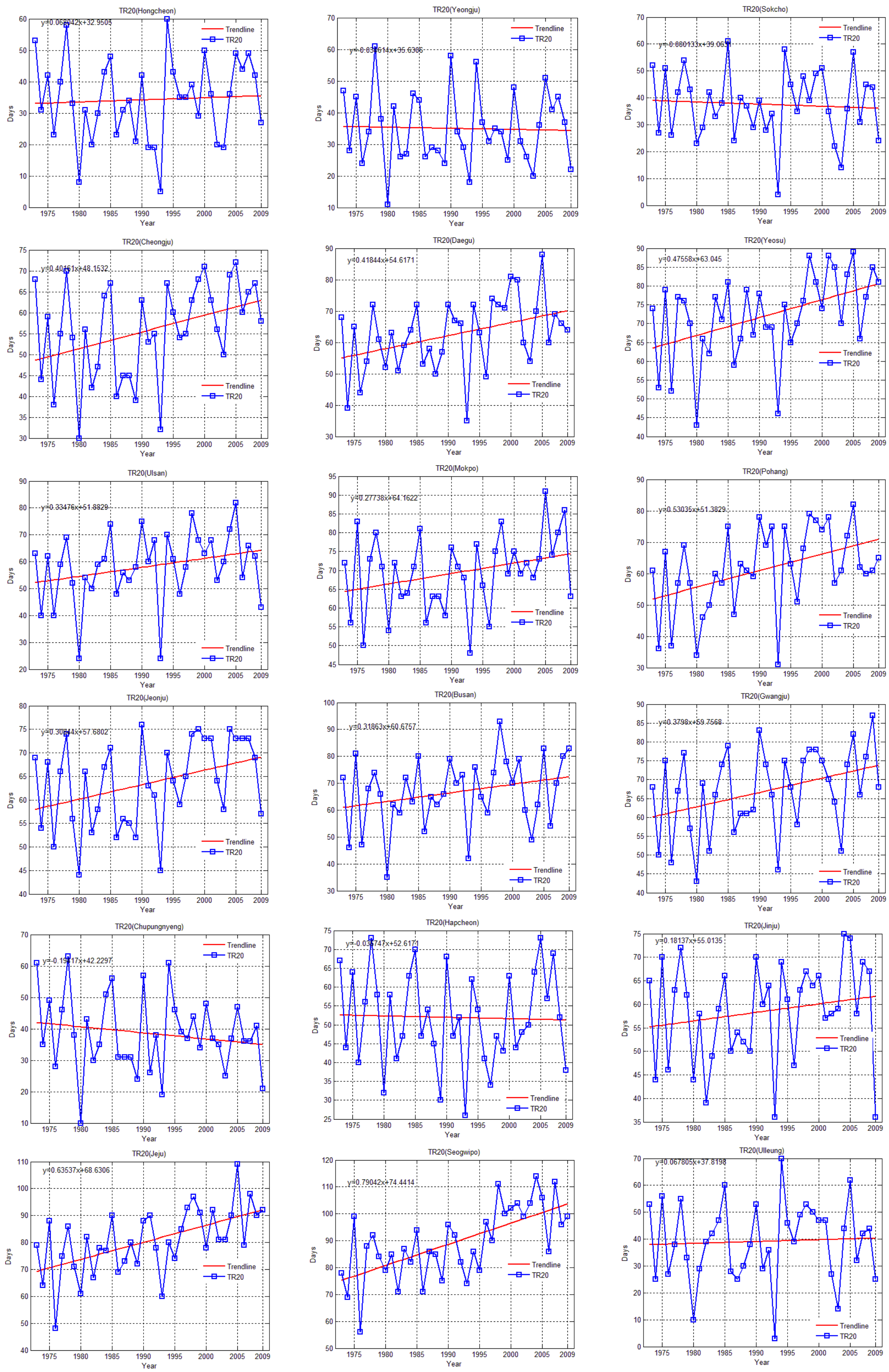

Figure B.12 TR20 at 24 stations

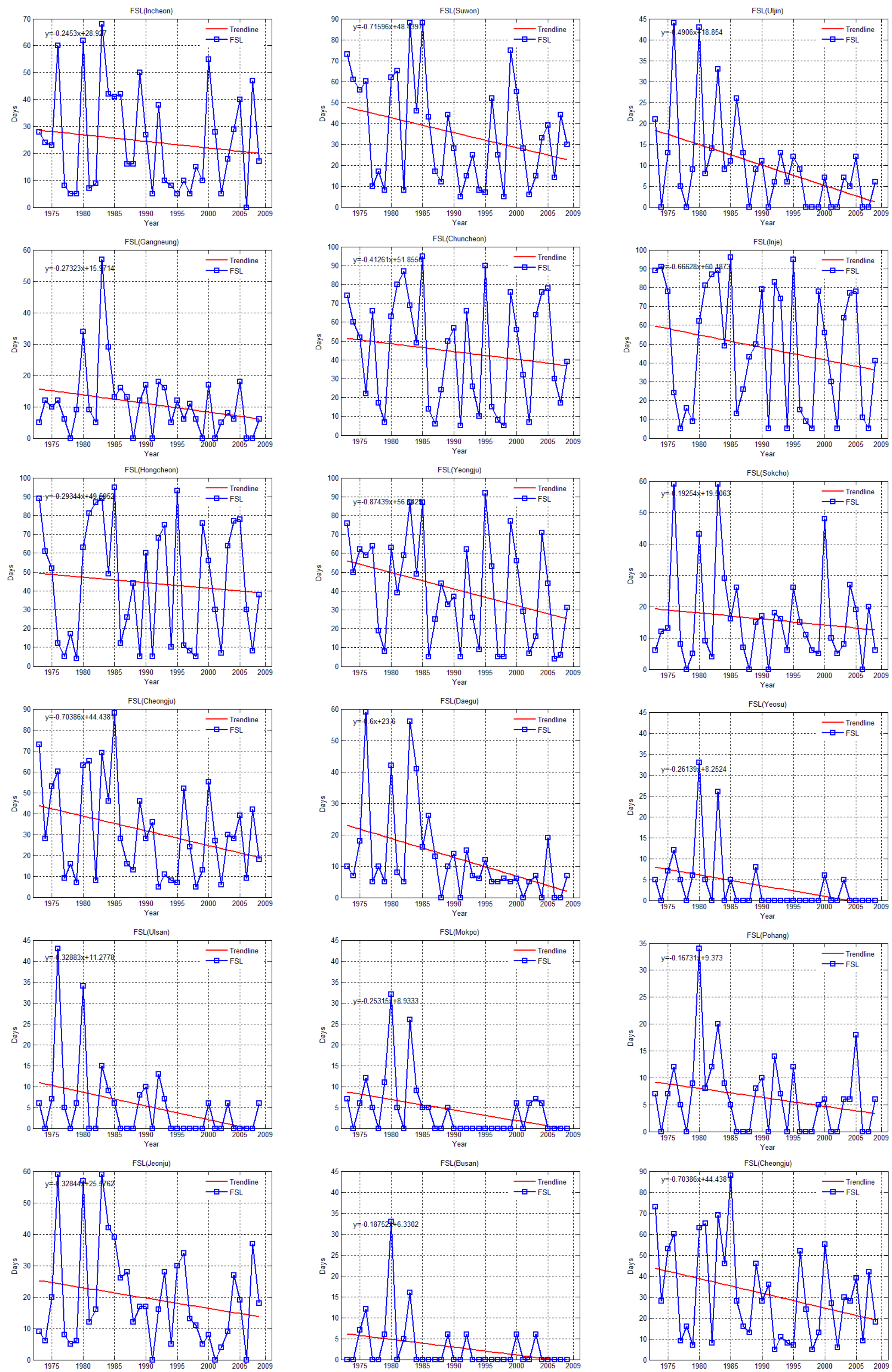
FSL(Incheon)
FSL(Suwon)
FSL(Uljin)
FSL(Gangneung)
FSL(Chuncheon)
FSL(Inje)
FSL(Hongcheon)
FSL(Yeongju)
FSL(Sokcho)
FSL(Cheongju)
FSL(Daegu)
FSL(Yeosu)
FSL(Ulsan)
FSL(Mokpo)
FSL(Pohang)
FSL(Jeonju)
FSL(Busan)
FSL(Cheongju)
Trendline
FSL
Days
Year

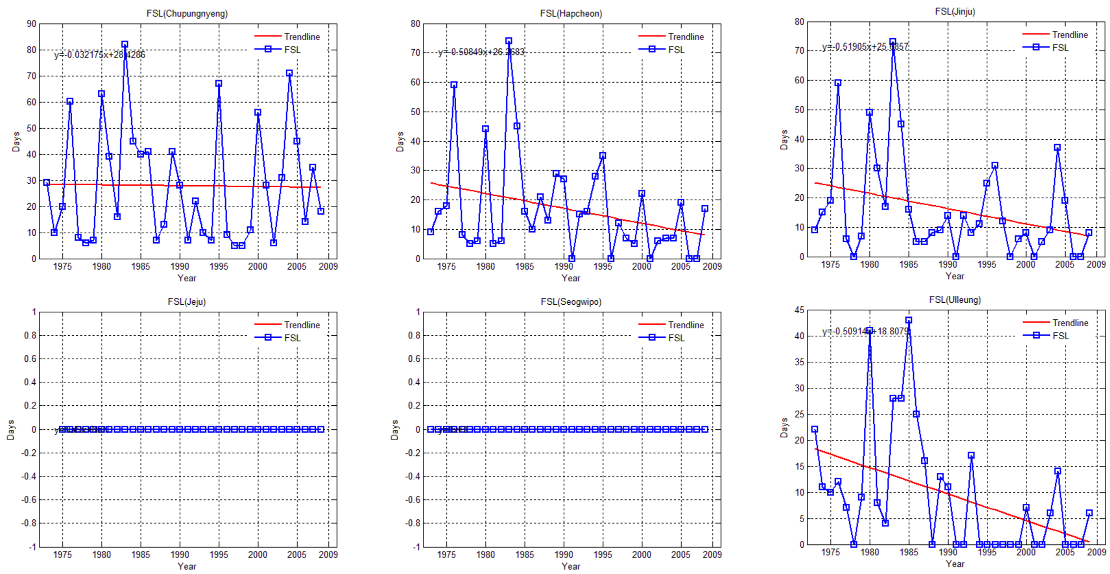

Figure B.13 FSL at 24 stations

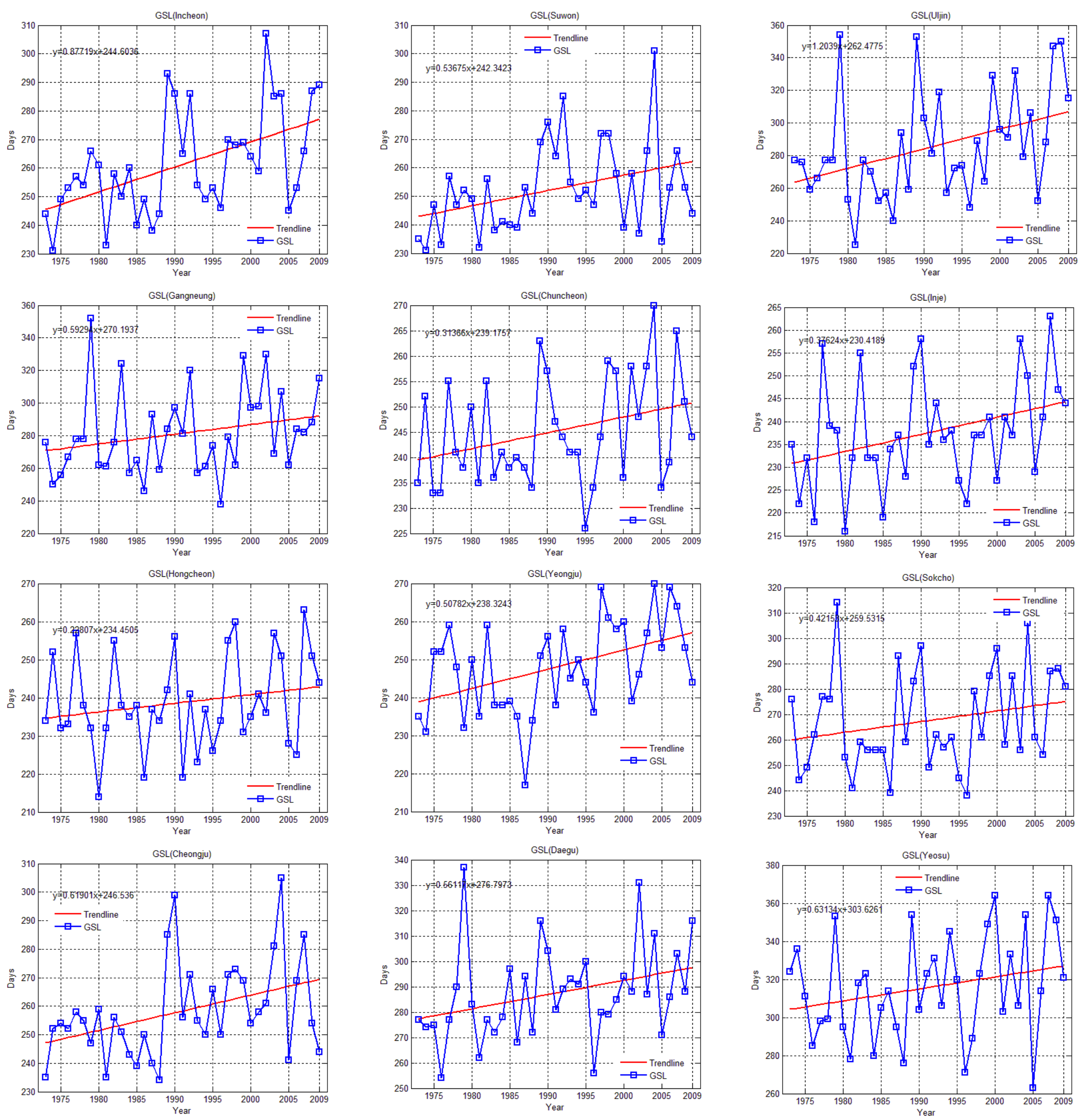

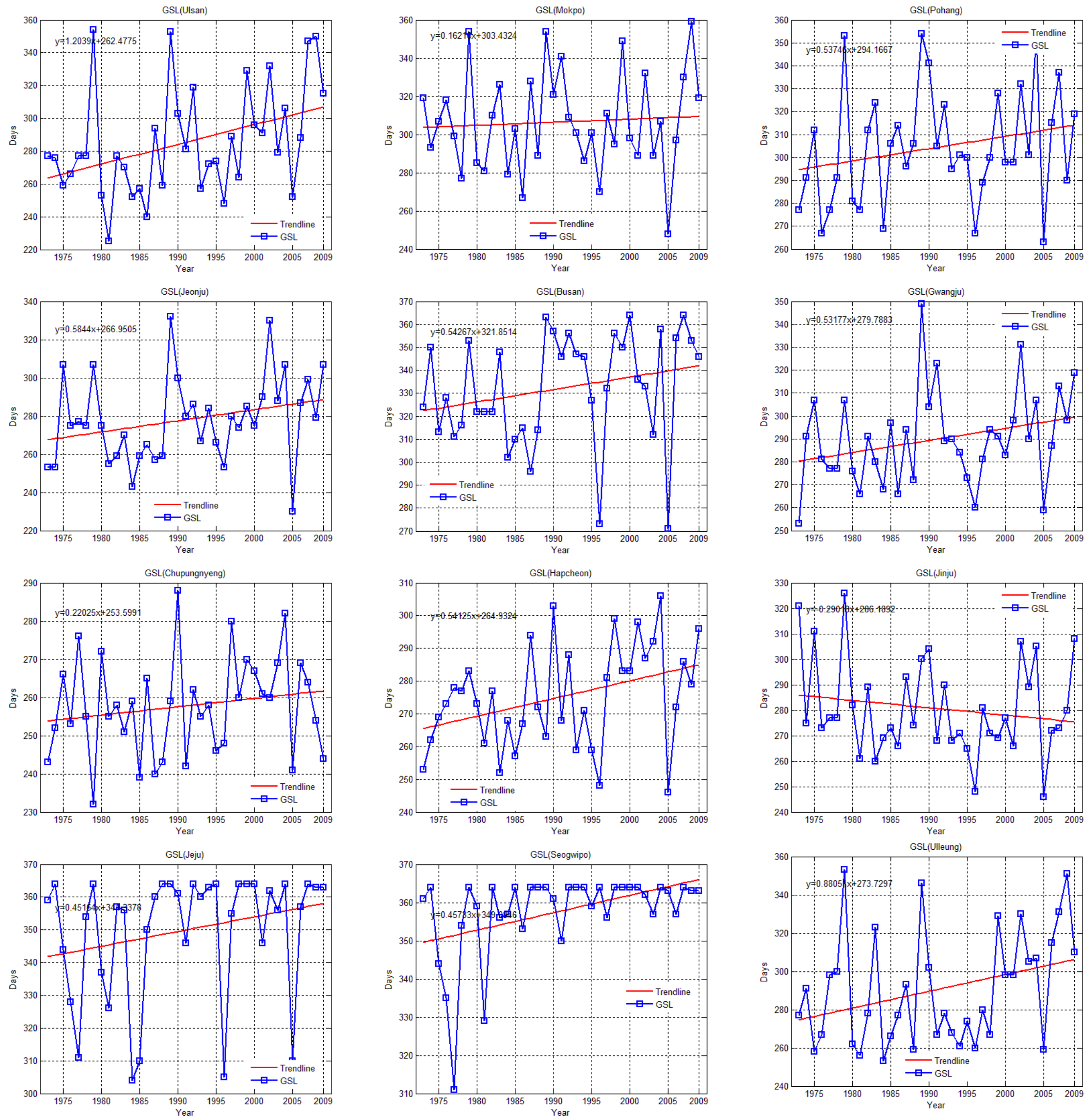

Figure B.14 GSL at 24 stations

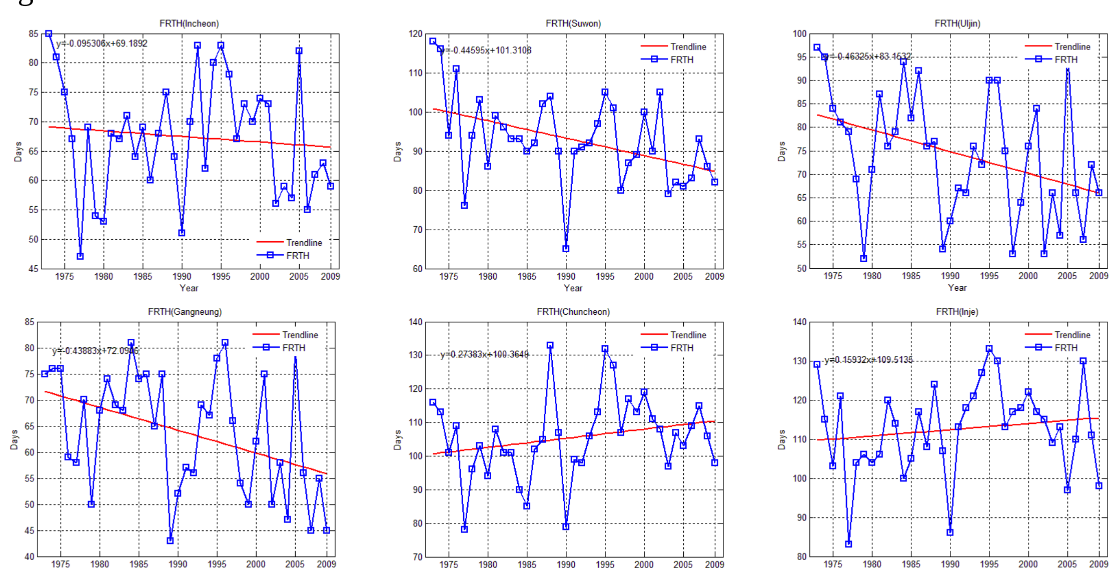

Figure B.15 FRTH at 24 stations

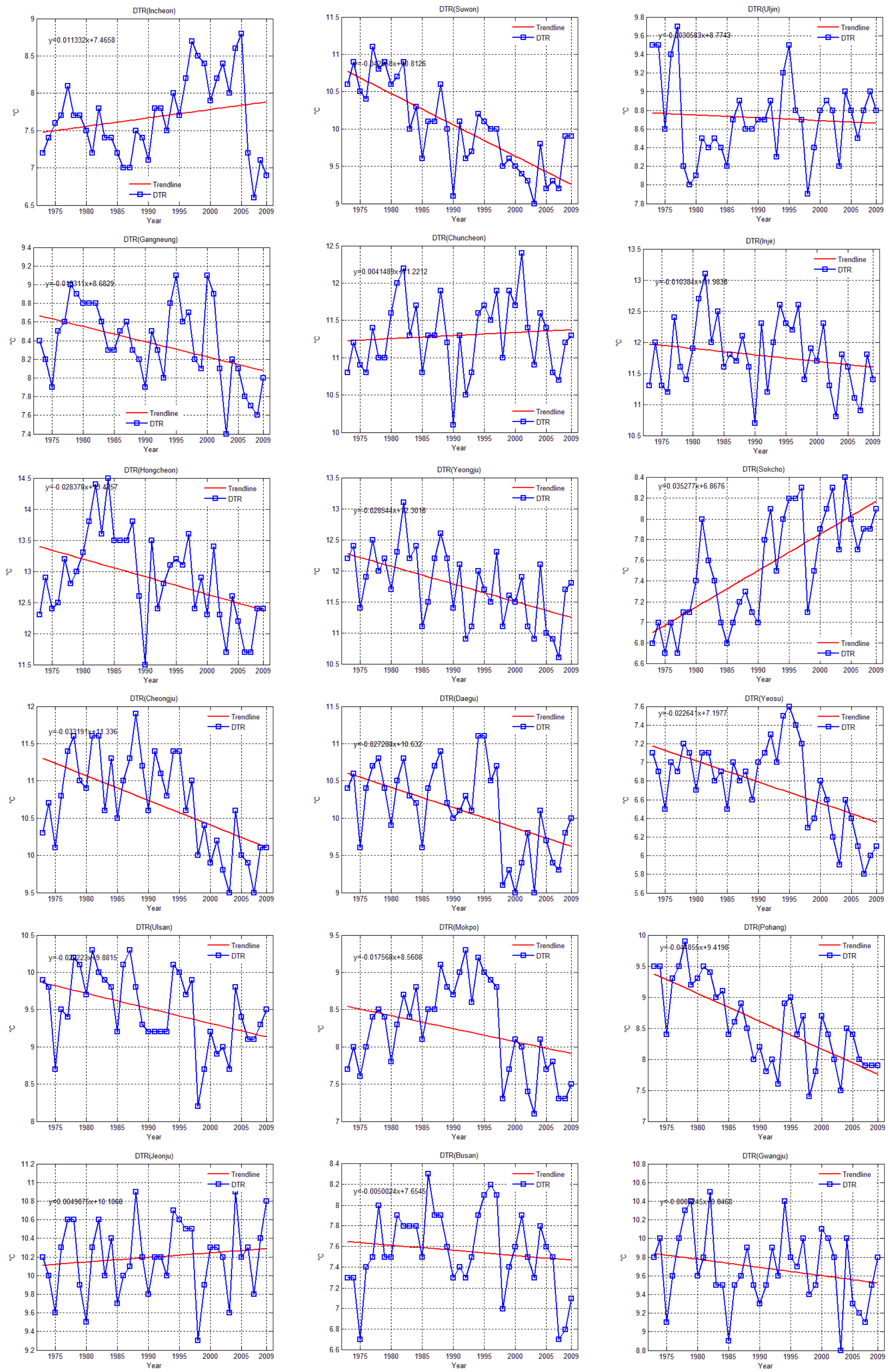
DTR(Incheon)
y=0.011332x+7.4658
DTR(Suwon)
DTR(Uljin)
DTR(Gangneung)
DTR(Chuncheon)
DTR(Inje)
DTR(Hongcheon)
DTR(Yeongju)
DTR(Sokcho)
y=0.035277x+6.8676
DTR(Cheongju)
DTR(Daegu)
y=-0.027288x+10.632
DTR(Yeosu)
y=-0.022641x+7.1977
DTR(Ulsan)
DTR(Mokpo)
y=-0.017568x+8.5608
DTR(Pohang)
DTR(Jeonju)
DTR(Busan)
y=-0.0050024x+7.6545
DTR(Gwangju)
Trendline
DTR
Year
℃

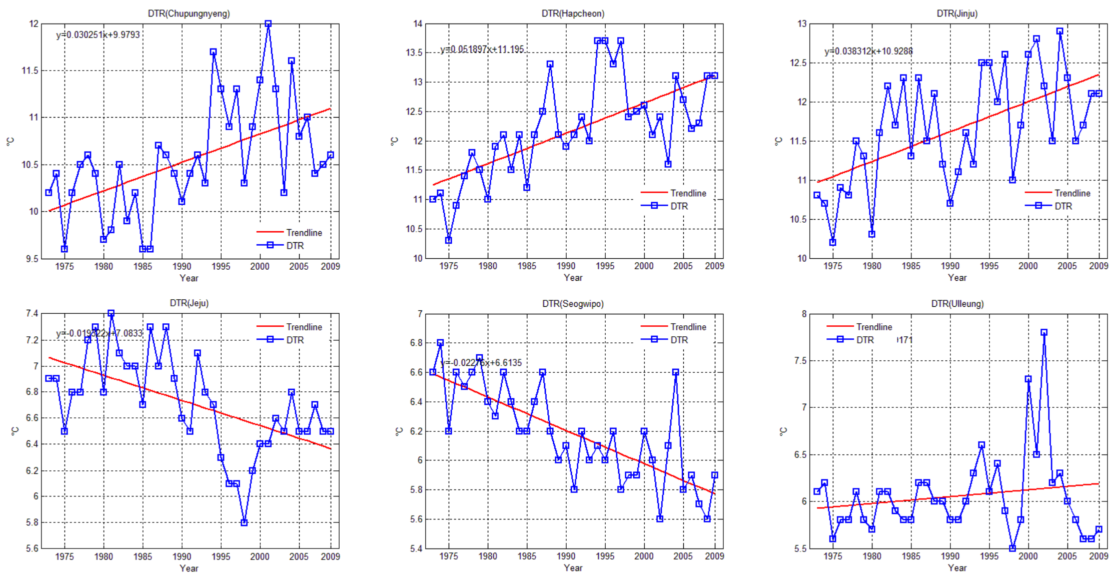

Figure B.16 DTR at 24 stations

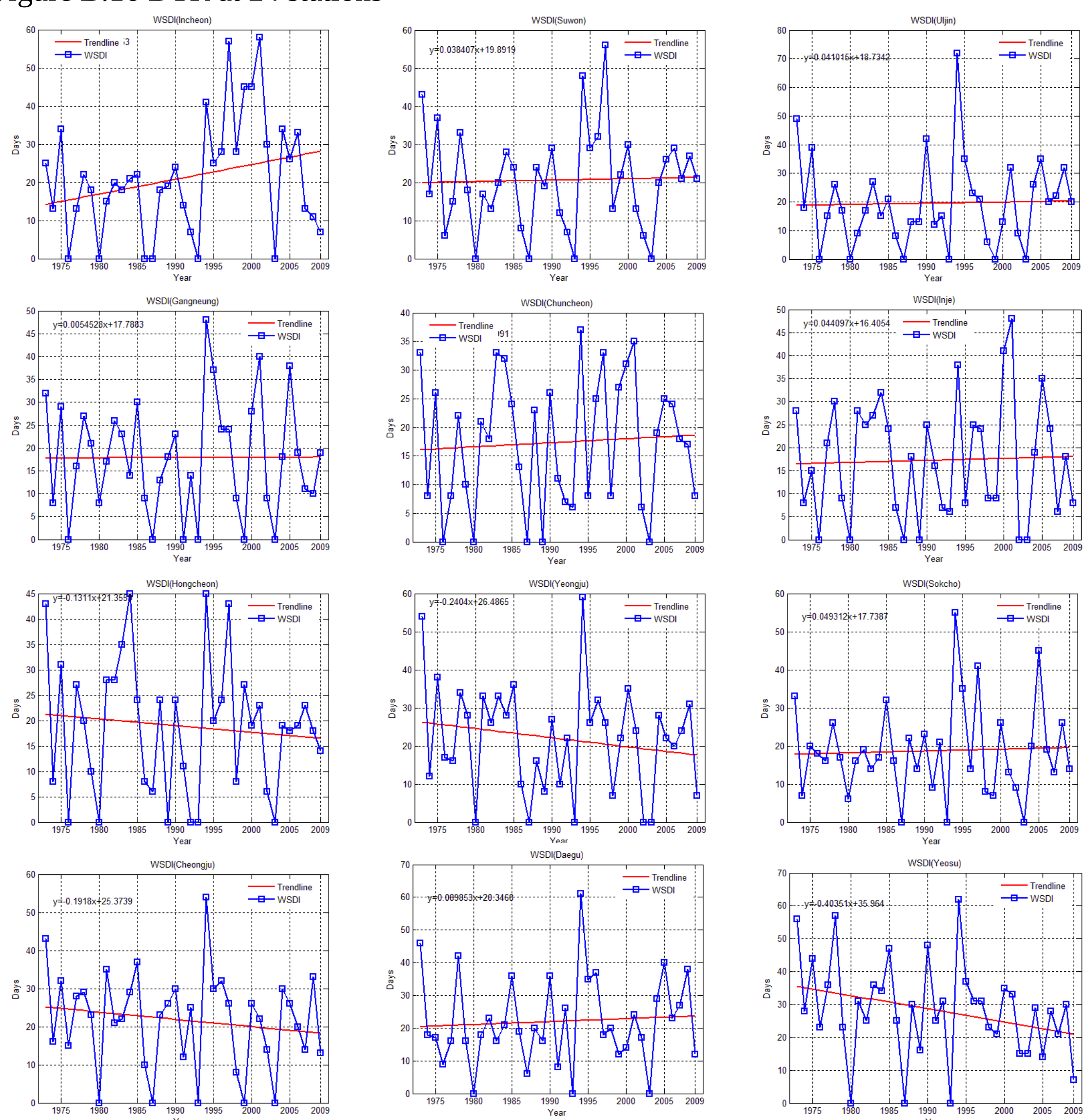

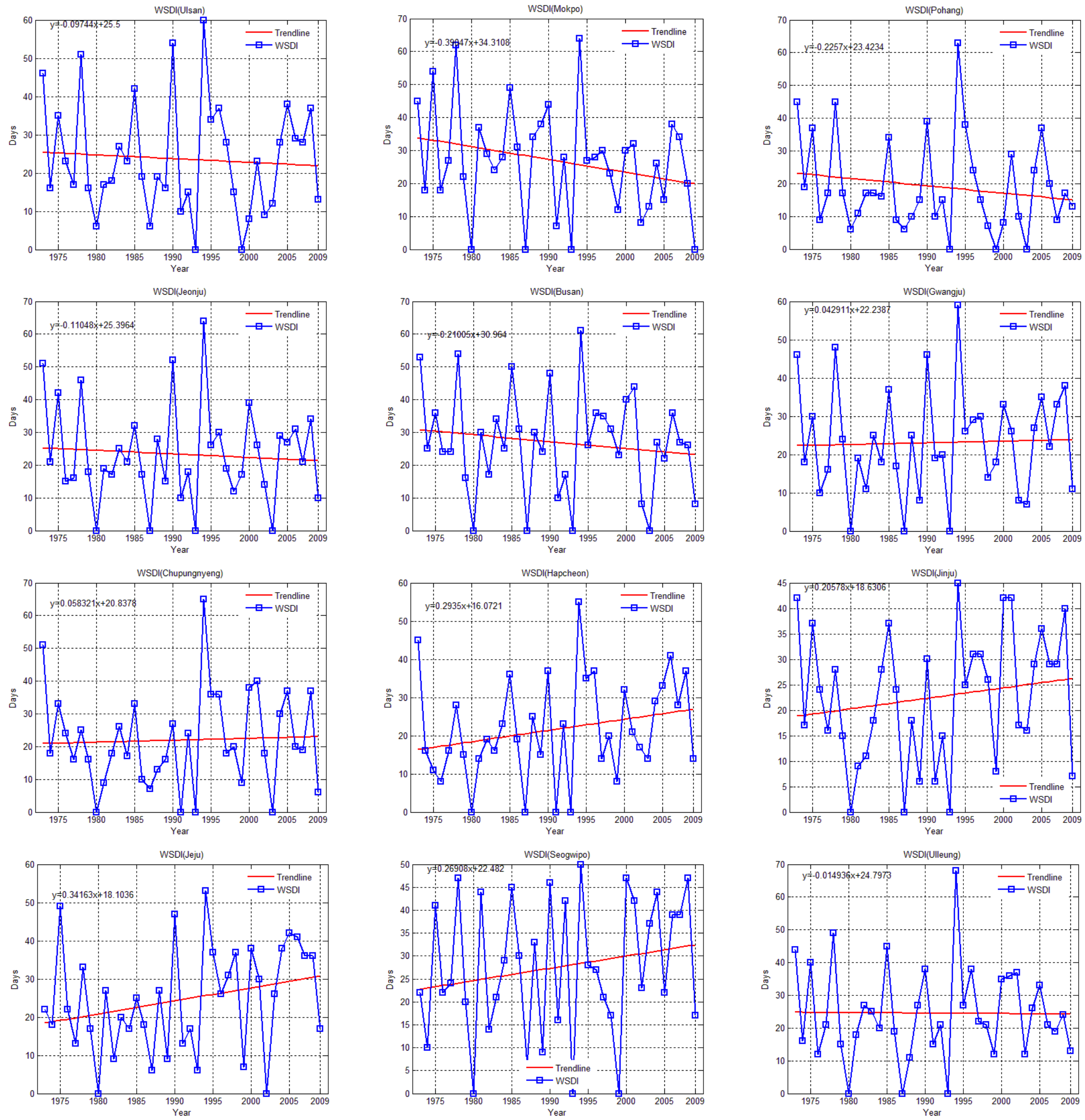

Figure B.17 WSDE at 24 stations

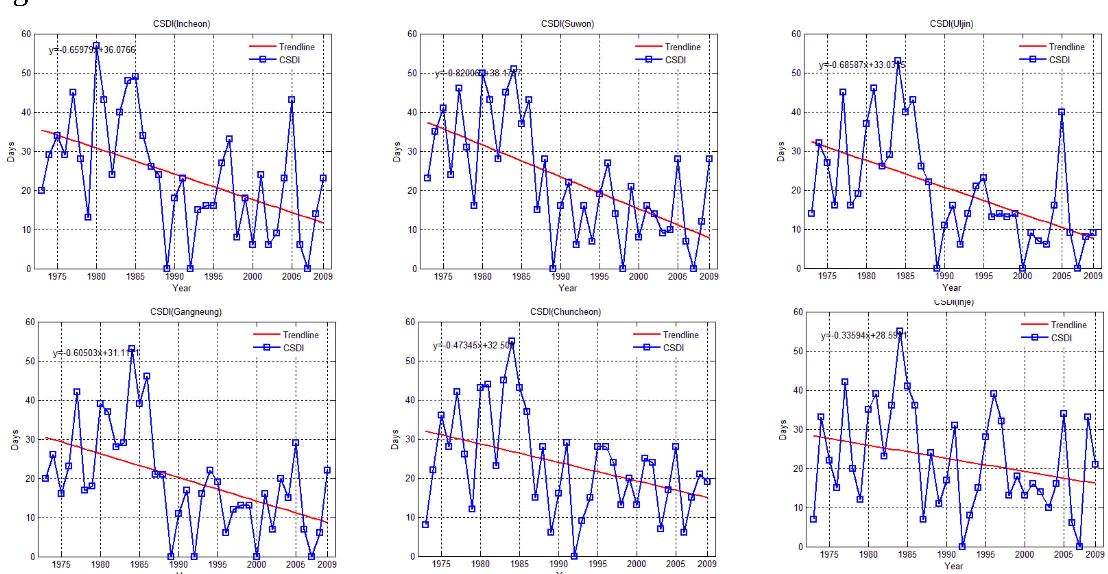

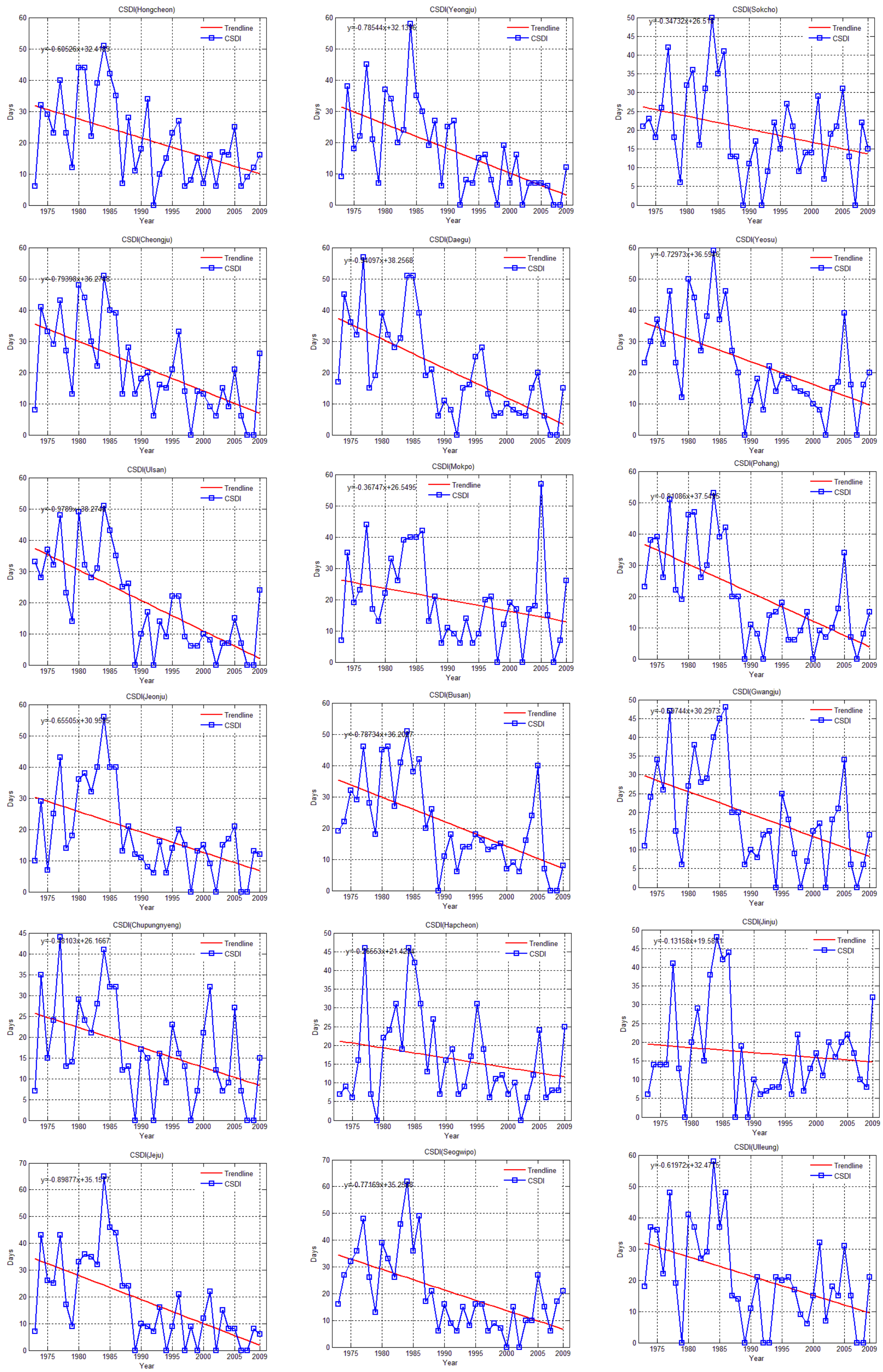

Figure B.18 CSDI at 24 stations